All-Optical Signal Processing
in
Quadratic Nonlinear Materials

Steffen Kjær Johansen

IMM

This document was prepared with LaTeX.

Preface

This dissertation is written in partial fulfillment of the requirements for the degree of *Doctor of Philosophy*, Ph.D., from the *Technical University of Denmark*. The work has been supported financially by the Danish Research Agency through the Graduate School in Nonlinear Science, the Technical University of Denmark, the Generalitat de Catalunya, and the European Union through the Improving Human Potential program (Contract HPRI-CT-1999-00071). Most of the numerical work was done at CESCA-CEPBA-CIRI. Support for the project supervision via the Danish Technical Research Council (Talent Grant No. 26-00-0355) is also acknowledged. The research was carried out partly at the Department of Informatics and Mathematical Modelling (IMM) of the Technical University of Denmark and partly at the Department of Signal Theory and Communications (TSC) of the Technical University of Catalonia.

Regarding the actual scientific work performed during the last three years, I want to thank my supervisors Res. Associate Prof. Ole Bang (IMM), Prof. Lluís Torner (TSC), and Associate Prof. Mads Peter Sørensen (IMM) in particular. I am also indebted to Prof. Peter Leth Christiansen (IMM) for his non-trivial involvement in ensuring the financial support for the project.

The main part of the work presented here has been published in the two appended papers. The chapters 2 and 3 are meant to give a brief introduction to the scientific content of the papers. Chapter 4 is a spin-off of chapter 2 and the results presented here have not yet been published. The introduction in chapter 1 aims at placing the scientific contribution of this dissertation in a broader perspective whereas the epilogue in chapter 5 is meant to summarise and conclude on the work. Chapter 1 and 5 should be understandable for everybody with an interest in *All-Optical Signal Processing in Quadratic Nonlinear Materials*.

Copenhagen, August 31, 2002

Steffen Kjær Johansen

List of appended papers

1 Steffen Kjær Johansen, Ole Bang, and Mads Peter Sørensen,
Escape angles in bulk $\chi^{(2)}$ soliton interactions,
Physical Review E, Volume 65, 026601 (February 2002).

2 Steffen Kjær Johansen, Silvia Carrasco, Lluís Torner, and Ole Bang,
Engineering of spatial solitons in two-period QPM structures,
Optics Communications, Volume 203, Issue 3-6, pp. 393-402 (March 2002).

Summary

The focal point of the research presented here is all-optical signal processing via nonlinearities. The objective has been to investigate the interaction between optical signals via nonlinearities and how these nonlinearities can be engineered to serve specific purposes.

The nonlinear response of materials with a second order nonlinearity, the so-called $\chi^{(2)}$ materials, is faster and stronger than that of more conventional materials with a cubic nonlinearity. The $\chi^{(2)}$ materials support spatial solitons consisting of two coupled components, the fundamental wave (FW) and its second harmonic (SH).

During this project the interaction between such spatial solitons has been investigated theoretically through perturbation theory and experimentally via numerical simulations. The outcome of this research is *new theoretical tools* for quantitatively predicting the *escape angle*, i.e. the angle of incidence below which the solitons will fuse and above which they will move apart. Head-on collision experiments are not comprised within the model assumptions, but even so expressions predicting the so-called inwards escape angle are proposed and numerically verified for certain cases. Chapter 2 and paper 1 are dedicated to this part of the research. In chapter 4 the generality of the theoretical approach is emphasized with the derivation and verification of equivalent tools for media with a saturable nonlinearity.

The strength of the $\chi^{(2)}$ nonlinearity strongly depends on the phase mismatch between the FW and the SH. Via quasi-phase-matching (QPM) the phase mismatch and hence the nonlinearity is effectively brought under control through periodic sign reversal of the nonlinearity. On the average QPM changes the quadratic nonlinearity and induces new cubic nonlinearities in the system. The engineering and exploitation of these cubic nonlinearities in *two-period QPM wave-guides* has been another area of investigation. Introducing the second period might make *practical engineering of the nonlinearities* possible. A major result is the discovery that cubic nonlinearities leads to an *enhancement of the bandwidth for soliton generation*. This part of the research is presented in Chapter 3 and paper 2.

Dansk resumé

Stikordene for den forskning, der præsenteres her, er "all-optical" signal behandling ved hjælp af ikke-lineariteter. Specifikt har målet været at undersøge optiske signalers vekselvirkning gennem ikke-lineariteter, og hvordan disse ikke-lineariteter kan skræddersys til bestemte formål.

Materialer med en kvadratisk ikke-linearitet, de såkaldte $\chi^{(2)}$ materialer, har vist sig at have ikke blot en kraftig ikke-linearitet, men også et ekstremt hurtigt respons sammenlignet med de mere udbredte materialer med en kubisk ikke-linearitet. I $\chi^{(2)}$ materialer kan der eksiteres rumlige solitoner bestående af to koplede felter, den fundamentale bølge (FW) og dens anden harmoniske (SH).

I dette projekt er vekselvirkningen mellem to sådanne rumlige solitoner blevet undersøgt teoretisk ved hjælp af perturbationsregning og eksperimentelt gennem numeriske simuleringer. Resultatet er *nyt teoretisk værktøj*, der kan forudsige den kritiske indfaldsvinkel, under hvilken solitonerne vil smelte sammen. Frontale sammenstød falder uden for model-antagelserne, men under visse forudsætninger kan der alligevel opstilles udtryk, som viser sig at være korrekte. Kapitel 2 og artikel 1 er dedikeret til denne del af forskningen. I kapitel 4 eftervises den generelle metode gennem udledning og verificering af tilsvarende værktøjer for materialer med en mætbar ikke-linearitet.

Den kvadratiske ikke-linearitets styrke afhænger kraftigt af om faserne mellem den FW og den SH er tilpasset hinanden. Tilpasningen kan ske ved hjælp af kvasi-fase tilpasning (QPM), der grundlæggende er en periodisk inversion af ikke-linearitetens fortegn. QPM ændrer den midlede kvadratiske ikke-linearitet og inducerer nye midlede kubiske ikke-lineariteter i systemet. Specielt er der blevet forsket i metoder til manipulering og udnyttelse af disse kubiske ikke-lineariteter for *to-periode QPM bølgeledere*. Med to perioder burde det være praktisk muligt at udnytte de midlede ikke-lineariteter. Et vigtigt resultat er opdagelsen af, at *kubiske ikke-lineariteter udvider båndbredden for generering af solitoner*. Denne del af forskningen er præsenteret i kapitel 3 og i artikel 2.

Contents

CHAPTER 1

Introduction

The field of nonlinear optics is immense and it comprises several autonomous areas of research. In this introduction the focus will be on the processes leading to spatial soliton formation and interaction in quadratic materials.

1.1   The quest for nonlinear light control

In 1961, shortly after the invention of the laser, a group around P. Franken generated the second harmonic (SH) of an optical wave by passing it through a quartz crystal [1]. Besides the discovery in 1893 of Pockels' effect[1] this was he first observation of a nonlinear optical event and as such it marked the beginning of the field of nonlinear optics [2, 3].

The second harmonic generation (SHG) process is based on the $\chi^{(2)}$ nonlinearity, which is the quadratic nonlinearity arising from photon-electron interactions. In general three waves are mixed in a $\chi^{(2)}$ crystal. This situation is refered to as type-II vectorial interaction. Type-I interaction of which SHG is an example, is degenerate three-wave mixing where two waves have the same polarization and same fundamental wavelength (FW). In SHG the photons at the FW are repeatedly up-converted

---

[1]Friedrich Pockels discovered that the refractive index in certain crystals changes linearly with the amplitude of an applied electric field.

via SHG ($\omega + \omega \rightarrow 2\omega$) and then down-converted via ($2\omega - \omega \rightarrow \omega$). Because of the repeatedness of the process the $\chi^{(2)}$ nonlinearity is often refered to as the cascaded nonlinearity. The conversion efficiency depends strongly on the wave vector mismatch $\Delta k = k_{2\omega} - 2k_\omega$ because the energy that down-converts experience a phase shift with respect to the original FW. Realizing a small mismatch and hence a considerable conversion efficiency was difficult in the early years of nonlinear optics. However, in 1967 Ostrovskii [4] recognized the importance of the phase shift in the FW, which becomes an almost linear function of propagation distance at large phase mismatches, thus mimicking the third order nonlinearity known from the cubic nonlinear Schrödinger equation (NLS).

In the late 1980s and early 1990s experiments close to the phase match condition were made [5, 6]. These experiments showed a strong phase shift, larger than π, due to cascading. The availability of materials such as polymers and semiconductors with very strong $\chi^{(2)}$ nonlinearities and relatively low loss led to a series of articles [7, 8] which rediscovered the potential exploitation of the cascaded nonlinearity. During the 1990s all-optical switching devices like the directional coupler, the Mach-Zehnder interferometer, and the optical transistor were proposed [9]-[11] and demonstrated in type-I [12] and in type-II [13]-[15] interactions.

Quadratic solitons in optics

Besides SHG the field of nonlinear optics also comprises temporally and spatially coherent structures, i.e. temporal and spatial solitary waves. The key feature in temporally coherent structures is the balance between group-velocity dispersion, i.e. the spreading of the pulse due to different velocities of the different frequency components, and self-phase modulation, i.e. the phase shift induced through the nonlinearity changing the phase of different frequency components with different amounts. Analogous spatially coherent structures depends upon the balance between refraction and self-focusing. Self-focusing arises when a continuous wave (CW) via the change in the intensity dependent refractive index creates a wave guide in the medium. When this self-created wave guide equals the diffraction of the CW the wave experiences self-trapping and a spatial soliton has emerged. In $\chi^{(2)}$ materials trapping is a result of interaction between the FW and its SH rather than a result of a refractive index change.

In 1974 Karamzin and Sukhorukov and later in 1981 Kanashov and Rubenschik predicted the existence of spatial solitons in $\chi^{(2)}$ materials [16]-[18], but due to the experimental limitation to high mismatch regimes the observed quadratic effects were very small. Hence the area was deemed experimentally exotic and largely "left in the dark" for the next couple of decades.

The close-to-phase-matching experiments around 1990 spawned a new interest in the spatial solitons. In a series of publications the solitons were studied analytically in waveguides, i.e. in media where trapping occurs in one transverse direction [19]-[30], and in bulk with trapping in two transverse directions [31]-[34], and likewise in type-II [35]-[40].

In the mid 1990s spatial solitons were experimentally observed [41]-[43] in $\chi^{(2)}$ materials and all-optical switching was demonstrated exploiting type-II [44]. In 1998 temporal solitons were also observed in a $\chi^{(2)}$ material [45].

Soliton interaction

The interaction between spatial solitons was from the start showed an immense interest due to the obvious potential applications in photonics [46]. An intriguing feature of solitons is their particle-like behavior during collision. In 1D Kerr media collisions are fully elastic due to integrability of the NLS equation [47, 48]. In contrast $\chi^{(2)}$ media are described by non-integrable equations [49] and soliton collisions are therefore inelastic, displaying both fusion, repulsion, annihilation, and generation of additional solitons [50, 51].

Fusion and crossing of spatial $\chi^{(2)}$ solitons was investigated numerically in type-I [52]-[55] and in type-II [56, 40]. Experimental observations confirming the numerics were later made [57]-[60].

Variational theories [61, 62], which are able to predict critical launch angles and relative phases separating regimes of collision and no collision [56]-[63], were developed. More recently elegant non-planar effective particle theories have predicted the absence of spiraling for type-I solitons [65, 66].

Quasi-phase-matching

Quasi-phase-matching (QPM) is a major alternative over conventional phase matching in many laser applications based on frequency-conversion processes in quadratic nonlinear media. Lately remarkable progress has been made in the periodic poling of lithium niobate technique for both two-dimensional bulk media and waveguides [67, 68]. This has refueled the interest in QPM even though it was proposed [2, 3] and even demonstrated [69, 70] in the early years of nonlinear optics.

Besides other practical advantages, QPM can be used to tailor the nonlinearity of the material to form complex structures. For example, engineerable pulse compression

in frequency-doubling schemes in synthetic QPM gratings has been demonstrated in aperiodically poled lithium niobate and KTP [71]-[74], and transverse QPM gratings have been made, both for shaping second-harmonic beams and to extend the spectral coverage of optical parametric oscillators [75, 76]. Bandwidth enhanced parametric interactions can be obtained in modulated-period structures [77], multiple nonlinear interactions can be achieved in quasi-periodic schemes [78]-[82], and simultaneous generation of multiple color laser light has been demonstrated in QPM waveguides [83] and QPM crystals [84]. QPM engineering also finds novel important applications beyond pure frequency-conversion devices, and generation of enhanced cascading phase-shifts [85] and all-optical diode operation [86] have been demonstrated.

Spatial solitons are supported by QPM media [87]-[91] and have been observed in periodically poled lithium niobate [92]. Perturbative approaches suggest that the averaged field equations should include induced averaged cubic nonlinearities [93]-[95]. Such terms, modifying the average properties of CW waves [96, 97] and the soliton families of the averaged equations [93]-[98], can be analyzed as sustained by competing quadratic and effective cubic nonlinearities [99]-[103].

The question thus naturally arises whether and how QPM engineering can be employed to bring the effective cubic nonlinearities to compete with the quadratic in the average fields. One solution is to add a strong dc-part to the nonlinear QPM grating, i.e. as done in [104, 105]. This adds a term to the induced Kerr terms, which is proportional to the QPM grating period and the dc-value squared, and thus can be large [95]. Another potentially more versatile technique is to modulate the QPM period with a second longer period, as it was shown theoretically in [94]. This introduces an extra degree of freedom, which can be used to engineer the effective quadratic and induced averaged cubic nonlinearity.

References

[1] P. A. Franken, A. E. Hill, C. W. Peters, and G. Weinreich, "Generation of Optical Harmonics," Phys. Rev. Lett. **7**, 118–119 (1961).

[2] J. A. Armstrong, N. Bloembergen, and P. Pershan, "Interaction Between Light Waves in a Nonlinear Dielectric," Phys. Rev. **127**, 1918 (1962).

[3] P. A. Franken and J. F. Ward, "Optical Harmonics and Nonlinear Phenomena," Rev. Mod. Phys. **35**, 23–39 (1963).

[4] L. A. Ostrovskii, "Self-action of Light in Crystals," Sov. Phys. JETP **5**, 272–275 (1967).

[5] N. R. Belashenkov, S. V. Gagarskii, and M. V. Inochkin, "Nonlinear refraction of light on second-harmonic generation," Opt. Spectrosk. (USSR) **66**, 1383–1386 (1989).

[6] R. DeSalvo, D. J. Hagan, M. Sheik-Bahae, G. I. Stegeman, E. V. Stryland, and H. Vanherzeele, "Self-focusing and self-defocusing by cascaded second-order effects in KTP," Opt. Lett. **17**, 28–30 (1992).

[7] G. I. Stegeman, M. Sheik-Bahae, E. V. Stryland, and G. Assanto, "Large non-linear phase shifts in second-order nonlinear-optical processes," Opt. Lett. **18**, 13–15 (1993).

[8] R. Schiek, "Nonlinear refraction caused by cascaded second-order nonlinearity in optical waveguide structures," J. Opt. Soc. Am. B **10**, 1848–1855 (1993).

[9] D. C. Hutchings, J. S. Aitchison, and C. N. Ironside, "All-optical switching based on nondegenrate phase shifts from a cascaded second-order nonlinearity," Opt. Lett. **18**, 793–795 (1993).

[10] G. Assanto, G. I. Stegeman, M. Sheik-Bahae, and E. V. Stryland, "All-optical switching devices based on large nonlinear phase shifts from second harmonic generation," Appl. Phys. Lett. **62**, 1323–1325 (1993).

[11] G. Assanto, A. Laureti-Palma, C. Sibilia, and M. Bertolotti, "All-optical switching via second harmonic generation in a nonlinearly asymmetric directional coupler," Opt. Commun. **110**, 599–603 (1994).

[12] Y. Baek, R. Schiek, and G. I. Stegeman, "All-optical switching in a hybrid Mach-Zehnder interferometer as a result of cascaded second-order nonlinearity," Opt. Lett. **20**, 2168–2170 (1995).

[13] G. Assanto, I. Torelli, and S. Trillo, "All-optical processing by means of vectorial interactions in second-order cascading: novel approaches," Opt. Lett. **19**, 1720–1722 (1994).

[14] G. Assanto, Z. Wang, D. J. Hagan, and E. V. Stryland, "All-optical switching via nonlinear cascading in type II second-harmonic generation," Appl. Phys. Lett. **67**, 2120–21223 (1995).

[15] G. Assanto, G. I. Stegeman, M. Sheik-Bahae, and E. V. Stryland, "Coherent Interactions for All-Optical Signal Processing via Quadratic Nonlinearities," IEEE J. Quantum Electron. **31**, 673–681 (1995).

[16] Y. N. Karamzin and A. P. Sukhorukov, "Nonlinear Interaction of Diffracted Light Beams in a Medium with Quadratic Nonlinearity: Mutual Focusing of Beams and Limitation on the Efficiency of Optical Frequency Converters," Sov. Phys. JETP **20**, 339–342 (1967).

[17] Y. N. Karamzin and A. P. Sukhorukov, "On mutual focusing of intense light beams in media with quadratic nonlinearity," Zh. Eksp. Teor. Fiz. **68**, 834–847 (1975).

[18] A. A. Kanashov and A. M. Rubenchik, "On diffraction and Dispersion Effect on Three Wave Interaction," Physica D **4**, 122–134 (1981).

[19] K. Hayata and M. Koshiba, "Multidimensional Solitons in Quadratic Nonlinear Media," Phys. Rev. Lett. **71**, 3275–3278 (1993).

[20] M. J. Werner and P. D. Drummond, "Simulton solutions for the parametric amplifier," J. Opt. Soc. Am. B **10**, 2390–2393 (1993).

[21] M. J. Werner and P. D. Drummond, "Strongly coupled nonlinear parametric solitary waves," Opt. Lett. **19**, 613–615 (1994).

[22] L. Torner, C. R. Menyuk, and G. I. Stegeman, "Excitation of solitons with cascaded $\chi^{(2)}$ nonlinearities," Opt. Lett. **19**, 1615–1617 (1994).

[23] C. R. Menyuk, R. Schiek, and L. Torner, "Solitary waves due to $\chi^{(2)} : \chi^{(2)}$ cascading," J. Opt. Soc. Am. B **11**, 2434–2443 (1994).

[24] L. Torner, C. R. Menyuk, and G. I. Stegeman, "Bright solitons with second-order nonlinearities," J. Opt. Soc. Am. B **12**, 889–897 (1995).

[25] A. V. Buryak and Y. S. Kivshar, "Spatial optical solitons governed by quadratic nonlinearity," Opt. Lett. **19**, 1612–1614 (1994).

[26] L. Torner, "Stationary solitary waves with second-order nonlinearities," Opt. Commun. **114**, 136–140 (1995).

[27] A. V. Buryak and Y. S. Kivshar, "Solitons due to second harmonic generation," Phys. Lett. A **197**, 407–412 (1995).

[28] D. E. Pelinovsky, A. V. Buryak, and Y. S. Kivshar, "Instability of Solitons Governed by Quadratic Nonlinearities," Phys. Rev. Lett. **75**, 591–595 (1995).

[29] L. Torner, D. Mihalache, D. Mazilu, and N. N. Akhmediev, "Stability of spatial solitary waves in quadratic media," Opt. Lett. **20**, 2183–2185 (1995).

[30] L. Torner, W. E. Torruellas, , G. I. Stegeman, and C. R. Menyuk, "Beam steering by $\chi^{(2)}$ trapping," Opt. Lett. **20**, 1952–1953 (1995).

[31] V. K. M. L. Bergé, J. J. Rasmussen, and J. Wyller, "Formation of stable solitons in quadratic nonlinear media," Phys. Rev. A **52**, 28–31 (1995).

[32] L. Torner, C. R. Menyuk, W. E. Torruellas, and G. I. Stegeman, "Two-dimensional solitons with second-order nonlinearities," Opt. Lett. **20**, 13–15 (1995).

[33] L. Torner, D. Mihalache, D. Mazilu, E. M. Wright, W. E. Torruellas, and G. I. Stegeman, "Stationary trapping of light beams in bulk second-order nonlinear media," Opt. Commun. **121,** 149–155 (1995).

[34] L. Torner and E. M. Wright, "Soliton excitation and mutual locking of light beams in bulk quadratic nonlinear crystals," J. Opt. Soc. Am. B **13,** 864–875 (1996).

[35] H. T. Tran, "Self-induced phase-matching and three-wave bright spatial solitons in quadratic media," Opt. Commun. **118,** 581–586 (1995).

[36] A. Kobyakov, U. Peschel, and F. Lederer, "Vectorial type-II interaction in cascaded quadratic nonlinearities - an analytic approach," Opt. Commun. **124,** 184–194 (1994).

[37] B. A. Malomed, D. Anderson, and M. Lisak, "Three-wave interaction solitons in a dispersive medium with quadratic nonlinearity," Opt. Commun. **126,** 251–254 (1996).

[38] A. V. Buryak, Y. S. Kivshar, and S. Trillo, "Stability of Three-Wave Parametric Solitons in Diffractive Quadratic Media," Phys. Rev. Lett. **77,** 5210–5213 (1996).

[39] G. Leo, G. Assanto, and W. E. Torruellas, "Beam pointing control with spatial solitary waves in quadratic nonlinear media," Opt. Commun. **134,** 223–226 (1997).

[40] G. Leo and G. Assanto, "Collisional interactions of vectorial spatial solitary waves in type II frequency-doubling media," J. Opt. Soc. Am. B **14,** 3151–3161 (1997).

[41] W. E. Torruellas, Z. Wang, D. J. Hagan, E. V. Stryland, G. I. Stegeman, L. Torner, and C. R. Menyuk, "Observation of Two-Dimensional Spatial Solitary Waves in a Quadratic Medium," Phys. Rev. Lett. **74,** 5036–5039 (1995).

[42] W. E. Torruellas, Z. Wang, L. Torner, and G. I. Stegeman, "Observation of mutual trapping and dragging of two-dimensional spatial solitary waves in a quadratic medium," Opt. Lett. **20,** 1949–1951 (1995).

[43] R. Schiek, Y. Baek, and G. I. Stegeman, "One-dimensional spatial solitary waves due to cascaded second-order nonlinearities in planar waveguides," Phys. Rev. E **53,** 1138–1141 (1996).

[44] W. E. Torruellas, G. Assanto, B. L. Lawrence, F. Fuerst, and G. I. Stegeman, "All-optical switching by spatial walkoff compensation and solitary-wave locking," Appl. Phys. Lett. **68,** 1449–1451 (1996).

[45] P. D. Trapani, D. Caironi, G. Valiulis, A. Dubietis, R. Danielius, and A. Piskarskas, "Observation of Temporal Solitons in Second-harmonic Generation with Tilted Pulses," Phys. Rev. Lett. **81**, 570–573 (1998).

[46] S. Lan, E. DelRe, Z. Chen, M. feng Shih, and M. Segev, "Directional coupler with soliton-induced waveguides," Opt. Lett. **24**, 475–477 (1999).

[47] V. E. Zakharov and A. B. Shabat, "Exact Theory of Two-Dimensional Self-Focusing and One-Dimensional Self-Modulation of Waves in Nonlinear Media," Zh. Eksp. Teor. Fiz. **61**, 118–134 (1971).

[48] V. E. Zakharov and A. B. Shabat, "Interaction Between Solitons in a Stable Medium," Zh. Eksp. Teor. Fiz. **64**, 1627–39 (1973).

[49] S. Lafortune, P. Winternitz, and C. R. Menyuk, "Solutions to the optical cascading equations," Phys. Rev. E **58**, 2518–2525 (1998).

[50] L. Torner, J. P. Torres, and C. R. Menyuk, "Fission and self-deflection of spatial solitons by cascading," Opt. Lett. **21**, 462–464 (1996).

[51] M. C. Santos, "Dynamic Y-branched structures in quadratic nonlinear media," Opt. Commun. **180**, 167–177 (2000).

[52] A. V. Buryak, Y. S. Kivshar, and V. V. Steblina, "Self-trapping of light beams and parametric solitons in diffractive quadratic media," Phys. Rev. A **52**, 1670–1674 (1995).

[53] D.-M. Baboiu, G. I. Stegeman, and L. Torner, "Interaction of one-dimensional bright solitary waves in quadratic media," Opt. Lett. **20**, 2282–2284 (1995).

[54] C. Etrich, U. Peschel, F. Lederer, and B. Malomed, "Collision of solitary waves in media with a second-order nonlinearity," Phys. Rev. A **52**, 3444–3447 (1995).

[55] D.-M. Baboiu and G. I. Stegeman, "Solitary-wave interactions in quadratic media near type I phase-matching conditions," J. Opt. Soc. Am. B **14**, 3143–3150 (1997).

[56] B. Costantini, C. D. Angelis, A. Barthelemy, A. L. Palma, and G. Assanto, "Polarization-multiplexed $\chi^{(2)}$ solitary-wave interactions," Opt. Lett. **22**, 1376–1378 (1997).

[57] Y. Baek, R. Schiek, G. I. Stegeman, I. Baumann, and W. Sohler, "Interactions between one-dimensional quadratic solitons," Opt. Lett. **22**, 1550–1552 (1997).

[58] R. Schiek, Y. Baek, G. I. Stegeman, and W. Sohler, "Interactions between one-dimensional quadratic soliton-like beams," Optical and Quantum Electronics **30**, 861–879 (1998).

[59] A. Barthélémy, B. Bourliaguet, V. Kermene, B. Costantini, C. D. Angelis, D. Modotto, and G. Assanto, "Interactions of type II vectorial spatial solitary waves in materials with quadratic non-linearity," Optical and Quantum Electronics **30**, 923–935 (1998).

[60] B. Costantini, C. D. Angelis, A. Barthelemy, B. Bourliaguet, and V. Kermene, "Collisions between type II two-dimensional quadratic solitons," Opt. Lett. **23**, 424–426 (1998).

[61] K. A. Gorshkov and L. A. Ostrovsky, "Interactions of Solitons in Nonintegrable Systems: Direct Perturbation Methods and Applications," Physica D **1**, 428–438 (1981).

[62] D. Anderson and M. Lisak, "Variational Approach to Incoherent Two-Soliton Interaction," Physica Scripta **33**, 193–196 (1986).

[63] V. V. Steblina, Y. S. Kivshar, M. Lisak, and B. Malomed, "Self-guided beams in a diffractive $\chi^{(2)}$ medium: variational approach," Opt. Commun. **118**, 345–352 (1995).

[64] C. B. Clausen, P. L. Christiansen, and L. Torner, "Perturbative approach to the interaction of solitons in quadratic nonlinear media," Opt. Commun. **136**, 185–192 (1997).

[65] V. V. Steblina, Y. S. Kivshar, M. Lisak, and B. Malomed, "Scattering and spiraling of solitons in a bulk quadratic medium," Opt. Commun. **23**, 156–158 (1998).

[66] A. V. Buryak and V. V. Steblina, "Soliton collisions in bulk quadratic media: comprehensive analytical and numerical study," J. Opt. Soc. Am. B **16**, 245–255 (1999).

[67] K. El Hadi, M. Sundheimer, P. Aschieri, P. Baldi, M. P. De Micheli, and D. B. Ostrowsky, "Quasi-phase-matched parametric interactions in proton-exchanged lithium niobate waveguides," J. Opt. Soc. Am. B **14**, 3197–3203 (1997).

[68] P. Baldi, M. P. De Micheli, K. E. Hadi, S. Nouh, A. C. Cino, P. Aschieri, and D. B. Ostrowsky, "Proton exchanged waveguides in LiNbO3 and LiTaO3 for integrated lasers and nonlinear frequency converters," Opt. Eng. **37**, 1193–1202 (1998).

[69] A. Szilagyi, A. Hordvik, and H. Schlossberg, "A quasi-phase-matching technique for efficient optical mixing and frequency doubling," J. Appl. Phys. **47**, 2025–2032 (1976).

[70] J. P. van der Ziel, M. Ilegems, P. W. Foy, and R. M. Mikulyak, "Phase-matched second harmonic generation in a periodic GaAs waveguide," Appl. Phys. Lett. **29**, 775–777 (1976).

[71] M. A. Arbore, M. M. Fejer, M. E. Fermann, A. Hariharan, A. Galvanauskas, and D. Harter, "Frequency doubling of femtosecond erbium-fiber soliton lasers in periodically poled lithium niobate," Opt. Lett. **22,** 13–15 (1997).

[72] M. A. Arbore, A. Galvanauskas, D. Harter, M. H. Chou, and M. M. Fejer, "Engineerable compression of ultrashort pulses by use of second-harmonic generation in chirped-period-poled lithium niobate," Opt. Lett. **22,** 1341–1343 (1997).

[73] P. Loza-Alvarez, D. T. Reid, P. Faller, M. Ebrahimzadeh, W. Sibbett, H. Karlsson, and F. Laurell, "Simultaneous femtosecond-pulse compression and second-harmonic generation in aperiodically poled KTiOPO$_4$," Opt. Lett. **24,** 1071–1073 (1999).

[74] G. Imeshev, M. A. Arbore, M. M. Fejer, Galvanauskas, M. Fermann, and D. Harter, "Ultrashort-pulse second-harmonic generation with longitudinally nonuniform quasi-phase-matching gratings: pulse compression and shaping," J. Opt. Soc. Am. B **17,** 304–318 (2000).

[75] G. Imeshev, M. Proctor, and M. M. Fejer, "Lateral patterning of nonlinear frequency conversion with transversely varying quasi-phase-matching gratings," Opt. Lett. **23,** 673–675 (1998).

[76] P. E. Powers, T. J. Kulp, and S. E. Bisson, "Continuous tuning of a continuous-wave periodically poled lithium niobate optical parametric oscillator by use of a fan-out grating design," Opt. Lett. **23,** 159–162 (1998).

[77] K. Mizuuchi, K. Yamamoto, M. Kato, and H. Sato, "Broadening of the Phase-Matching Bandwidth in Quasi-Phase-Matched Second Harmonic Generation," IEEE J. Quantum Electron. **30,** 1596–1604 (1994).

[78] S.-N. Zhu, Y.-Y. Zhu, and N.-B. Ming, "Quasi-Phase-Matched Third-Harmonic Generation in a Quasi-Periodic Optical Superlattice," Science **278,** 843–846 (1997).

[79] K. Fradkin-Kashi and A. Arie, "Multiple-Wavelength Quasi-Phase-Matched Nonlinear Interactions," IEEE J. Quantum Electron. **35,** 1649–1656 (1999).

[80] M. H. Chou, K. R. Parameswaran, M. M. Fejer, and I. Brener, "Multiple-channel wavelength conversion by use of engineered quasi-phase-matching structures in LiNbO$_3$ waveguides," Opt. Lett. **24,** 1157–1159 (1999).

[81] H. Liu, Y. Y. Zhu, S. N. Zhu, C. Zhang, and N. B. Ming, "Aperiodic optical superlattices engineered for optical frequency conversion," Appl. Phys. Lett. **79,** 728–730 (2001).

[82] K. Fradkin-Kashi, A. A. nad Pavel Urenski, and G. Rosenman, "Multiple Non-linear Optical Interactions with Arbitrary Wave Vector Differences," Phys. Rev. Lett. **88,** 023903 (2002).

[83] P. Baldi, C. G. Treviño-Palacios, G. I. Stegeman, M. P. De Micheli, D. B. Ostrowsky, D. Delacourt, and M. Papuchon, "Simultaneous generation of red, green and blue light in room temperature periodically poled lithium niobate waveguides using single source," Elect. Lett. **31,** 1350–1351 (1995).

[84] J. Capmany, "Simultaneous generation of red, green, and blue continuous-wave laser radiation in Nd^{3+}-doped aperiodically poled lithium niobate," Appl. Phys. Lett. **78,** 144–146 (2001).

[85] M. Cha, "Cascaded phase shift and intensity modulation in aperiodic quasi-phase-matched gratings," Opt. Lett. **23,** 250–252 (1998).

[86] K. Gallo, G. Assanto, K. R. Parameswaran, and M. M. Fejer, "All-optical diode in a periodically poled lithium niobate waveguide," Appl. Phys. Lett. **79,** 314–316 (2001).

[87] L. Torner, C. B. Clausen, O. Bang, P. L. Christiansen, Y. S. Kivshar, and M. M. Fejer, "Soliton Control by QPM Engineering," Optics & Photonics News **10,** 44 (1999).

[88] L. Torner, C. B. Clausen, and M. M. Fejer, "Adiabatic shaping of quadratic solitons," Opt. Lett. **23,** 903–905 (1998).

[89] C. B. Clausen and L. Torner, "Spatial switching of quadratic solitons in engineered quasi-phase-matched structures," Opt. Lett. **24,** 7–9 (1999).

[90] C. B. Clausen, O. Bang, Y. S. Kivshar, and P. L. Christiansen, "Quasi-Periodic Envelope Solitons," Phys. Rev. Lett. **83,** 4740–4743 (1999).

[91] S. Carrasco, J. P. Torres, L. Torner, and R. Schiek, "Engineerable generation of quadratic solitons in synthetic phase matching," Opt. Lett. **25,** 1273–1275 (2000).

[92] B. Bourliaguet, V. Couderc, A. Barthélémy, G. W. Ross, P. G. R. Smith, D. C. Hanna, and C. D. Angelis, "Observation of quadratic spatial solitons in periodically poled lithium niobate," Opt. Lett. **24,** 1410–1412 (1999).

[93] C. B. Clausen, O. Bang, and Y. S. Kivshar, "Spatial Solitons and Induced Kerr Effects in QPM Media," Phys. Rev. Lett. **78,** 4749–4752 (1997).

[94] O. Bang, C. B. Clausen, P. L. Christiansen, and L. Torner, "Engineering competing nonlinearities," Opt. Lett. **24,** 1413–1415 (1999).

[95] J. F. Corney and O. Bang, "Solitons in quadratic nonlinear photonic crystals," Phys. Rev. E **64,** 047601 (2001).

[96] A. Kobyakov, F. Lederer, O. Bang, and Y. S. Kivshar, "Nonlinear phase shift and all-optical switching in quasi-phase-matched quadratic media," Opt. Lett. **23,** 506–508 (1998).

[97] O. Bang, T. W. Graversen, and J. F. Corney, "Accurate switching intensities and length scales in quasi-phase-matched materials," Opt. Lett. **26**, 1007–1009 (2001).

[98] J. F. Corney and O. Bang, "Modulational Instability in Periodic Quadratic Nonlinear Materials," Phys. Rev. Lett. **87**, 133901 (2001).

[99] A. V. Buryak, Y. S. Kivshar, and S. Trillo, "Optical solitons supported by competing nonlinearities," Opt. Lett. **20**, 1961–1963 (1995).

[100] O. Bang, "Dynamical equations for wave packets in materials with both quadratic and cubic responses," J. Opt. Soc. Am. B **14**, 51–61 (1997).

[101] L. Bergé, O. Bang, J. J. Rasmussen, and V. K. Mezentsev, "Self-focusing and solitonlike structures in materials with competing quadratic and cubic nonlinearities," Phys. Rev. E **55**, 3555–3570 (1997).

[102] O. Bang, L. Bergé, and J. J. Rasmussen, "Wave collapse in bulk media with quadratic and cubic responses," Opt. Commun. **146**, 231–235 (1998).

[103] O. Bang, Y. S. Kivshar, A. V. Buryak, A. D. Rossi, and S. Trillo, "Two-dimensional solitary waves in media with quadratic and cubic nonlinearity," Phys. Rev. E **58**, 5057–5069 (1998).

[104] A. S. Helmy, D. C. Hutchings, T. C. Kleckner, J. H. Marsh, A. C. Bryce, J. M. Arnold, C. R. Stanley, J. S. Aitchison, C. T. A. Brown, K. Moutzouris, and M. Ebrahimzadeh, "Quasi phase matching in GaAs-AlAs superlattice waveguides through bandgap tuning by use of quantum-well intermixing," Opt. Lett. **25**, 1370–1372 (2000).

[105] Y. Shuto, T. Watanabe, S. Tomaru, I. Yokohama, M. Hikita, and M. Amano, "Quasi-Phase-Matched Second-Harmonic Generation in Diazo-Dye-Substituted Polymer Waveguides," IEEE J. Quantum Electron. **33**, 349–357 (1997).

CHAPTER 2

Interaction in $\chi^{(2)}$ media

In this chapter soliton interaction in media with a second-order nonlinearity is considered. Soliton interaction has been investigated before [1]-[3]. These contributions made it possible to predict the fusion distance and yielded valuable insights regarding the significance of the phase-difference between the solitons. However, models for solitons launched with a nonzero angle of incidence with respect to each other have not been developed.

As depicted in Fig. 2.1, the aim is to predict quantitatively the escape angle. In the planar interaction case the inwards escape angle is defined as the angle of incidence below which two identical solitons will fuse and above which they will pass through each other. The outwards escape angle is defined as the angle below which two identical solitons will turn around and fuse and above which they will continue to move apart.
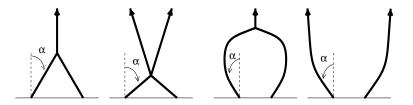

Figure 2.1: The escape angle concept.

In a symmetric setup with identical solitons the interaction problem can be reduced to that of an effective particle in a well-potential [3]. In the first section this effective particle approach is presented. The derivation of the full set of soliton interaction equations, i.e. the general analytical model describing nonplanar interaction of non-identical solitons, involves extensive perturbation theory. This part has therefore been placed in appendix A.

The chapter should be viewed merely as an introduction since the main results and conclusions have already been published in paper 1. However, the paper deals only with the 2D in-plane case. Thus in the second section of this chapter new results for the outwards escape angle in 1D are presented and in the third section an example of spiraling, the 2D nonplanar case, is given.

Regarding the inwards escape angle it has only been been possible to numerically verify the theoretical expression for perfect phase-matching conditions in the 2D in-plane case. Attempts to verify expressions for other cases, i.e. for nonzero phase mismatches in 2D and for both zero and nonzero phase mismatches in 1D, have so far proved futile. Note that this is not surprising since all model assumptions (see section 2.1) are violated in this case. For further discussion of the inwards escape angle the reader is refered to paper 1, where the results for the 2D in-plane case have been published.

2.1 The effective particle approach

Beam propagation under type-I second harmonic generation (SHG) conditions in lossless bulk $\chi^{(2)}$ materials is considered. The 1D slab waveguide version is trivially recovered by separating the linear variation in y out of the equations below. The system of normalized dimensionless dynamical equations describing the evolution of the slowly varying envelope of the fundamental wave (FW), $A_1 = A_1(x, y, z)$, and its second harmonic (SH), $A_2 = A_2(x, y, z)$, is [4, 5]

$$i\frac{\partial A_1}{z} + \tfrac{1}{2}\nabla_\perp^2 A_1 + A_1^* A_2 = 0, \tag{2.1a}$$

$$i\frac{\partial A_2}{z} + \tfrac{1}{4}\nabla_\perp^2 A_2 - \beta A_2 + A_1^2 = 0. \tag{2.1b}$$

z is the propagation variable, and $\nabla_\perp^2 = \partial^2/\partial x^2 + \partial^2/\partial y^2$ accounts for diffraction in the transverse (x, y)-plane. The normalized phase mismatch is $\beta = l_d(2k_1 - k_2)$, where l_d is the diffraction length of the fundamental and k_1 and k_2 are the wave numbers of the FW and SH, respectively. Equations (2.1) conserve the power $P = \int(|A_1|^2 + |A_2|^2)d\vec{r}_\perp$ and the vector momentum $\vec{M} = \int \text{Im}(A_1^*\nabla_\perp A_1 + A_2^*\nabla_\perp A_2)d\vec{r}_\perp$, where $\int d\vec{r}_\perp \equiv \int \int_{-\infty}^{\infty} dxdy$. The system (2.1) is known to have a one-parameter

family of radially symmetric bright 2D solitons of the form $A_1(\vec{r}) = V(r; \lambda)\exp(i\lambda z)$ and $A_2(\vec{r}) = W(r; \lambda)\exp(i2\lambda z)$ where $\lambda > \max(0; -\beta/2)$ is the internal soliton parameter and $r = \sqrt{x^2 + y^2}$. Furthermore a gauge transformation can be applied to find the soliton profiles V and W moving with transverse velocities ν_x and ν_y. The general three parameter soliton profiles are given by

$$V(x - \nu_x z, y - \nu_y z; \lambda, \nu_x, \nu_y) = V(x, y; \lambda - \tfrac{1}{2}\nu_x - \tfrac{1}{2}\nu_y)e^{-i(\nu_x x + \nu_y y)}, \qquad (2.2a)$$

$$W(x - \nu_x z, y - \nu_y z; \lambda, \nu_x, \nu_y) = W(x, y; \lambda - \tfrac{1}{2}\nu_x - \tfrac{1}{2}\nu_y)e^{-i2(\nu_x x + \nu_y y)}. \qquad (2.2b)$$

In the following a superposition of two solitons is considered. The field components can be expressed as

$$A_1 = \sum_{j=1,2} V^{(j)}(x - x^{(j)}, y - y^{(j)})e^{i\phi^{(j)} z}, \qquad (2.3a)$$

$$A_2 = \sum_{j=1,2} W^{(j)}(x - x^{(j)}, y - y^{(j)})e^{2i\phi^{(j)} z}, \qquad (2.3b)$$

where $x^{(j)}$ and $y^{(j)}$ give the soliton center positions in the transverse plane, and $\phi^{(j)}$ is the accumulated phase of soliton j. The transverse velocities of the solitons are given by $\dot{x}^{(j)}$ and $\dot{y}^{(j)}$, where dot denotes differentiation with respect to the propagation coordinate.

In appendix A the general set of soliton interaction equations, i.e. the general analytical model describing weak nonplanar interaction between the two solitons (2.3), is derived. The derivation is based on a perturbative approach and the solitons are assumed to be far apart with only a small overlap of the soliton tails. The functional forms of the non-interacting soliton profiles are then retained during interaction. The changes in the shape due to the interaction come about as a result of slowly varying soliton parameters $x^{(j)}$, $y^{(j)}$, and $\phi^{(j)}$.

If the solitons are identical with no phase difference between them and they are launched placed opposite each other in the transverse plane, then the two sets of soliton parameters reduce to one, $\lambda = \lambda^{(1)} = \lambda^{(2)}$, $x^{(1)} = -x^{(2)}$, $y^{(1)} = -y^{(2)}$. Under these conditions there can be no net transfer of energy between the solitons and since the initial overlap is assumed small it can be assumed that the individual soliton powers do not change, i.e. $\partial P/\partial z = 0$. With this in mind it is only necessary to consider two out of the six interaction equations (A.25, with $\eta = 1$ and $\gamma = 0$). Without loss of generality the two remaining equations (A.25b) and (A.25c) for

soliton 1 are chosen,

$$\frac{\partial M_x^{(1)}}{\partial Z} + \frac{\partial U^{(1)}}{\partial x^{(1)}} = 0, \tag{2.4a}$$

$$\frac{\partial M_y^{(1)}}{\partial Z} + \frac{\partial U^{(1)}}{\partial y^{(1)}} = 0, \tag{2.4b}$$

where the interaction potential $U^{(1)}$ is

$$U^{(1)} = -\text{Re} \int \left(V^{*(1)2} W^{(2)} + 2V^{(1)} W^{*(1)} V^{(2)} \right) d\vec{r}_\perp. \tag{2.5}$$

The system (2.4) can be derived from the Lagrangian

$$L = \dot{X} M_x + \dot{Y} M_y - U. \tag{2.6}$$

In (2.6) $X = x^{(1)} = -x^{(2)}$ and $Y = y^{(1)} = -y^{(2)}$. The soliton index has been removed because of unambiguousness. By exploiting the gauge transformation (2.2), (2.6) can be rewritten as

$$L = \left(\dot{X}^2 + \dot{Y}^2 \right) P - U, \tag{2.7}$$

with interaction potential U given by

$$U = -\int \Bigg(V^2(x - X, y - Y) W(x + X, y + Y) \cos(2\Delta)$$

$$+ 2V(x - X, y - Y) V(x + X, y + Y) W(x - X, y - Y) \cos(\Delta) \Bigg) d\vec{r}_\perp, \tag{2.8}$$

where $\Delta = 2\dot{X} X + 2\dot{Y} Y$. In a classical framework (2.7) is nothing more than the Lagrangian for a particle with mass P and kinetic energy $E_{\text{kin}} = (\dot{X}^2 + \dot{Y}^2) P/2$ moving in a potential $U = U(X, Y, \dot{X}, \dot{Y})$.[1]

Even though the potential is two-dimensional and nonuniform in the (X, Y)-plane the general idea can be appreciated by the one-dimensional case illustrated in Fig. 2.2. The particle, placed in the potential, will be affected by forces trying to drag it towards the bottom of the potential. To escape the barrier the particle must have sufficient kinetic energy, E_{kin}. The sufficient kinetic energy is the equivalent amount of potential energy, E_{pot}, at the location of the particle. Put in another way, the total energy, E_{tot}, of the system must be zero, i.e. $E_{\text{tot}} = E_{\text{kin}} + E_{\text{pot}} = 0$. Equivalently the solitons, in the soliton interaction picture, will continue apart if their outwards velocities initially are above some critical value. If initially the velocities are below

---

[1]In paper 1 the system is further reduced by introducing cylindrical coordinates with $R = \sqrt{X^2 + Y^2}$. Though the reduction is illustrative, it is of little practical use, because $\dot{R} \neq \dot{X}^2 + \dot{Y}^2$ is difficult to relate to the real system.
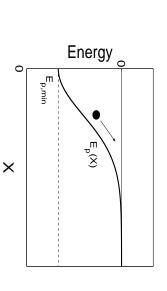
Figure 2.2: Illustration of classical particle facing a potential barrier.

that value the solitons are trapped. Whether they then fuse or pass through each other is impossible to predict with the theory presented here. Based on experience however, it is known that for small phase mismatches the solitons tend to fuse, whereas for larger phase mismatches, where the system becomes effectively cubic, some oscillations of the solitons around each other can occur before they eventually fuse. In the effective particle picture this would correspond to introducing damping into the system.

Hence, determination of the outwards escape velocities for a given problem simply becomes a question of solving

$$(\nu_x^2 + \nu_y^2)\, P(\lambda, \beta) + U(\lambda, \beta, x_0, y_0; \nu_x, \nu_y) = 0, \qquad (2.9)$$

where $x_0 = X(z = 0)$ and $y_0 = Y(z = 0)$ is the initial center position in the transverse plane and $\nu_x = \dot{X}(z = 0)$ and $\nu_y = \dot{Y}(z = 0)$ are the initial transverse velocities. Because U depends on the transverse velocities this equation is in general transcendental. Note that the angle α and the transverse velocity ν along a transverse direction are related through $\alpha = \mathrm{Arctan}\nu$ (see Fig. 2.1).

2.2 Outwards escape angle in the 1D case

To illustrate the method outlined above, soliton interaction in a 1D slab waveguide is considered. Fig. 2.3 shows a typical numerical experiment where two solitons of equal power are launched with opposite outwards angles. The figure shows how the solitons fuse, if they are launched with an outwards angle below some critical value, and how they continue to move apart, if the angle is greater than the critical value. In order to determine the critical angle the following transcendental equation must be solved

$$\nu_c^2 P(\lambda, \beta) = -U(\lambda, \beta, x_0; \nu_c), \qquad (2.10)$$
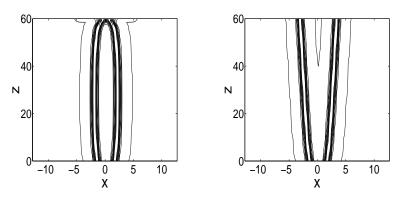
Figure 2.3: Contour plots illustrating interaction in 1D quadratic media. Here $\beta = 20$ and the two solitons are identical with individual powers $P = 198.8$. In both cases the initial separation is $2x_0 = 3$. In the left plot the solitons are launched with outwards angles $\alpha \approx 4.6°$ and in the right plot they are launched with $\alpha \approx 4.9°$.

where ν_c is the critical transverse velocity ν_x for which (2.10) is satisfied, i.e. $\nu_c = \nu_c(\beta, \lambda, x_0)$. The interaction potential is

$$U = -\int \left(V^2(x - x_0)W(x + x_0)\cos(4x_0\nu_x) \right.$$

$$\left. +2V(x - x_0)W(x - x_0)V(x + x_0)\cos(2x_0\nu_x)\right)dx. \qquad (2.11)$$

In general the analytical expressions for the soliton profiles V and W are not known
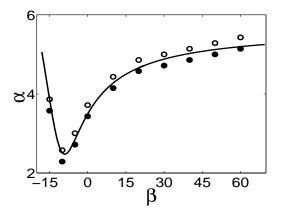

Figure 2.4: Outwards escape angle, α_c, in degrees as a function of the phase mismatch, β, for 1D interaction in a quadratic material. FWHM=1 and $x_0 = 1.5$. A ($\bullet$) is the result of a numerical experiment where the solitons fused, whereas a ($\circ$) is the result of an experiment where they escaped, i.e. continued to move apart.

and they must be found by numerical methods. Note that for a given β, the individual soliton characteristics, such as the power, P, and the full-width at half-maximum, FWHM, are functions only of the soliton propagation parameter λ. Approximations for the profiles do exist, but it turns out that the functional form of the soliton tale, i.e. $V(x), W(x)$ for $x \gg$ FWHM, is very important, and that the tales of the standard trial functions, i.e. a Gaussian or a sech, are not close enough.

In Fig. 2.4 the outwards escape angle is shown as a function of the phase mismatch β. The initial separation of the soliton centers, $2x_0 = 3$, and the initial width of the solitons, FWHM=1, are kept constant. The figure shows both the analytically found curve and results of numerical experiments like the one in Fig. 2.3. For $\beta \approx -19$ there is no longer any soliton parameter λ yielding FWHM=1. This is due to the fact that the soliton width goes to infinity when λ approaches the cut off value $-\beta/2$. For positive values of β it was always numerically possible to find a λ fulfilling FWHM=1 though it cannot be ruled out that a cut off value exists. The soliton characteristics for the different phase mismatches are shown in Fig. 2.5.
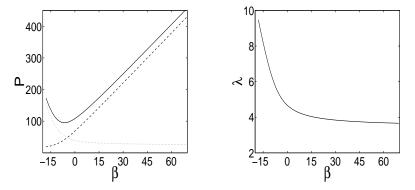
Figure 2.5: Characteristics for the interacting solitons of Fig. 2.4. On the left figure the full curve shows the total power, the dashed curve shows the power in the FW, and the dotted curve shows the power in the SH. The right figure shows how the soliton propagation parameter λ changes.

The experiments are seen to agree with the theoretical predictions. The minimum around $\beta = -10$ is global. Note that the angles are expected to be small due to the small initial overlap and correspondingly weak coupling. The overlap is small for all β because the FWHM instead of the power is chosen to be constant. As a curiosity it might be added that in the limit of $\beta \to \infty$ the 1D cubic nonlinear Schrödinger equation is expected to be recovered. Hence the interaction between the solitons should show signs of the integrability of that system, i.e. the escape angle should go to zero. This is obviously not what is observed in Fig. 2.4. To explain this apparent discrepancy it suffices to note that in the limit $\beta \to \infty$ the power goes to infinity as a consequence of the fixed width. This inhibits the system from entering the effective cubic regime.

2.3   Spiraling

As mentioned in the introduction of this chapter, spiraling is the 2D nonplanar interaction case. The situation is somewhat more complicated than in the 1D case or the 2D in-plane case where the potential is effectively one-dimensional. In the 2D nonplanar case the potential is also two-dimensional and in general nonuniform in x_0 and y_0. The transcendental equation (2.9) is the one to be solved in order to find the critical velocities ν_x and ν_y. Notice that the potential

$$U = -\int \left(V^2(x - x_0, y - y_0) W(x + x_0, y + y_0) \cos(2\Delta) \right.$$

$$\left. + 2V(x - x_0, y - y_0) V(x + x_0, y + y_0) W(x - x_0, y - y_0) \cos(\Delta) \right) d\vec{r}_\perp, \ \ (2.12)$$

through $\Delta = 2\nu_x x_0 + 2\nu_y y$ depends on the sign of the transverse velocities. Hence the signs of transverse velocities are still of importance. Notice also that the theory does not distinguish between a given set of velocities (ν_x, ν_y) and the same set with inverted signs, $(-\nu_x, -\nu_y)$. This can be understood by reexamining the effective particle picture discussed above. If both signs are positive, then the particle faces the barrier as illustrated in Fig. 2.2. However, if the signs are inverted, then the particle crosses the bottom of the barrier before it eventually faces the potential barrier. In the 1D soliton interaction picture crossing the bottom of the potential corresponds to the solitons passing through each other, a situation which is not correctly described by the theory. In the 2D nonplanar case, the potential is also two-dimensional and the particle does not necessarily have to cross the bottom of the potential. Hence, correct predictions are a possibility, though no effort to verify this experimentally has been made.

To conclude this section the result of a numerical experiment on spiraling with both angles chosen in the outwards direction is shown in Fig. 2.6. In the figure all parameters but the transverse velocity in the x-direction are kept constant. Evidently raising ν_x from 0.088 in the left plot to 0.089 in the right plot is enough for the solitons to no longer fuse. In angles these numbers correspond to $\alpha \approx 5°$ and $\alpha \approx 5.1°$, respectively. The critical velocity ν_c as calculated from (2.9) is $\nu_c \approx 0.088$.
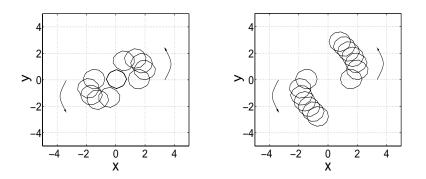
Figure 2.6: Sequences spaced $z = 15$ apart of soliton positions illustrating spiraling. The arrows indicate direction of revolution. The curves are equi-intensity curves of the FW with $I = 3.5$. In the left plot $\nu_x = 0.088$ and in the right plot $\nu_x = 0.089$ (Predicted: $\nu_c \approx 0.088$). The rest of the parameters are the same for both plots: $\beta = 5$, $P \approx 122$, FWHM=1, $x_0 = 1.5$, $y_0 = 0$, and $\nu_y = 0.05$.

References

[1] C. B. Clausen, P. L. Christiansen, and L. Torner, "Perturbative approach to the interaction of solitons in quadratic nonlinear media," Opt. Commun. **136,** 185–192 (1997).

[2] B. Costantini, C. D. Angelis, A. Barthelemy, A. L. Palma, and G. Assanto, "Polarization-multiplexed $\chi^{(2)}$ solitary-wave interactions," Opt. Lett. **22,** 1376–1378 (1997).

[3] A. V. Buryak and V. V. Steblina, "Soliton collisions in bulk quadratic media: comprehensive analytical and numerical study," J. Opt. Soc. Am. B **16,** 245–255 (1999).

[4] C. R. Menyuk, R. Schiek, and L. Torner, "Solitary waves due to $\chi^{(2)} : \chi^{(2)}$ cascading," J. Opt. Soc. Am. B **11,** 2434–2443 (1994).

[5] O. Bang, "Dynamical equations for wave packets in materials with both quadratic and cubic responses," J. Opt. Soc. Am. B **14,** 51–61 (1997).

CHAPTER 3

Two-period QPM media

This chapter is dedicated to soliton engineering with two-period quasi-phase-matching (QPM) in $\chi^{(2)}$ crystals like the one depicted in Fig. 3.1 (for reviews, see [1, 2]). As opposed to one-period QPM the introduction of a second period should make it practically possible to engineer the effective competing nonlinearities. The main con-
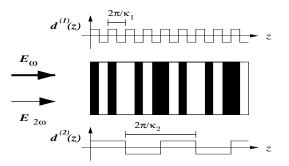

Figure 3.1: Two-period QPM grating.

clusions have already been published in paper 2 and this chapter is meant only to give a brief presentation of the idea of QPM in general and of the averaged equations and nonlinearities for two-period QPM in particular. With a few examples on the soliton properties the theoretical predictions are verified in the end of the chapter.

Though reasonably straight forward, the shear size of the involved expressions makes the actual derivation of the averaged equations and the induced averaged nonlinearities somewhat difficult. Hence this has been put in appendix B.

3.1   Governing equations and basic soliton features

The dimensionless equations governing the propagation of coupled beams in a lossless QPM slab waveguide are [3, 4]

$$i\frac{\partial E_1}{\partial z} + \frac{1}{2}\frac{\partial^2 E_1}{\partial x^2} + d(z)E_1^* E_2 e^{-i\beta z} = 0, \tag{3.1a}$$

$$i\frac{\partial E_2}{\partial z} + \frac{\alpha}{2}\frac{\partial^2 E_2}{\partial x^2} + d(z)E_1^2 e^{i\beta z} = 0, \tag{3.1b}$$

where $E_1 = E_1(x, z)$ is the slowly varying envelope of the fundamental wave (FW) and $E_2 = E_2(x, z)$ the second harmonic (SH). β is the intrinsic wave-vector phase mismatch and the spatial periodic modulation of the nonlinearity is described by the grating function $d(z)$ whose amplitude is normalized to 1, and whose domain length is defined as $\Lambda = \pi/\kappa$, where κ is the real and positive spatial grating frequency, the so-called QPM frequency.

In its basic form QPM aims at counteracting the large wave vector phase mismatch, $\beta \sim 1000$, which is inherent in most quadratic materials and causes poor second harmonic generation efficiency. In more mathematical terms a large β results in fast varying exponentials, $e^{i\beta z}$, in (3.1). These exponentials tend to average out the effect of the nonlinearity. If a grating with the right periodicity is introduced then the mth Fourier component of the grating function *quasi matches* β. This results in an effective mismatch $\epsilon = \beta - m\kappa \approx 1$ and on average the nonlinearity is non-vanishing.

However, on average the grating also induces cubic nonlinearities [5]. The strengths of these induced cubic nonlinearities depend on the QPM frequency and hence offers a way of engineering spatial solitons. The problem with one-period QPM is that the average cubic nonlinearities are very small since they are inversely proportional to $\kappa \sim \beta$. With a grating function characterized by two QPM frequencies, like the one depicted in Fig. 3.1, one could hope to obtain yet another degree of freedom in order to effectively engineer the solitons, i.e. to use one QPM frequency to eliminate the intrinsic phase mismatch and the other to engineer the averaged cubic nonlinearities. The grating function for a two-period grating structure like the one depicted in Fig. 3.1 is characterized by the QPM frequencies κ_1 and κ_2 and can be represented by its Fourier series

$$d(z) = \sum_k d_k^{(1)} \exp(ik\kappa_1 z) \times \sum_l d_l^{(2)} \exp(il\kappa_2 z), \tag{3.2}$$

where the summations are over all integers (k, l) from $-\infty$ to ∞. In (3.2) $d_k^{(1)}$ and $d_l^{(2)}$ are the Fourier components of the primary and the superimposed secondary grating, respectively. For square grating functions only the odd harmonics enters into the expansion, $d_{2l+1} = 2/i\pi(2l+1)$ and $d_{2l} = 0$.

The actual analysis of beam propagation performed here relies heavily on the assumption that the amplitude profiles of the beams are slowly varying. Put in other words, it is assumed that all initial transients have died out and some oscillatory but otherwise stationary state has developed. Only then it makes sense to talk about averaged and/or induced nonlinearities and averaged fields. In case of a one-periodic structure the expansion of the beams in a Fourier series is straight forward since the higher order modes simply are harmonics of the single QPM frequency. In a two-period structure the situation is a bit more subtle since cross-harmonics are expected to arise, i.e. higher order modes at some superposition of both QPM frequencies. However, here it is assumed that such cross-harmonics do not arise or at least that they are negligible. This assumption is justified by the agreement between theoretical predictions and numerical experiments.

The Fourier expansions for the two-period structure become

$$w(x, z) = w_0(x, z) + \sum_{q \neq 0} w_q(x, z)e^{iq\kappa_1 z} + \sum_{q \neq 0} \omega_q(x, z)e^{iq\kappa_2 z}, \qquad (3.3a)$$

$$v(x, z) = v_0(x, z) + \sum_{q \neq 0} v_q(x, z)e^{iq\kappa_1 z} + \sum_{q \neq 0} \nu_q(x, z)e^{iq\kappa_2 z}, \qquad (3.3b)$$
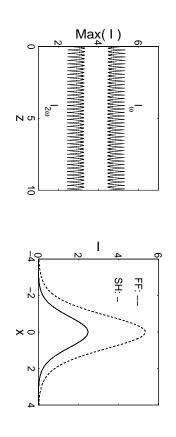
with $w = E_1$ and $v = E_2 e^{-i\epsilon z}$. $\epsilon = \beta - m\kappa_1 - n\kappa_2$ is the new effective phase mismatch where m and n are the QPM orders related to the primary and secondary grating, respectively. The expansions are valid under the additional assumption that the Fourier components are located far apart in order to avoid overlap between the peaks.

In appendix B the equations governing the averaged fields w_0 and v_0 are derived together with the averaged nonlinearities. Their final form is

$$i\frac{\partial w_0}{\partial z} + \frac{1}{2}\frac{\partial^2 w_0}{\partial x^2} + \eta w_0^* v_0 + \gamma(|w_0|^2 - |v_0|^2)w_0 = 0, \qquad (3.4a)$$

$$i\frac{\partial v_0}{\partial z} + \frac{\alpha}{2}\frac{\partial^2 v_0}{\partial x^2} - \epsilon v_0 + \eta w_0^2 - 2\gamma|w_0|^2 v_0 = 0. \qquad (3.4b)$$

Equations (3.4) with the characteristic cubic terms appearing as self-phase and cross-phase modulation of the FW but only cross-phase modulation for the SH are not unique to two-period QPM. They have the same form regardless of the specific type of grating, the parameters merely being given as sums over the Fourier coefficients of the grating [5]-[7].

Figure 3.2: Soliton evolution in real two-period crystal with $(\kappa_1, \kappa_2) = (13, 195)$. The initial condition is for $\eta = -0.3786$, $\gamma = 0.0072$, $\epsilon = 0$, and $\lambda = 0.4$. Left figure shows the evolution of the peak intensities. Right figure shows the intensity profiles of the initial condition.

In case of square grating functions the strengths of the averaged nonlinearities reduces to

$$\eta = -\frac{4}{\pi^2}\left(\frac{1}{mn} - \sum_s \frac{1}{(2s+m)\left(2s\frac{\kappa_1}{\kappa_2}+n\right)}\right),\tag{3.5a}$$

$$\gamma = -\frac{16}{\pi^4}\left(\frac{1}{n\kappa_1}\sum_{q\neq 0,r} \frac{1}{2q(2r+n)\left(2q-2r\frac{\kappa_2}{\kappa_1}+m\right)\left(2q-2r\frac{\kappa_2}{\kappa_1}+m\right)(m+2q)}\right.$$
$$\left.+\frac{1}{m\kappa_2}\sum_{q\neq 0,s} \frac{1}{2q(2s+m)\left(2q-2s\frac{\kappa_1}{\kappa_2}+n\right)(n+2q)}\right).\tag{3.5b}$$

r and s must be chosen such that the terms in the parenthesis of the denominators of (3.5) yield integers. Otherwise the Fourier components of (3.2) are not defined. Still it is reasonably obvious that there is ample room for engineering of the averaged nonlinearities. The main parameters are the QPM frequencies κ_1 and κ_2 with cubic terms inversely proportional to these. However, the sum in (3.5a), which effectively reduces the numerical value of the quadratic nonlinearity, is seen to depend solely on the ratio κ_1/κ_2. Compared to the one-period case this adds new features to the system. With two periods the same quadratic nonlinearity can be realized at large QPM frequencies with effectively no induced averaged cubic nonlinearity or at low QPM frequencies with significant induced averaged cubic nonlinearity. If the ratio between the frequencies is big then the sum in (3.5a) does not contribute. If furthermore one of the frequencies is of the order $\beta \sim 1000$ and the other of the order 1

then by choosing 1st order QPM, i.e. $m = n = 1$, (3.5) reduces to

$$\eta = -\frac{4}{\pi^2}, \qquad \gamma = \frac{4}{\kappa_2 \pi^2} \left(1 - \frac{8}{\pi^2} \right),$$ (3.6)

effectively mimicking the one-period QPM system.

The system (3.4) with competing nonlinearities supports a family of solitons that can be found by substituting $w_0 = u_1 \exp(i\lambda z)$ and $v_0 = u_2 \exp(i\lambda z)$ into (3.4) and solving the resulting boundary value problem with numerical methods. In Fig. 3.2 one example on the evolution of such a soliton is shown. With the two periods chosen to $(\kappa_1, \kappa_2) = (13, 195)$ the nonlinearities must be calculated numerically via (3.5) and thus this is an example of how the ratio between the frequencies come into play.
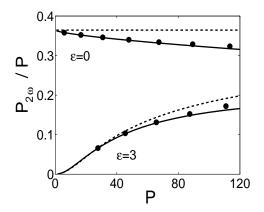

Figure 3.3: Fraction of power in the SH for the two-period QPM system with $(\kappa_1, \kappa_2) = (997, 13)$ as a function of total power. Solid line and •: Theoretical and numerically measured values, respectively. Dashed curves: Zero-order approximation, $\gamma = 0$. The value of ϵ is indicated at each pair of curves.

In Fig. (3.3) a series of simulations is presented to verify the model in the effective one-period limit where the averaged nonlinearities are given by (3.6). Soliton initial conditions are launched in a real two-period structure with κ_1 chosen to be a high prime and κ_2 a small prime. Choosing primes is an effective way of reducing (3.5) to (3.6). The fraction of power in the SH after any initial transient has died out is measured and compared to the theoretically predicted value. Besides verifying the model in the one-period limit, Fig. (3.3) also illustrates an important example of soliton engineering, namely how one via the QPM frequencies can tailor the power sharing between the FW and the SH.

For more details and further examples the reader is refered to paper 2. One important result presented in the paper is the discovery that the averaged cubic nonlinearities

leads to an increase in the bandwidth for soliton generation [8], i.e. the interval of phase mismatches for which soliton generation is broadened at a given input power launched only in the the FW.

References

[1] R. L. Byer, "Quasi-phasematched nonlinear interactions and devices," J. Nonlinear Opt. Phys. **6,** 549–592 (1997).

[2] M. M. Fejer, in *Beam shaping and control with nonlinear optics*, F. Kajzar and R. Reinisch, eds., (Plenum Press, New York, 1998), pp. 375–406.

[3] C. R. Menyuk, R. Schiek, and L. Torner, "Solitary waves due to $\chi^{(2)} : \chi^{(2)}$ cascading," J. Opt. Soc. Am. B **11,** 2434–2443 (1994).

[4] O. Bang, "Dynamical equations for wave packets in materials with both quadratic and cubic responses," J. Opt. Soc. Am. B **14,** 51–61 (1997).

[5] C. B. Clausen, O. Bang, and Y. S. Kivshar, "Spatial solitons and induced Kerr effects in QPM media," Phys. Rev. Lett. **78,** 4749–4752 (1997).

[6] J. F. Corney and O. Bang, "Solitons in quadratic nonlinear photonic crystals," Phys. Rev. E **64,** 047601 (2001).

[7] O. Bang, C. B. Clausen, P. L. Christiansen, and L. Torner, "Engineering competing nonlinearities," Opt. Lett. **24,** 1413–1415 (1999).

[8] L. Torner, J. P. Torres, D. Artigas, D. Mihalache, and D. Mazilu, "Soliton content with quadratic nonlinearities," Opt. Commun. **164,** 153–159 (1999).

Soliton interaction in saturable media

The investigation of interaction in saturable media closely follows the procedure outlined in chapter 2. Hence the theory will be presented with less comments and in less detail. Though the theory is immediately applicable to the 2D interaction case, only media with one transverse direction will be considered here.
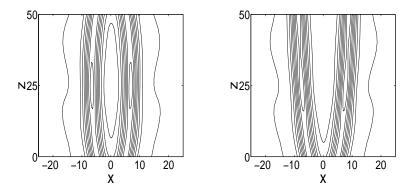

Figure 4.1: Contour plots illustrating interaction in 1D saturable media. Here $\lambda = 0.2 \Rightarrow P \approx 2.7$. In both cases the initial separation is $2x_0 = 10$. In the left plot the solitons are launched with outwards angles $\alpha \approx 10.8°$ and in the right plot they are launched with $\alpha \approx 11.9°$.

In the first section the outwards escape angle is considered. The derivation of the interaction potential can be found in appendix C. It follows the same Lagrangian approach as the derivation of the potential for quadratic media in appendix A. In the second section numerical results on the inwards escape angle are presented. This section should be viewed as an up-to-the-minute account on work in progress.

4.1   The outwards escape angle

The evolution of the envelope $\psi = \psi(x, z)$ in a medium with a saturable nonlinearity is governed by the nonlinear Schrödinger equation

$$i\frac{\partial \psi}{\partial z} + \frac{\partial \psi}{\partial x} + \frac{|\psi|^2}{1 + |\psi|^2}\psi = 0. \tag{4.1}$$

The power, P, and the momentum along the x-axis, M, are conserved quantities.

$$P = \int_{-\infty}^{\infty} |\psi|^2 dx, \qquad M = \frac{i}{2}\int_{-\infty}^{\infty}\left(\psi\frac{\partial \psi^*}{\partial x} - \psi^*\frac{\partial \psi}{\partial x}\right) dx. \tag{4.2}$$

Stable solitons of the form $\psi(x, z) = V(x)\exp(i\lambda z)$ are known to exist for $0 < \lambda < 1$. Solitons moving with transverse velocity ν can be found by the gauge transformation

$$V(x - \nu z; \lambda, \nu) = V(x; \lambda - \frac{1}{4}\nu)e^{-\frac{i}{2}\nu x}. \tag{4.3}$$

In the limit $\lambda \to 0$ the nonlinearity is effectively cubic. Hence it is possible to approximate the solitons with the standard 1D sech-type solitons for the cubic Schrödinger equation. However, the sech-approximation is not very good for $\lambda \to 1$ and since the entire λ-interval is considered here, the exact numerically found solitons are used.

In appendix C the soliton interaction equations for weak interaction in 2D are derived. The 1D version is found by trivial elimination of the y-dimension. By following the same line of arguments as in section 2.1, remembering in particular the assumption of weakly overlapping solitons, the outwards escape angle for the interaction between two identical solitons in a symmetrical setup with no phase difference between them can be found via the transcendental equation

$$\nu^2 P(\lambda) = -U(\lambda, x_0; \nu), \tag{4.4}$$

with the interaction potential U given as

$$U = \int_{-\infty}^{\infty}\left(\ln\frac{g}{(1 + V^2(x - x_0))(1 + V^2(x + x_0))} - \frac{h}{1 + V^2(x + x_0)}\right) dx, \tag{4.5}$$
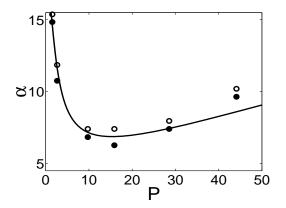
Figure 4.2: Outwards escape angle, α_c, in degrees as a function of the power for 1D interaction in a medium with a saturable nonlinearity. $x_0 = 5$ has been kept constant. A ($\bullet$) is the result of a numerical experiment where the solitons fused, whereas a ($\circ$) is the result of an experiment where they escaped, i.e. continued to move apart.

where

$$g = 1 + V^2(x - x_0) + V^2(x + x_0) + h, \quad h = 2V(x - x_0)V(x + x_0)\cos(\nu x_0). \quad (4.6)$$

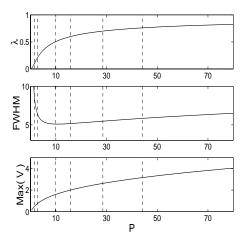In the above x_0 is the initial location of the soliton center on the x-axis.

Figure 4.3: Soliton characteristics for the interacting solitons of Fig. 4.2. The top, middle and bottom graphs show how the soliton parameter, the width, and the peak amplitude, respectively, change with power. The dashed lines indicate the powers of the numerical experiments from Fig. 4.2.

In Fig. 4.2 the analytically found escape curve is plotted as a function of soliton power, $P = P(\lambda)$, and tested against numerical experiments. One of the numerical experiments is shown in Fig. 4.1. The initial separation, $2x_0 = 10$, has been kept constant. At powers $P < 50$ the experimental data matches the analytical predictions very well. At higher powers the agreement is less accurate. The reason for this apparent inaccuracy is a breakdown in the assumptions for high powers. The combination of higher power and an ever increasing soliton width with power, as shown in Fig. 4.3, eventually results in too much power being located in the overlap for the interaction to be considered weak. Note that had the initial separation been kept constant at a higher value, then the graph would have been accurate for higher powers, but at the price of smaller escape angles at low powers. In the other limit, for small λ, the FWHM at some point also becomes bigger than the initial separation leading to an almost complete overlap of the solitons and a breakdown in the model assumptions. The parameter settings chosen here is a compromise focusing on verifying the theory, i.e. the interaction potential (4.5), for relatively big angles.

4.2   The inwards escape angle: head-on collisions

Fig. 4.4 shows data for the inwards escape angle (see Fig. 2.1) in a 1D saturable medium. The three graphs are for three different values of the soliton parameter λ and they show the power content, C_{win}, in the window $x \in [-15; 15]$ at a distance of 5 times the initial collision point. C_{win} is defined as the remaining power within a given window divided with the total launched power. The choice of measuring C_{win} at 5 times the initial collision point is made to ensure consistency in the numerical experiments, the number 5 being somewhat arbitrarily chosen.

For two solitons launched with initial separation $2x_0 = 40$ and initial transverse velocity $\nu = 0.1 \Rightarrow \alpha \approx 5.7°$ the initial collision point is at $z = 200$ and the measurement of C_{win} takes place at $z = 1000$. All simulations have been performed by applying the standard split-step method with a step-size of $\Delta z = 10^{-3}$. Since some radiation is expected it is important to simulate in a sufficiently large x-interval. Here this interval has been chosen to $x \in [-409.6; 409.6]$ with 8192 points of discretization.

Fig. 4.4 reflects the complexity of the saturable system. In the limit where $\lambda \to 0$ the system effectively mimics the cubic nonlinear Schrödinger equation and the interaction between solitons is expected to show signs of the integrability of that system, i.e. they should pass through each other unaffected. However, in the previous section, it was shown that the theory predicts an attractive force between the solitons for all $\lambda \neq 0$. Combining the integrability with an attractive force leads to the behavior illustrated in Fig. 4.5 for small applied angles. The solitons initially pass

Figure 4.4: Relative power content, C_{win}, in the window $x \in [-15; 15]$ at a distance of 5 times the initial collision point as a function of inwards angle of incidence and for different soliton parameters (λ is indicated on each graph.). The discrete points are the outcome of experiments whereas the full curves in between the points only serve to help the eye.

Figure 4.5: Contour plots illustrating what happens for low values of the applied angle (here $\alpha \approx 5.7°$). $\lambda = 0.5 \Rightarrow P \approx 9.4$.

through each other, but because of the attraction they eventually turn around and collide again. This process repeats itself over and over. Eventually the solitons fuse because of the radiation shed during the multiple collisions. The propagation distance

between two consecutive collisions gets smaller for $\lambda \to 1$ and for $\alpha \to 0°$. The behavior described here accounts for the numerical results for small angles in Fig. 4.4. Here most of the power is still in the window of measurement, i.e. $C_{win} \sim 1$.
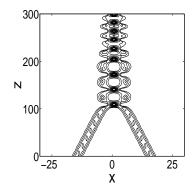
At some angle of incidence the attractive force is no longer strong enough to make the solitons turn around and hence they continue to move apart. This is illustrated in Fig. 4.6(a) and holds for all λ. Power is shed as radiation when the angle of incidence
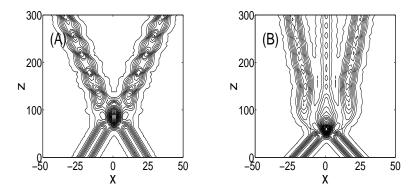

Figure 4.6: Contour plots illustrating what happens for values of the angle of incidence being big enough to counteract the attractive force (A: $\alpha \approx 11.3°$. B: $\alpha \approx 16.7°$). $\lambda = 0.95 \Rightarrow P \approx 746$.

is raised even further. When the power shedding is strong enough, a new stable state is formed between the two original solitons. This is illustrated in Fig. 4.6(b). Notice that after the collision the two original solitons move apart slower than the solitons from Fig. 4.6(a) even though they were launched with a higher angle of incidence. The amount of power in the new state depends on the amount of power shed as radiation during the collision. This in turn depends on the angle of incidence and on the soliton parameter, i.e. how close the system is to the integrable limit. In this way the part of Fig. 4.4 from $\alpha \sim 15°$ can be explained. For $\lambda = 0.95$ the system is far from the integrable limit and a lot of radiation is shed during collision which is the reason for the relatively strong formation of new states observed in the figure. For $\lambda = 0.5$ the system is still far from the integrable limit, but already much less radiation is shed during the collisions resulting in lower C_{win} than observed for $\lambda = 0.95$. For $\lambda = 0.2$ the system is close to the integrable limit and almost no radiation is shed during the collision.

When the angle is raised beyond a certain point, C_{win} is seen to diminish again. This could be a consequence of less interaction time, i.e. the solitons pass through each other so fast that they have little time to affect each other.

One curious feature of the graphs in Fig. 4.4 is not easily explained. For $\lambda = 0.95$ and for $\lambda = 0.5$ the spikes after the initial drop in C_{win} are unexpected. The immediate

explanation would be that C_{win} is measured in between oscillations of the type shown in Fig. 4.5. However, this is not so. This can be seen for example from the simulation in Fig. 4.6(a). This simulation is located in the $C_{win} \sim 0$ region between the initial drop and the two spikes for $\lambda = 0.95$ in Fig. 4.4, but it clearly shows no sign of the two solitons turning around and colliding again. Hence the explanation must be looked for elsewhere. In particular it must be ruled out that the numerics in some way can provoke the spikes. This remains to be investigated.

CHAPTER 5

Epilogue

Besides being a requirement, a dissertation is also the natural place to conclude
and summarize on the work performed during the years spent in pursuit of the
Ph.D. degree. The work presented here has evolved around two distinct areas of
quadratic (or $\chi^{(2)}$) nonlinear optics: soliton interaction and soliton engineering with
quasi-phase-matching (QPM) gratings. The direct applicational motivation behind
any research undertaken in either of these areas is the wish to construct all-optical
switching devices to be implemented in optical circuitry.

Exploiting optical nonlinearities for switching devices is interesting mainly because
of the fast response. The $\chi^{(2)}$ nonlinearity arises through mutual interaction of two
beams rather than through a refractive index change which is the case for the tradi-
tional cubic (or $\chi^{(3)}$) nonlinearity. The $\chi^{(2)}$ nonlinearity holds several advantages over
the $\chi^{(3)}$ nonlinearity. The response of the $\chi^{(2)}$ nonlinearity can be made stronger than
that of the $\chi^{(3)}$ nonlinearity and the propagation of two-dimensional bright spatial
$\chi^{(2)}$ solitons is stable which is not the case for two-dimensional spatial $\chi^{(3)}$ solitons.
Another desired feature is the non-integrability of the $\chi^{(2)}$ system in the sense that it
is not possible to find an inverse scattering transform. This leads to inelastic interac-
tion between the beams with a rich spectrum of possible outcomes of the collisions.

Spatial soliton collisions have been analyzed earlier via variational approaches. All
of these earlier works dealt with solitons assumed to be parallelly launched and
as such they could only give qualitative predictions of the outcome of a collision.

One of the main achievements presented here is the incorporation of launch angles into the model. For identical solitons the variational approach leads to the classical mechanical problem of a single particle moving in a potential. In this picture the angle of incidence between two colliding solitons is merely the velocity of the particle whereas the potential reflects the forces acting between the solitons. In the simplest case the escape angle is found by determining the corresponding particle velocity for which the total energy in the effective particle picture is zero. *Thus it has been possible for the first time to predict quantitatively the outcome of the interaction between two solitons, i.e. to put a numerical value on the escape angle below which solitons will fuse and above which they will move apart.*

The generality of the method used to describe soliton interaction is emphasized by the fact that it has been able to correctly predict the escape angles for all the cases where it has been employed during this work, i.e. both in one and two-dimensional $\chi^{(2)}$ media and in one-dimensional saturable media. However, the theory generally fails to predict the outcome in the special case of head-on collisions between two solitons. This is not surprising since the model assumption of weakly interacting solitons is severely violated when the solitons pass through each other. What is more surprising is that it actually predicts the correct results for certain cases. *It has been possible to establish a very simple expression based on a Gaussian approximation in the perfect phase matching case in one-dimensional $\chi^{(2)}$ media relating soliton power with escape angle, i.e. the angle below which solitons will fuse and above which they will pass through each other.* The fact that this result has been obtained leaves hope that it could be possible to predict the correct results in the general head-on collision case. One way to go about it would be to include higher order terms in the perturbation theory.

Regarding the research performed on soliton engineering with QPM *the main result has been the derivation of an averaged model describing soliton propagation in two-period QPM structures.* Traditionally QPM has been employed to reduce the huge intrinsic phase mismatch and more recently also to engineer the solitons. However, with one-period QPM it is difficult to achieve both a reduction of the phase mismatch and effective engineering. Hence additional techniques like phase matching via temperature tuning are normally required. Soliton engineering is not just an academic issue. It is of paramount importance whenever light with a certain intensity profile crosses from one medium to another, i.e. from a fiber to a switching crystal. If the soliton generation process in the crystal reshapes the profile too much, power and hence information is lost as radiation. It is a fundamental issue to be able to produce and operate such components as simply as possible. *With two-period QPM both reduction of the phase mismatch and effective engineering can be achieved at room temperature without employing other techniques.*

Two-period QPM introduces new means of manipulating the induced $\chi^{(2)}$ and $\chi^{(3)}$ nonlinearities which on average control beam propagation in the crystal. In one-

period QPM the strength of the induced $\chi^{(3)}$ nonlinearity is determined solely by the size of the domain length, the shorter the domain length the weaker the nonlinearity. With two periods it is necessary to take into account also the ratio between the two periods, the lower the ratio the higher the strength of the $\chi^{(3)}$ nonlinearity. *In two-period QPM also the induced $\chi^{(2)}$ nonlinearity depends on this ratio and hence, in principle, engineering of this nonlinearity is possible.*

Another more fundamental discovery made during the QPM part of this work is the fact that $\chi^{(3)}$ *nonlinearities in general enhances the soliton generation bandwidth, i.e. the range of wavelength dependent effective phase mismatches where solitons can be generated* when a given beam profile, here sech-type, is launched in the crystal. For a given power the generation process depends critically on the phase mismatch and generation is only achieved within a narrow band stretching from perfect phase matching and not far into the positive region. In a physical setup this would correspond to a narrow interval of wavelengths which potentially imposes severe constraints on the other network components. With this in mind it is easy to understand why broadening of this bandwidth is highly desired. Introducing $\chi^{(3)}$ nonlinearities via QPM into the system has been shown to do just that and *examples with practically realistic parameter settings illustrate how the bandwidth can be almost doubled.*

Even though the field of quadratic nonlinear optics has been heavily investigated in recent years there is still plenty of discoveries to be made and much research to be performed. This is in particular the case on the level of fine tuning the field to practical purposes but also on the level of fundamental physics. With regards to soliton engineering with QPM it is safe to say that only the top of the iceberg has been revealed and that many potentially very interesting grating structures still remain to be discovered. It is the hope of the author of this thesis that others may gain inspiration through the work presented here and that it may assist in achieving the ultimate goal: cost efficient and manageable all-optical signal processing in nonlinear materials.

Appendix A

Interaction equations for combined $\chi^{(2)}$ and $\chi^{(3)}$ media

In this appendix the general set of soliton interaction equations, i.e. the general analytical model describing nonplanar interaction between two solitons, will be derived. The underlying assumption is that the functional forms of the non-interacting soliton profiles are retained during interaction. The changes in the shape due to the interaction come about as a result of slowly varying soliton parameters.

The propagation of two coupled beams in a medium exhibiting both a $\chi^{(2)}$ and a $\chi^{(3)}$ response is governed by the two coupled dimensionless differential equations

$$i\frac{\partial A_1}{\partial z} + \frac{1}{2}\nabla_\perp^2 A_1 + \eta A_1^* A_2 + \gamma\left(\zeta_1|A_1|^2 + \frac{\rho}{2}|A_2|^2\right)A_1 = 0, \qquad (A.1a)$$

$$i\frac{\partial A_2}{\partial z} + \frac{1}{4}\nabla_\perp^2 A_2 - \beta A_2 + \eta A_1^2 + \gamma\left(\zeta_2|A_2|^2 + \rho|A_1|^2\right)A_2 = 0, \qquad (A.1b)$$

where $A_1 = A_1(x,y,z)$ is the fundamental wave (FW) and $A_2 = A_2(x,y,z)$ is the second harmonic (SH). Equations (A.1) are the Euler-Lagrange equations of the Lagrangian density

$$\mathcal{L} = i\left(A_1\frac{\partial A_1^*}{\partial z} - A_1^*\frac{\partial A_1}{\partial z}\right) + \frac{i}{2}\left(A_2\frac{\partial A_2^*}{\partial z} - A_2^*\frac{\partial A_2}{\partial z}\right) + \nabla_\perp A_1\cdot\nabla_\perp A_1^* + \frac{1}{4}\nabla_\perp A_2\cdot\nabla_\perp A_2^*$$

$$+\beta|A_2|^2 - \eta\left(A_1^{*2}A_2 + A_1^2 A_2^*\right) - \gamma\left(\zeta_1|A_1|^4 + \frac{\zeta_2}{2}|A_2|^4 + \rho|A_1|^2|A_2|^2\right). \qquad (A.2)$$

For intrinsic $\chi^{(3)}$ normally $\eta = 1$ whereas γ determines the strength of the cubic nonlinearity as compared to the quadratic and $\eta = 1$, $\zeta_1 = \frac{1}{2}$, $\zeta_2 = 1$, and $\rho = 2$. For QPM-induced $\chi^{(3)}$ terms $\zeta_2 = 0$ whereas the rest of the coefficients are determined by the specific QPM grating function. The system is known to conserve the power $P = \int (|A_1|^2 + |A_2|^2) d\vec{r}_\perp$ and the momentum $\vec{M} = \int \mathrm{Im}(A_1^* \nabla_\perp A_1 + A_2^* \nabla_\perp A_2) d\vec{r}_\perp$, where $\int d\vec{r}_\perp \equiv \int \int_{-\infty}^{\infty} dx dy$.

Substitution of a superposition of two overlapping localized fields,

$$A_1 = A_1^{(1)}(x - x^{(1)}, y - y^{(1)}, z) + A_1^{(2)}(x - x^{(1)}, y - y^{(1)}, z), \qquad \text{(A.3a)}$$

$$A_2 = A_2^{(1)}(x - x^{(2)}, y - y^{(2)}, z) + A_2^{(2)}(x - x^{(2)}, y - y^{(2)}, z), \qquad \text{(A.3b)}$$

where $x^{(j)}$ and $y^{(j)}$ is the field off-set in the transverse plane, into the Lagrangian density (A.2) yields

$$\mathcal{L} = \mathcal{L}^{(1)} + \mathcal{L}^{(2)} + \mathcal{L}_c + \mathcal{L}_c^*, \qquad \text{(A.4)}$$

where $\mathcal{L}^{(1)}$ and $\mathcal{L}^{(2)}$ are the no-interaction Lagrangian densities, i.e. (A.2) with $A_{1,2}$ replaced by $A_{1,2}^{(1)}$ or $A_{1,2}^{(2)}$. The coupling Lagrangian, $\mathcal{L}_c$, is given by

$$
\begin{aligned}
\mathcal{L}_c = {} & i \left(A_1^{(1)} \frac{\partial A_1^{*(2)}}{\partial z} - \frac{\partial A_1^{(1)}}{\partial z} A_1^{*(2)} \right) + \frac{i}{2} \left(A_2^{(1)} \frac{\partial A_2^{*(2)}}{\partial z} - \frac{\partial A_2^{(1)}}{\partial z} A_2^{*(2)} \right) \\
& + \nabla_\perp A_1^{(1)} \cdot \nabla_\perp A_1^{*(2)} + \frac{1}{4} \nabla_\perp A_2^{(1)} \cdot \nabla_\perp A_2^{*(2)} + \beta \left(A_2^{*(1)} A_2^{(2)} + A_2^{(1)} A_2^{*(2)} \right) \\
& - \eta \left[A_1^{(1)^2} A_2^{*(2)} + A_1^{(2)^2} A_2^{*(1)} + 2 \left(A_1^{(1)} A_1^{(2)} \left(A_2^{*(1)} + A_2^{*(2)} \right) \right) \right] \\
& - \gamma \left[\zeta_1 \left(A_1^{(1)^2} A_1^{*(2)^2} + 2|A_1^{(1)}|^2 |A_1^{(2)}|^2 + 2 A_1^{(1)} A_1^{*(2)} \left(|A_1^{(1)}|^2 + |A_1^{(2)}|^2 \right) \right) \right. \\
& \qquad + \frac{\zeta_2}{2} \left(A_2^{(1)^2} A_2^{*(2)^2} + 2|A_2^{(1)}|^2 |A_2^{(2)}|^2 + 2 A_2^{(1)} A_2^{*(2)} \left(|A_2^{(1)}|^2 + |A_2^{(2)}|^2 \right) \right) \\
& \qquad + \rho \left(\frac{1}{2} |A_1^{(1)}|^2 |A_2^{(2)}|^2 + \frac{1}{2} |A_1^{(2)}|^2 |A_2^{(1)}|^2 + A_2^{(1)} A_2^{*(2)} \left(|A_1^{(1)}|^2 + |A_1^{(2)}|^2 \right) \right. \\
& \qquad \qquad \left. \left. + A_1^{(1)} A_1^{*(2)} \left(A_2^{(1)} A_2^{*(2)} + A_2^{*(1)} A_2^{(2)} + |A_2^{(1)}|^2 + |A_2^{(2)}|^2 \right) \right) \right]. \qquad \text{(A.5)}
\end{aligned}
$$

From (A.4) a set of eight coupled differential equations can be derived, one for each of the four field components and one for each of their conjugates. The set constitutes

the new governing equations. The equations for the FW $A_1^{(1)}$ and its SH $A_2^{(1)}$ are

$$
i\frac{\partial A_1^{(1)}}{\partial z} + \frac{1}{2}\nabla_\perp^2 A_1^{(1)} + \eta A_1^{*(1)} A_2^{(1)} + \gamma\left(\zeta_1|A_1^{(1)}|^2 + \frac{\rho}{2}|A_2^{(1)}|^2\right)A_1^{(1)}
$$

$$
+\left[i\frac{\partial A_1^{(2)}}{\partial z} + \frac{1}{2}\nabla_\perp^2 A_1^{(2)} + \eta A_1^{*(2)} A_2^{(2)} + \gamma\left(\zeta_1|A_1^{(2)}|^2 + \frac{\rho}{2}|A_2^{(2)}|^2\right)A_1^{(2)}\right]
$$

$$
+\eta\left[A_1^{*(1)} A_2^{(2)} + A_2^{(1)} A_1^{*(2)}\right]
$$

$$
+\gamma\zeta_1\left[A_1^{*(1)} A_1^{(2)2} + A_1^{(1)2} A_1^{*(2)} + 2A_1^{(1)}|A_1^{(2)}|^2 + 2|A_1^{(1)}|^2 A_1^{(2)}\right] \qquad \text{(A.6a)}
$$

$$
+\gamma\frac{\rho}{2}\left[A_1^{(1)}|A_2^{(2)}|^2 + A_1^{(2)}|A_2^{(1)}|^2 + \left(A_1^{(1)} + A_1^{(2)}\right)\left(A_2^{(1)} A_2^{*(2)} + A_2^{*(1)} A_2^{(2)}\right)\right] = 0,
$$

$$
i\frac{\partial A_2^{(1)}}{\partial z} + \frac{1}{4}\nabla_\perp^2 A_2^{(1)} - \beta A_2^{(1)} + \eta A_1^{(1)2} + \gamma\left(\zeta_2|A_2^{(1)}|^2 + \rho|A_1^{(1)}|^2\right)A_2^{(1)}
$$

$$
+\left[i\frac{\partial A_2^{(2)}}{\partial z} + \frac{1}{4}\nabla_\perp^2 A_2^{(2)} - \beta A_2^{(2)} + \eta A_1^{(2)2} + \gamma\left(\zeta_2|A_2^{(2)}|^2 + \rho|A_1^{(2)}|^2\right)A_2^{(2)}\right]
$$

$$
+2\eta A_1^{(1)} A_1^{(2)}
$$

$$
+\gamma\zeta_2\left[A_2^{*(1)} A_2^{(2)2} + A_2^{(1)2} A_2^{*(2)} + 2A_2^{(1)}|A_2^{(2)}|^2 + 2A_2^{(2)}|A_2^{(1)}|^2\right] \qquad \text{(A.6b)}
$$

$$
+\gamma\rho\left[|A_1^{(2)}|^2 A_2^{(1)} + |A_1^{(1)}|^2 A_2^{(2)} + \left(A_1^{(1)} A_1^{*(2)} + A_1^{*(1)} A_1^{(2)}\right)\left(A_2^{(1)} + A_2^{(2)}\right)\right] = 0.
$$

Because of symmetry the equations for $A_1^{(2)}$ and $A_2^{(2)}$ are thus far exactly the same. It is emphasised that up until now no assumptions have been made and equations (A.6) are exact.

The system (A.1) is known to have symmetric bright soliton solutions of the form $A_1(x,y,z) = V(x,y;\lambda)\exp(i\lambda z)$ and $A_2(x,y,z) = W(x,y;\lambda)\exp(i2\lambda z)$. λ is the soliton propagation parameter taking on different values depending on the type of medium, i.e. on the parameters η, γ, ζ_1, ζ_2, and ρ. Furthermore a gauge transformation can be applied and soliton profiles V and W moving with transverse velocities ν_x and ν_y can be found. The general three parameter soliton profiles are given by

$$
V\left(x - \nu_x z, y - \nu_y z; \lambda, \nu_x, \nu_y\right) = V(x,y; \lambda - \frac{1}{2}\nu_x - \frac{1}{2}\nu_y)e^{-i(\nu_x x + \nu_y y)}, \qquad \text{(A.7a)}
$$

$$
W\left(x - \nu_x z, y - \nu_y z; \lambda, \nu_x, \nu_y\right) = W(x,y; \lambda - \frac{1}{2}\nu_x - \frac{1}{2}\nu_y)e^{-i2(\nu_x x + \nu_y y)}. \qquad \text{(A.7b)}
$$

With this in mind the interaction between solitons is now assumed weak and hence all the interaction terms in the expressions above are assumed to be small compared to the terms with components from $A_n^{(1)}$ or $A_n^{(2)}$ only. Under this assumption it is reasonable to expect that the functional forms of the solitons (A.7) are left unchanged, i.e. that the changes are adiabatic and solely due to slowly varying soliton parameters.

In terms of perturbation theory the parameters depend on a slow propagation variable $Z = \epsilon z$, where ϵ is a small parameter, and they can be expressed as

$$x^{(j)}(z) = \int_0^z \nu_x^{(j)}(Z')\mathrm{d}Z' + x_0^{(j)} \quad \Rightarrow \quad \frac{\partial x^{(j)}(z)}{\partial z} = \nu_x^{(j)}(Z), \qquad (\text{A.8a})$$

$$y^{(j)}(z) = \int_0^z \nu_y^{(j)}(Z')\mathrm{d}Z' + y_0^{(j)} \quad \Rightarrow \quad \frac{\partial y^{(j)}(z)}{\partial z} = \nu_y^{(j)}(Z), \qquad (\text{A.8b})$$

$$\phi^{(j)}(z) = \int_0^z \lambda^{(j)}(Z')\mathrm{d}Z' + \phi_0^{(j)} \quad \Rightarrow \quad \frac{\partial \phi^{(j)}(z)}{\partial z} = \lambda^{(j)}(Z), \qquad (\text{A.8c})$$

where $x^{(j)}$ and $y^{(j)}$ give the soliton center positions in the transverse plane, and $\phi^{(j)}$ is the accumulated phase of the soliton. Subscript 0 denotes initial values. Substituting solitons on the form

$$A_1^{(j)}(x,y,z) = V^{(j)}(x - x^{(j)}, y - y^{(j)})e^{i\phi^{(j)}}, \qquad (\text{A.9a})$$

$$A_2^{(j)}(x,y,z) = W^{(j)}(x - x^{(j)}, y - y^{(j)})e^{i2\phi^{(j)}}, \qquad (\text{A.9b})$$

into (A.6) yields

$$\frac{1}{2}\nabla_\perp^2 V^{(1)} - i\nu_x^{(1)}\frac{\partial V^{(1)}}{\partial x} - i\nu_y^{(1)}\frac{\partial V^{(1)}}{\partial y} - \lambda^{(1)}V^{(1)}$$

$$+\eta V^{*(1)}W^{(1)} + \gamma\left(\zeta_1|V^{(1)}|^2 + \frac{\rho}{2}|W^{(1)}|^2\right)V^{(1)} =$$

$$-\epsilon\left(i\frac{\partial V^{(1)}}{\partial Z} - \frac{\partial \phi^{(1)}}{\partial Z}V^{(1)}\right) - \eta\left[V^{*(1)}W^{(2)} + W^{(1)}V^{*(2)}\right]e^{2i\phi}$$

$$-\gamma\left(2\zeta_1|V^{(2)}|^2 + \frac{\rho}{2}|W^{(2)}|^2\right)V^{(1)}$$

$$-\gamma\zeta_1\left[V^{*(1)}V^{(2)^2}e^{2i\phi} + V^{(1)^2}V^{*(2)}e^{-i\phi} + 2|V^{(1)}|^2V^{(2)}e^{i\phi}\right] \qquad (\text{A.10a})$$

$$-\gamma\frac{\rho}{2}\left[V^{(2)}|W^{(1)}|^2e^{i\phi} + \left(V^{(1)} + V^{(2)e^{i\phi}}\right)\left(W^{(1)}W^{*(2)}e^{-2i\phi} + W^{*(1)}W^{(2)}e^{2i\phi}\right)\right],$$

$$\frac{1}{4}\nabla_\perp^2 W^{(1)} - i\nu_x^{(1)}\frac{\partial W^{(1)}}{\partial x} - i\nu_y^{(1)}\frac{\partial W^{(1)}}{\partial y} - \left(2\lambda^{(1)} + \beta\right)W^{(1)}$$

$$+\eta V^{(1)^2} + \gamma\left(\zeta_2|W^{(1)}|^2 + \rho|V^{(1)}|^2\right)W^{(1)} =$$

$$-\epsilon\left(i\frac{\partial W^{(1)}}{\partial Z} - 2\frac{\partial \phi^{(1)}}{\partial Z}W^{(1)}\right) - 2\eta V^{(1)}V^{(2)}e^{i\phi}$$

$$-\gamma\left(2\zeta_2|W^{(2)}|^2 + \rho|V^{(2)}|^2\right)W^{(1)}$$

$$-\gamma\zeta_2\left[W^{*(1)}W^{(2)^2}e^{-4i\phi} + W^{(1)^2}W^{*(2)}e^{-2i\phi} + 2W^{(2)}|W^{(1)}|^2e^{2i\phi}\right] \qquad (\text{A.10b})$$

$$-\gamma\rho\left[|V^{(1)}|^2W^{(2)}e^{2i\phi} + \left(V^{(1)}V^{*(2)}e^{-i\phi} + V^{*(1)}V^{(2)}e^{i\phi}\right)\left(W^{(1)} + W^{(2)}e^{2i\phi}\right)\right].$$

In (A.10) $\phi = \phi^{(2)} - \phi^{(1)}$ is the phase difference between the solitons. Note that a part of the $\chi^{(3)}$ interaction terms is independent of the phase difference and that the ϵ terms stem from $\partial/\partial z = \partial/\partial z + \epsilon\partial/\partial Z$. In (A.10) the terms from (A.6) with only $A_n^{(2)}$ field components, i.e. the terms in the square brackets of equations (A.6), have been excluded. This is done in advance, knowing that their contribution to first order will be trivially zero.

Next $V^{(j)}$ and $W^{(j)}$ are expanded into asymptotic series according to

$$V^{(j)}(x,y,z) = V_0^{(j)}(x - x^{(j)}, y - y^{(j)}) + \sum_{n=1}^{\infty} \epsilon^n V_n^{(j)}(x,y,z), \qquad \text{(A.11a)}$$

$$W^{(j)}(x,y,z) = W_0^{(j)}(x - x^{(j)}, y - y^{(j)}) + \sum_{n=1}^{\infty} \epsilon^n W_n^{(j)}(x,y,z). \quad \text{(A.11b)}$$

All interaction terms are then assumed to be higher order terms and from (A.10) it is then obvious that to the zeroth order only the left-hand sides of (A.10a) and (A.10b) contribute and that the resulting equations are simply the no-interaction equations from which the solitons are determined. Collecting terms to the first order yields

$$
\begin{aligned}
&\frac{1}{2}\nabla_\perp^2 V_1^{(1)} - i\nu_x^{(1)}\frac{\partial V_1^{(1)}}{\partial x} - i\nu_y^{(1)}\frac{\partial V_1^{(1)}}{\partial y} - \lambda^{(1)} V_1^{(1)} \\
&\qquad + \eta\left(V_0^{*(1)}W_1^{(1)} + V_1^{*(1)}W_0^{(1)}\right) + \gamma\left(2\zeta_1|V_0^{(1)}|^2 + \frac{\rho}{2}|W_0^{(1)}|^2\right)V_1^{(1)} \\
&\qquad\quad + \gamma\left(\zeta_1 V_0^{(1)} V_1^{*(1)} + \frac{\rho}{2}\left(W_0^{(1)}W_1^{*(1)} + W_0^{*(1)}W_1^{(1)}\right)\right)V_0^{(1)} = \\
&-\epsilon\left(i\frac{\partial V_0^{(1)}}{\partial Z} - \frac{\partial\phi^{(1)}}{\partial Z}V_0^{(1)}\right) - \eta\left[V_0^{*(1)}W_0^{(2)}e^{2i\phi} + W_0^{(1)}V_0^{*(2)e^{-i\phi}}\right] \\
&-\gamma\left(2\zeta_1|V_0^{(2)}|^2 + \frac{\rho}{2}|W_0^{(2)}|^2\right)V_0^{(1)} \\
&-\gamma\zeta_1\left[V_0^{*(1)}V_0^{(2)\,2}e^{2i\phi} + V_0^{(1)\,2}V_0^{*(2)}e^{-i\phi} + 2|V_0^{(1)}|^2 V_0^{(2)}e^{i\phi}\right] \qquad\qquad \text{(A.12)} \\
&-\gamma\frac{\rho}{2}\left[V_0^{(2)}|W_0^{(1)}|^2 e^{i\phi} + \left(V_0^{(1)} + V_0^{(2)e^{i\phi}}\right)\left(W_0^{(1)}W_0^{*(2)}e^{-2i\phi} + W_0^{*(1)}W_0^{(2)}e^{2i\phi}\right)\right],
\end{aligned}
$$

and

$$
\begin{aligned}
\frac{1}{4}\nabla_\perp^2 W_1^{(1)} &- i\nu_x^{(1)}\frac{\partial W_1^{(1)}}{\partial x} - i\nu_y^{(1)}\frac{\partial W_1^{(1)}}{\partial y} - \left(2\lambda^{(1)} + \beta\right)W_1^{(1)} \\
&+ 2\eta V_0^{(1)}V_1^{(1)} + \gamma\left(2\zeta_2|W_0^{(1)}|^2 + \rho|V_0^{(1)}|^2\right)W_1^{(1)} \\
&\quad + \gamma\left(\zeta_2 W_0^{(1)}W_1^{*(1)} + \rho\left(V_0^{(1)}V_1^{*(1)} + V_0^{*(1)}V_1^{(1)}\right)\right)W_0^{(1)} = \\
-\epsilon&\left(i\frac{\partial W_0^{(1)}}{\partial Z} - 2\frac{\partial\phi^{(1)}}{\partial Z}W_0^{(1)}\right) - 2\eta V_0^{(1)}V_0^{(2)}e^{i\phi} \\
-\gamma&\left(2\zeta_2|W_0^{(2)}|^2 + \rho|V_0^{(2)}|^2\right)W_0^{(1)} \\
-\gamma\zeta_2&\left[W_0^{*(1)}W_0^{(2)^2}e^{-4i\phi} + W_0^{(1)^2}W_0^{*(2)}e^{-2i\phi} + 2W_0^{(2)}|W_0^{(1)}|^2e^{2i\phi}\right] \\
-\gamma\rho&\left[|V_0^{(1)}|^2 W_0^{(2)}e^{2i\phi} + \left(V_0^{(1)}V_0^{*(2)}e^{-i\phi} + V_0^{*(1)}V_0^{(2)}e^{i\phi}\right)\left(W_0^{(1)} + W_0^{(2)}e^{2i\phi}\right)\right].
\end{aligned}
\tag{A.13}
$$

The full system of equations describing the first order correction to soliton 1 due to the interaction with soliton 2 is given by (A.12-A.13) and their conjugates. By rotating the superscripts, i.e. $(1) \leftrightarrow (2)$, the system to solve in order to find the correction to soliton 2 due to interaction with soliton 1 is immediately recovered. Solving these equations for $W_1^{(j)}$ and $V_1^{(j)}$ would be a non-trivial task to perform. However, one way of continuing is to apply Fredholms alternative and find solvability conditions for solutions to exist. It is from these conditions that the final set of interaction equations will be derived.

If the matrix operator $\hat{K}$ is given by

$$
\hat{K} = \left[\begin{array}{cccc}
A1 & A2 & A3 & A4 \\
B1 & B2 & B3 & B4 \\
A3^* & A4^* & A1^* & A2^* \\
B3^* & B4^* & B1^* & B2^*
\end{array}\right],
\tag{A.14}
$$

where

$$
A1 = \frac{1}{2}\nabla_\perp^2 - i\nu_x^{(1)}\frac{\partial}{\partial x} - i\nu_y^{(1)}\frac{\partial}{\partial y} - \lambda^{(1)} + \gamma\left(2\zeta_1|V_0^{(1)}|^2 + \frac{\rho}{2}|W_0^{(1)}|^2\right),
\tag{A.15a}
$$

$$
A2 = \eta V_0^{*(1)} + \gamma\frac{\rho}{2}V_0^{(1)}W_0^{*(1)},
\tag{A.15b}
$$

$$
A3 = \eta W_0^{(1)} + \gamma\zeta_1 V_0^{(1)^2},
\tag{A.15c}
$$

$$
A4 = \gamma\frac{\rho}{2}V_0^{(1)}W_0^{(1)},
\tag{A.15d}
$$

and

$$B1 = \eta V_0^{(1)} + \gamma \frac{\rho}{2} V_0^{*(1)} W_0^{(1)}, \tag{A.16a}$$

$$B2 = \frac{1}{8}\nabla_\perp^2 - \frac{i}{2}\nu_x^{(1)}\frac{\partial}{\partial x} - \frac{i}{2}\nu_y^{(1)}\frac{\partial}{\partial y} - \left(\lambda^{(1)} + \frac{\beta}{2}\right) + \gamma\left(\zeta_2|W_0^{(1)}|^2 + \frac{\rho}{2}|V_0^{(1)}|^2\right), \tag{A.16b}$$

$$B3 = \gamma \frac{\rho}{2} V_0^{(1)} W_0^{(1)}, \tag{A.16c}$$

$$B4 = \gamma \frac{\zeta_2}{2} W_0^{(1)^2}, \tag{A.16d}$$

then the full system for soliton 1 can be put on matrix form

$$\hat{K}\begin{bmatrix} V_1^{(1)} \\ W_1^{(1)} \\ V_1^{*(1)} \\ W_1^{*(1)} \end{bmatrix} = i\frac{\partial}{\partial Z}\begin{bmatrix} -V_0^{(1)} \\ -\frac{1}{2}W_0^{(1)} \\ V_0^{*(1)} \\ \frac{1}{2}W_0^{*(1)} \end{bmatrix} + \begin{bmatrix} V_0^{(1)} \\ W_0^{(1)} \\ V_0^{*(1)} \\ W_0^{*(1)} \end{bmatrix}\frac{\partial \phi^{(1)}}{\partial Z}$$

$$-\eta\begin{bmatrix} V_0^{*(1)}W_0^{(2)}e^{i2\phi} + W_0^{(1)}V_0^{*(2)}e^{-i\phi} \\ V_0^{(1)}V_0^{(2)}e^{i\phi} \\ V_0^{(1)}W_0^{*(2)}e^{-i2\phi} + W_0^{*(1)}V_0^{(2)}e^{i\phi} \\ V_0^{*(1)}V_0^{*(2)}e^{-i\phi} \end{bmatrix} - \gamma\begin{bmatrix} \left(2\zeta_1|V_0^{(2)}|^2 + \frac{\rho}{2}|W_0^{(2)}|^2\right)V_0^{(1)} \\ \left(\zeta_2|W_0^{(2)}|^2 + \frac{\rho}{2}|V_0^{(2)}|^2\right)W_0^{(1)} \\ \left(2\zeta_1|V_0^{(2)}|^2 + \frac{\rho}{2}|W_0^{(2)}|^2\right)V_0^{*(1)} \\ \left(\zeta_2|W_0^{(2)}|^2 + \frac{\rho}{2}|V_0^{(2)}|^2\right)W_0^{*(1)} \end{bmatrix}$$

$$-\gamma\begin{bmatrix} \zeta_1\left(V_0^{*(1)}V_0^{(2)^2}e^{2i\phi} + V_0^{(1)^2}V_0^{*(2)}e^{-i\phi} + 2|V_0^{(1)}|^2V_0^{(2)}e^{i\phi}\right) \\ \frac{\zeta_2}{2}\left(W_0^{*(1)}W_0^{(2)^2}e^{-4i\phi} + W_0^{(1)^2}W_0^{*(2)}e^{-2i\phi} + 2W_0^{(2)}|W_0^{(1)}|^2e^{2i\phi}\right) \\ \zeta_1\left(V_0^{(1)}V_0^{*(2)^2}e^{-2i\phi} + V_0^{*(1)^2}V_0^{(2)}e^{i\phi} + 2|V_0^{(1)}|^2V_0^{*(2)}e^{-i\phi}\right) \\ \frac{\zeta_2}{2}\left(W_0^{(1)}W_0^{*(2)^2}e^{4i\phi} + W_0^{*(1)^2}W_0^{(2)}e^{2i\phi} + +2W_0^{*(2)}|W_0^{(1)}|^2e^{-2i\phi}\right) \end{bmatrix} \tag{A.17}$$

$$-\gamma\frac{\rho}{2}\begin{bmatrix} V_0^{(2)}|W_0^{(1)}|^2e^{i\phi} + \left(V_0^{(1)} + V_0^{(2)}e^{i\phi}\right)\left(W_0^{(1)}W_0^{*(2)}e^{-2i\phi} + W_0^{*(1)}W_0^{(2)}e^{2i\phi}\right) \\ |V_0^{(1)}|^2W_0^{(2)}e^{2i\phi} + \left(V_0^{(1)}V_0^{*(2)}e^{-i\phi} + V_0^{*(1)}V_0^{(2)}e^{i\phi}\right)\left(W_0^{(1)} + W_0^{(2)}e^{2i\phi}\right) \\ V_0^{*(2)}|W_0^{(1)}|^2e^{-i\phi} + \left(V_0^{*(1)} + V_0^{*(2)}e^{-i\phi}\right)\left(W_0^{*(1)}W_0^{(2)}e^{2i\phi} + W_0^{(1)}W_0^{*(2)}e^{-2i\phi}\right) \\ |V_0^{(1)}|^2W_0^{*(2)}e^{-2i\phi} + \left(V_0^{*(1)}V_0^{(2)}e^{i\phi} + V_0^{(1)}V_0^{*(2)}e^{-i\phi}\right)\left(W_0^{*(1)} + W_0^{*(2)}e^{-2i\phi}\right) \end{bmatrix}.$$

Fredholms alternative states that the solution vector, $\bar{V}_h$, of the adjoint homogeneous system corresponding to (A.15) must be orthogonal to the right-hand side, $\bar{h}$, of our original problem, i.e. $\bar{V}_h^* \cdot \bar{h} = 0$. The known solutions of the homogeneous system

obtained from (A.15) are

$$V_{h1}^{(1)} = iV_0^{(1)}, \qquad\qquad W_{h1}^{(1)} = 2iW_0^{(1)}, \qquad\qquad (A.18a)$$

$$V_{h2}^{(1)} = \frac{\partial V_0^{(1)}}{\partial x} = -\frac{\partial V_0^{(1)}}{\partial x^{(1)}}, \quad W_{h2}^{(1)} = \frac{\partial W_0^{(1)}}{\partial x} = -\frac{\partial W_0^{(1)}}{\partial x^{(1)}}, \quad (A.18b)$$

$$V_{h3}^{(1)} = \frac{\partial V_0^{(1)}}{\partial y} = -\frac{\partial V_0^{(1)}}{\partial y^{(1)}}, \quad W_{h3}^{(1)} = \frac{\partial W_0^{(1)}}{\partial y} = -\frac{\partial W_0^{(1)}}{\partial y^{(1)}}, \quad (A.18c)$$

together with their conjugates. The solution (A.18a) yields the solvability condition

$$
\begin{aligned}
0 \;=\; & -\frac{\partial |V_0^{(1)}|^2}{\partial Z} - \frac{\partial |W_0^{(1)}|^2}{\partial Z} \\
& -i\eta \left(V_0^{(1)\,2} W_0^{*(2)} e^{-i2\phi} - V_0^{*(1)\,2} W_0^{(2)} e^{i2\phi} \right. \\
& \qquad\qquad \left. + V_0^{*(1)} W_0^{(1)} V_0^{*(2)} e^{-i\phi} - V_0^{(1)} W_0^{*(1)} V_0^{(2)} e^{i\phi} \right) \\
& -i\gamma\zeta_1 \left(V_0^{(1)\,2} V_0^{*(2)\,2} e^{-2i\phi} - V_0^{*(1)\,2} V_0^{(2)\,2} e^{2i\phi} \right. \\
& \qquad\qquad \left. + V_0^{(1)} |V_0^{(1)}|^2 V_0^{*(2)} e^{-i\phi} - V_0^{*(1)} |V_0^{(1)}|^2 V_0^{(2)} e^{i\phi} \right) \\
& -i\gamma\zeta_2 \left(W_0^{(1)\,2} W_0^{*(2)\,2} e^{-4i\phi} - W_0^{*(1)\,2} W_0^{(2)\,2} e^{4i\phi} \right. \\
& \qquad\qquad \left. + W_0^{(1)} |W_0^{(1)}|^2 W_0^{*(2)} e^{-2i\phi} - W_0^{*(1)} |W_0^{(1)}|^2 W_0^{(2)} e^{2i\phi} \right) \\
& -i\gamma\frac{\rho}{2} \left(V_0^{(1)} V_0^{*(2)} e^{-i\phi} - V_0^{*(1)} V_0^{(2)} e^{i\phi} \right) \times \\
& \qquad\qquad \left(W_0^{(1)} W_0^{*(2)} e^{-2i\phi} + W_0^{*(1)} W_0^{(2)} e^{2i\phi} + |W_0^{(1)}|^2 \right) \\
& -i\gamma\rho \left(W_0^{(1)} W_0^{*(2)} e^{-2i\phi} - W_0^{*(1)} W_0^{(2)} e^{2i\phi} \right) \times \\
& \qquad\qquad \left(V_0^{(1)} V_0^{*(2)} e^{-i\phi} + V_0^{*(1)} V_0^{(2)} e^{i\phi} + |V_0^{(1)}|^2 \right). \qquad (A.19)
\end{aligned}
$$

Integrating over the transverse plane yields

$$\frac{\partial P^{(1)}}{\partial Z} - \eta \frac{\partial U_{\chi^{(2)}}^{(1)}}{\partial \phi^{(1)}} - \gamma \frac{\partial U_{\chi^{(3)}}^{(1)}}{\partial \phi^{(1)}} = 0, \qquad\qquad (A.20)$$

where it has been exploited that $\partial/\partial\phi = -\partial/\partial\phi^{(1)}$. $P^{(1)}$ is the to the zeroth order conserved power. $U_{\chi^{(2)}}^{(1)}$ is the $\chi^{(2)}$ interaction potential given by

$$
\begin{aligned}
U_{\chi^{(2)}}^{(1)} \;=\; & -\frac{1}{2} \int \left(V_0^{*(1)\,2} W_0^{(2)} e^{i2\phi} + V_0^{(1)\,2} W_0^{*(2)} e^{-i2\phi} \right. \\
& \qquad\quad \left. + 2V_0^{(1)} W_0^{*(1)} V_0^{(2)} e^{i\phi} + 2V_{0,}^{*(1)} W_0^{(1)} V_0^{*(2)} e^{-i\phi} \right) d\vec{r}_\perp, (A.21)
\end{aligned}
$$

and $U_{\chi^{(3)}}^{(1)}$ is the $\chi^{(3)}$ interaction potential given by

$$
\begin{aligned}
U_{\chi^{(3)}}^{(1)} \;=\; & -\frac{\zeta_1}{2} \int \left(V_0^{*(1)^2} V_0^{(2)^2} e^{2i\phi} + V_0^{(1)^2} V_0^{*(2)^2} e^{-2i\phi} \right. \\
& \qquad\qquad \left. 2V_0^{*(1)} |V_0^{(1)}|^2 V_0^{(2)} e^{i\phi} + 2V_0^{(1)} |V_0^{(1)}|^2 V_0^{*(2)} e^{-i\phi} \right) d\vec{r}_\perp \\
& -\frac{\zeta_2}{4} \int \left(W_0^{*(1)^2} W_0^{(2)^2} e^{4i\phi} + W_0^{(1)^2} W_0^{*(2)^2} e^{-4i\phi} + \right. \\
& \qquad\qquad \left. 2W_0^{*(1)} |W_0^{(1)}|^2 W_0^{(2)} e^{2i\phi} + 2W_0^{(1)} |W_0^{(1)}|^2 W_0^{*(2)} e^{-2i\phi} \right) d\vec{r}_\perp \\
& -\frac{\rho}{2} \int \left(V_0^{*(1)} |W_0^{(1)}|^2 V_0^{(2)} e^{i\phi} + V_0^{(1)} |W_0^{(1)}|^2 V_0^{*(2)} e^{-i\phi} + \right. \\
& \qquad\qquad \left. W_0^{*(1)} |V_0^{(1)}|^2 W_0^{(2)} e^{2i\phi} + W_0^{(1)} |V_0^{(1)}|^2 W_0^{*(2)} e^{-2i\phi} \right) d\vec{r}_\perp \\
& -\frac{\rho}{2} \int \left(V_0^{(1)} V_0^{*(2)} e^{-i\phi} + V_0^{*(1)} V_0^{(2)} e^{i\phi} \right) \times \\
& \qquad\qquad \left(W_0^{(1)} W_0^{*(2)} e^{-2i\phi} + W_0^{*(1)} W_0^{(2)} e^{2i\phi} \right) d\vec{r}_\perp . \qquad (A.22)
\end{aligned}
$$

By inspection it is found that the solvability conditions pertaining to the solutions (A.18b) and (A.18c) can be expressed as

$$
\frac{\partial M_x^{(1)}}{\partial Z} + \eta \frac{\partial U_{\chi^{(2)}}^{(1)}}{\partial x^{(1)}} + \gamma \frac{\partial U_{\chi^{(3)}}^{(1)}}{\partial x^{(1)}} = 0, \qquad (A.23)
$$

and

$$
\frac{\partial M_y^{(1)}}{\partial Z} + \eta \frac{\partial U_{\chi^{(2)}}^{(1)}}{\partial y^{(1)}} + \gamma \frac{\partial U_{\chi^{(3)}}^{(1)}}{\partial y^{(1)}} = 0, \qquad (A.24)
$$

respectively. $M_x^{(1)}$ and $M_y^{(1)}$ are the to the zeroth order conserved momenta along the transverse axes.

If everywhere in equations (A.20-A.24) the superscripts are rotated, the equivalent equations for the the second soliton are found. To sum up, the full set of interaction equations governing the variation of two generally non-identical interacting solitons

in the general nonplanar case is

$$\frac{\partial P^{(1)}}{\partial Z} - \eta \frac{\partial U^{(1)}_{\chi^{(2)}}}{\partial \phi^{(1)}} - \gamma \frac{\partial U^{(1)}_{\chi^{(3)}}}{\partial \phi^{(1)}} = 0, \qquad (A.25a)$$

$$\frac{\partial M_x^{(1)}}{\partial Z} + \eta \frac{\partial U^{(1)}_{\chi^{(2)}}}{\partial x^{(1)}} + \gamma \frac{\partial U^{(1)}_{\chi^{(3)}}}{\partial x^{(1)}} = 0, \qquad (A.25b)$$

$$\frac{\partial M_y^{(1)}}{\partial Z} + \eta \frac{\partial U^{(1)}_{\chi^{(2)}}}{\partial y^{(1)}} + \gamma \frac{\partial U^{(1)}_{\chi^{(3)}}}{\partial y^{(1)}} = 0, \qquad (A.25c)$$

$$\frac{\partial P^{(2)}}{\partial Z} - \eta \frac{\partial U^{(2)}_{\chi^{(2)}}}{\partial \phi^{(2)}} - \gamma \frac{\partial U^{(2)}_{\chi^{(3)}}}{\partial \phi^{(2)}} = 0, \qquad (A.25d)$$

$$\frac{\partial M_x^{(2)}}{\partial Z} + \eta \frac{\partial U^{(2)}_{\chi^{(2)}}}{\partial x^{(2)}} + \gamma \frac{\partial U^{(2)}_{\chi^{(3)}}}{\partial x^{(2)}} = 0, \qquad (A.25e)$$

$$\frac{\partial M_y^{(2)}}{\partial Z} + \eta \frac{\partial U^{(2)}_{\chi^{(2)}}}{\partial y^{(2)}} + \gamma \frac{\partial U^{(2)}_{\chi^{(3)}}}{\partial y^{(2)}} = 0, \qquad (A.25f)$$

where

$$U^{(1)}_{\chi^{(2)}} = -\mathrm{Re} \int \left(V_0^{*(1)^2} W_0^{(2)} e^{i2\phi} + 2 V_0^{(1)} W_0^{*(1)} V_0^{(2)} e^{i\phi} \right) d\vec{r}_\perp, \qquad (A.26)$$

and

$$U^{(1)}_{\chi^{(3)}} = -\zeta_1 \mathrm{Re} \int \left(V_0^{*(1)^2} V_0^{(2)^2} e^{2i\phi} + 2 V_0^{*(1)} |V_0^{(1)}|^2 V_0^{(2)} e^{i\phi} \right) d\vec{r}_\perp$$

$$- \frac{\zeta_2}{2} \mathrm{Re} \int \left(W_0^{*(1)^2} W_0^{(2)^2} e^{4i\phi} + 2 W_0^{*(1)} |W_0^{(1)}|^2 W_0^{(2)} e^{2i\phi} \right) d\vec{r}_\perp$$

$$- \rho \, \mathrm{Re} \int \left(V_0^{*(1)} |W_0^{(1)}|^2 V_0^{(2)} e^{i\phi} + |V_0^{(1)}|^2 W_0^{*(1)} W_0^{(2)} e^{2i\phi} \right. \qquad (A.27)$$

$$\left. + V_0^{(1)} W_0^{*(1)} V_0^{*(2)} W_0^{(2)} e^{i\phi} + V_0^{*(1)} W_0^{*(1)} V_0^{(2)} W_0^{(2)} e^{3i\phi} \right) d\vec{r}_\perp.$$

$U^{(2)}_{\chi^{(2)}}$ and $U^{(2)}_{\chi^{(3)}}$ are found by rotating superscripts in (A.26) and (A.27).

Averaged equations for two-period QPM

The averaged equations and the induced averaged nonlinearities for two-period QPM gratings are derived in this appendix.

The dimensionless equations governing the propagation of two coupled beams in lossless QPM slab waveguides are

$$i\frac{\partial E_1}{\partial z} + \frac{1}{2}\frac{\partial^2 E_1}{\partial x^2} + d(z)E_1^* E_2 e^{-i\beta z} = 0, \qquad \text{(B.1a)}$$

$$i\frac{\partial E_2}{\partial z} + \frac{1}{4}\frac{\partial^2 E_2}{\partial x^2} + d(z)E_1^2 e^{i\beta z} = 0. \qquad \text{(B.1b)}$$

$E_1 = E_1(x, z)$ is the fundamental wave (FW) and $E_2 = E_2(x, z)$ is the second harmonic (SH). β is the intrinsic phase mismatch and the spatial periodic modulation of the nonlinearity is described by the grating function $d(z)$ whose amplitude has been normalized to 1. Here a two-period grating function is considered. Such a function can be represented by its Fourier series

$$d(z) \quad = \quad \sum_k d_k^{(1)} \exp(ik\kappa_1 z) \times \sum_l d_l^{(2)} \exp(il\kappa_2 z). \qquad \text{(B.2)}$$

In (B.2) $d_k^{(1)}$ and $d_l^{(2)}$ are the Fourier components and κ_1 and κ_2 the spatial QPM frequencies of the primary and the superimposed secondary grating, respectively. The

summations are over all integers (k, l) from $-\infty$ to ∞. Notice, that though the terms primary and secondary are used to distinguish the gratings, mathematically speaking they are of equal importance.

Insertion of (B.2) into system (B.1) yields

$$i\frac{\partial w}{\partial z} + \frac{1}{2}\frac{\partial^2 w}{\partial x^2} + d_m^{(1)}d_n^{(2)}w^*v + w^*vR^{(1)} = 0, \tag{B.3a}$$

$$i\frac{\partial v}{\partial z} + \frac{1}{4}\frac{\partial^2 v}{\partial x^2} - \epsilon v + d_{-m}^{(1)}d_{-n}^{(2)}w^2 + w^2R^{(2)} = 0, \tag{B.3b}$$

where

$$w = E_1, \qquad v = E_2 e^{-i\epsilon z}. \tag{B.4}$$

The residual phase mismatch has been defined as $\epsilon = \beta - m\kappa_1 + n\kappa_2$ with m and n being the QPM orders related to the primary and secondary grating, respectively. In (B.3) the Fourier coefficients from (B.2) pertaining to the QPM orders have been separated out of the sums and the R terms represent what is left of the sums and are given by

$$R^{(1)} = d_m^{(1)}\sum_{l\neq n}d_l^{(2)}e^{i(l-n)\kappa_2 z} + d_n^{(2)}\sum_{k\neq m}d_k^{(1)}e^{i(k-m)\kappa_1 z} +$$

$$\sum_{k\neq m}d_k^{(1)}e^{i(k-m)\kappa_1 z} \times \sum_{l\neq n}d_l^{(2)}e^{i(l-n)\kappa_2 z}, \tag{B.5a}$$

$$R^{(2)} = R^{(1)}|_{m\to -m, n\to -n}. \tag{B.5b}$$

Because of the periodic grating the beams start oscillating. The analysis in the following relies on an expansion of the beams in Fourier series. The Fourier components are assumed to be slowly varying during propagation, i.e. $|\partial w_q/\partial z| \ll \kappa_{1,2}|w_q|$ (with equivalent expressions for the other field components). It is also assumed that the higher order Fourier components are much smaller than the averaged ($q = 0$) dc-amplitudes, i.e. $|w_{q\neq 0}| \ll |w_0|$ (with equivalent expressions for the other field components). In case of a one-periodic structure the expansion of the beams in a Fourier series is straight forward since the higher order modes are simply harmonics of the single QPM frequency. In a two-period structure the situation is a bit more subtle. Cross-harmonics, i.e. higher order modes at some superposition of both QPM frequencies, could be expected to arise. In the case where the ratio between the QPM frequencies is an integer the cross-harmonics are already included in the sums. In other cases they are not, but the numerical experiments show that a model without cross-harmonics still yields correct results and hence they are neglected. The Fourier expansions become

$$w(x, z) = w_0(x, z) + \sum_{q\neq 0} w_q(x, z)e^{iq\kappa_1 z} + \sum_{q\neq 0}\omega_q(x, z)e^{iq\kappa_2 z}, \tag{B.6a}$$

$$v(x, z) = v_0(x, z) + \sum_{q\neq 0} v_q(x, z)e^{iq\kappa_1 z} + \sum_{q\neq 0}\nu_q(x, z)e^{iq\kappa_2 z}, \tag{B.6b}$$

and to lowest order the Fourier components of the qth higher order mode are easily found to be

$$w_q = \frac{d_n^{(2)}}{\kappa_1} w_0^* v_0 \frac{d_{[m+q]}^{(1)}}{q}, \qquad \omega_q = \frac{d_m^{(1)}}{\kappa_2} w_0^* v_0 \frac{d_{[n+q]}^{(2)}}{q}, \qquad \text{(B.7a)}$$

$$v_q = \frac{d_{-n}^{(2)}}{\kappa_1} w_0^2 \frac{d_{[-m+q]}^{(1)}}{q}, \qquad \nu_q = \frac{d_{-m}^{(1)}}{\kappa_2} w_0^2 \frac{d_{[-n+q]}^{(2)}}{q}, \qquad \text{(B.7b)}$$

where the terms in square brackets are the integer Fourier indices.

To find the equations which govern the propagation of the averaged fields w_0 and v_0, (B.6) is inserted into (B.3) and all non dc-terms are eliminated. Only the two lowest order contributions are taken into account and in the following the η-terms comprise the lowest order contributions whereas the ζ-terms comprise the first order contribution. The structure of the averaged equations is

$$i\frac{\partial w_0}{\partial z} + \frac{1}{2}\frac{\partial^2 w_0}{\partial x^2} + \eta_1 w_0^* v_0 + (\zeta_1 |w_0|^2 - \zeta_2 |v_0|^2) w_0 = 0, \qquad \text{(B.8a)}$$

$$i\frac{\partial v_0}{\partial z} + \frac{1}{4}\frac{\partial^2 v_0}{\partial x^2} - \epsilon v_0 + \eta_2 w_0^2 - 2\zeta_3 |w_0|^2 v_0 = 0. \qquad \text{(B.8b)}$$

To make the derivation of the nonlinearities more presentable the induced quadratic and cubic terms are considered in separate sections.

B.1   Induced quadratic nonlinearity

In (B.8a) η_1 is a sum of the only two dc-contributions in (B.3a) involving $w_0^* v_0$. One arises trivially from $d_m^{(1)} d_n^{(2)} w^* v$, i.e. $d_m^{(1)} d_n^{(2)} w_0^* v_0$. The other stems from $w_0^* v_0 R^{(1)}$, where only the double sum from $R^{(1)}$ in (B.5a) yields dc-terms. Thus

$$\eta_1 = d_m^{(1)} d_n^{(2)} + \sum_{k \neq m} d_k^{(1)} e^{i(k-m)\kappa_1 z} \times \sum_{l \neq n} d_l^{(2)} e^{i(l-n)\kappa_2 z}, \quad (k-m)\kappa_1 + (l-n)\kappa_2 = 0$$

$$= d_m^{(1)} d_n^{(2)} + \sum_{k \neq m} d_k^{(1)} d_{[-(k-m)\kappa_1/\kappa_2+n]}^{(2)}. \qquad \text{(B.9)}$$

Obviously the condition placed to the far right on the top line in (B.9) is the condition to be fulfilled for the contribution to be a dc-contribution. The index in the square brackets stems from this condition.

Likewise η_2 is determined from (B.3b),

$$
\begin{aligned}
\eta_2 &= d_{-m}^{(1)} d_{-n}^{(2)} + \sum_{k \neq -m} d_k^{(1)} e^{i(k+m)\kappa_1 z} \times \sum_{l \neq -n} d_l^{(2)} e^{i(l+n)\kappa_2 z}, \quad (k+m)\kappa_1 + (l+n)\kappa_2 = 0 \\
&= d_m^{(1)} d_n^{(2)} + \sum_{k \neq -m} d_k^{(1)} d_{[-(k+m)\kappa_1/\kappa_2 - n]}^{(2)}.
\end{aligned}
\tag{B.10}
$$

If the two QPM frequencies do not share harmonics, for instance if one is an irrational number, then there are no contributions from the R terms since the conditions $(k-m)\kappa_1 + (l-n)\kappa_2 = 0$ and $(k+m)\kappa_1 + (l+n)\kappa_2 = 0$ from (B.9) and (B.10), respectively, can never be fulfilled, i.e. the Fourier components do not exist. In this case

$$
\eta_1 = d_m^{(1)} d_n^{(2)}, \qquad \eta_2 = d_{-m}^{(1)} d_{-n}^{(2)}.
\tag{B.11}
$$

B.2   Induced cubic nonlinearity

The strengths of the induced averaged cubic nonlinearities ζ_1, ζ_2, and ζ_3 are deduced from $w^* v R^{(1)}$ and $w^2 R^{(2)}$ in (B.8a) and (B.8b), respectively. They take into account first order contributions with one dc-field component. The terms with two dc-components yielded the lowest order quadratic contribution. For the ζ_1 and ζ_2 nonlinearities the contributions thus stem from

$$
\left(w_0^* \sum_{q \neq 0} v_q e^{iq\kappa_1 z} + w_0^* \sum_{q \neq 0} \nu_q e^{iq\kappa_2 z} + v_0 \sum_{q \neq 0} w_q^* e^{-iq\kappa_1 z} + v_0 \sum_{q \neq 0} \omega_q^* e^{-iq\kappa_2 z} \right) \times
\tag{B.12}
$$

$$
\left(d_m^{(1)} \sum_{l \neq n} d_l^{(2)} e^{i(l-n)\kappa_2 z} + d_n^{(2)} \sum_{k \neq m} d_k^{(1)} e^{i(k-m)\kappa_1 z} + \sum_{k \neq m} d_k^{(1)} e^{i(k-m)\kappa_1 z} \sum_{l \neq n} d_l^{(2)} e^{i(l-n)\kappa_2 z} \right).
$$

The terms from (B.12) which will eventually make up the $\zeta_1 |w_0|^2 w_0$ nonlinearity in (B.8a) are

$$d_n^{(2)} w_0^* \sum_{q \neq 0} d_{[m-q]}^{(1)} v_q \qquad\qquad , (k-m)\kappa_1 + q\kappa_1 = 0 \qquad\qquad \text{(B.13a)}$$

$$+ \; d_m^{(1)} w_0^* \sum_{q \neq 0} d_{[n-q]}^{(2)} \nu_q \qquad\qquad , (l-n)\kappa_2 + q\kappa_2 = 0 \qquad\qquad \text{(B.13b)}$$

$$+ \; d_n^{(2)} w_0^* \sum_{q \neq 0} d_{[m-q\frac{\kappa_2}{\kappa_1}]}^{(1)} \nu_q \qquad\qquad , (k-m)\kappa_1 + q\kappa_2 = 0 \qquad\qquad \text{(B.13c)}$$

$$+ \; d_m^{(1)} w_0^* \sum_{q \neq 0} d_{[n-q\frac{\kappa_1}{\kappa_2}]}^{(2)} v_q \qquad\qquad , (l-n)\kappa_2 + q\kappa_1 = 0 \qquad\qquad \text{(B.13d)}$$

$$+ \; w_0^* \sum_{k \neq m,\, q \neq 0,\, k \neq m - q\kappa_2/\kappa_1} d_k^{(1)} d_{[(n-q)-(k-m)\frac{\kappa_1}{\kappa_2}]}^{(2)} \nu_q \;\;, (k-m)\kappa_1 + (l-n)\kappa_2 + q\kappa_2 = 0 \;\text{(B.13e)}$$

$$+ \; w_0^* \sum_{l \neq n,\, q \neq 0,\, l \neq n - q\kappa_1/\kappa_2} d_l^{(2)} d_{[(m-q)-(l-n)\frac{\kappa_2}{\kappa_1}]}^{(1)} v_q . \;\;, (k-m)\kappa_1 + (l-n)\kappa_2 + q\kappa_1 = 0 \;\text{(B.13f)}$$

By inspection it is easily found that not excluding $k = m$ in (B.13e) yields the extra contribution (B.13b) and not excluding $k = m - q\kappa_2/\kappa_1$ in (B.13e) yields the contribution (B.13c). Likewise not excluding $l = n$ and $l = n - q\kappa_1/\kappa_2$ in (B.13f) yields the contributions (B.13a) and (B.13d), respectively. Bearing this in mind and substituting the field components with index q with (B.7) in (B.13e) and (B.13f) leads to the general expression for ζ_1.

$$\zeta_1 = \frac{d_{-n}^{(2)}}{\kappa_1} \sum_{l,\, q \neq 0} \frac{d_l^{(2)} d_{[(m-q)-(l-n)\frac{\kappa_2}{\kappa_1}]}^{(1)} d_{[-m+q]}^{(1)}}{q} + \frac{d_{-m}^{(1)}}{\kappa_2} \sum_{k,\, q \neq 0} \frac{d_k^{(1)} d_{[(n-q)-(k-m)\frac{\kappa_1}{\kappa_2}]}^{(2)} d_{[-n+q]}^{(2)}}{q} . \text{(B.14)}$$

ζ_2 is determined from (B.12) in exactly the same way. For the sake of completeness, the terms corresponding to (B.13) are presented. They are

$$d_n^{(2)} v_0 \sum_{q \neq 0} d_{[m+q]}^{(1)} w_q^* \qquad\qquad , (k-m)\kappa_1 - q\kappa_1 = 0 \qquad\qquad \text{(B.15a)}$$

$$+ \; d_m^{(1)} v_0 \sum_{q \neq 0} d_{[n+q]}^{(2)} \omega_q^* \qquad\qquad , (l-n)\kappa_2 - q\kappa_2 = 0 \qquad\qquad \text{(B.15b)}$$

$$+ \; d_n^{(2)} v_0 \sum_{q \neq 0} d_{[m+q\frac{\kappa_2}{\kappa_1}]}^{(1)} \omega_q^* \qquad\qquad , (k-m)\kappa_1 - q\kappa_2 = 0 \qquad\qquad \text{(B.15c)}$$

$$+ \; d_m^{(1)} v_0 \sum_{q \neq 0} d_{[n+q\frac{\kappa_1}{\kappa_2}]}^{(2)} w_q^* \qquad\qquad , (l-n)\kappa_2 - q\kappa_1 = 0 \qquad\qquad \text{(B.15d)}$$

$$+ \; v_0 \sum_{k \neq m,\, q \neq 0,\, k \neq m + q\kappa_2/\kappa_1} d_k^{(1)} d_{[(n+q)-(k-m)\frac{\kappa_1}{\kappa_2}]}^{(2)} \omega_q^* \;\;, k-m)\kappa_1 + (l-n)\kappa_2 - q\kappa_2 = 0 \;\text{(B.15e)}$$

$$+ \; v_0 \sum_{l \neq n,\, q \neq 0,\, l \neq n + q\kappa_1/\kappa_2} d_l^{(2)} d_{[(m+q)-(l-n)\frac{\kappa_2}{\kappa_1}]}^{(1)} w_q^* . \;\;, (k-m)\kappa_1 + (l-n)\kappa_2 - q\kappa_1 = 0 \;\text{(B.15f)}$$

From (B.15) ζ_2 can now be deduced through the same line of arguments as used above for ζ_1.

$$\zeta_2 = \frac{d_n^{*(2)}}{\kappa_1} \sum_{l,\, q \neq 0} \frac{d_l^{(2)} d_{[(m+q)-(l-n)\frac{\kappa_2}{\kappa_1}]}^{(1)} d_{[m+q]}^{*(1)}}{q} + \frac{d_m^{*(1)}}{\kappa_2} \sum_{k,\, q \neq 0} \frac{d_k^{(1)} d_{[(n+q)-(k-m)\frac{\kappa_1}{\kappa_2}]}^{(2)} d_{[n+q]}^{*(2)}}{q}. \quad \text{(B.16)}$$

For the $\zeta_3 |w_0|^2 v_0$ nonlinearity the contributions stem from (B.8b), i.e. from

$$\left(2w_0 \sum_{q \neq 0} w_q e^{iq\kappa_1 z} + 2w_0 \sum_{q \neq 0} \omega_q e^{iq\kappa_2 z} \right) \times$$

$$\left(d_{-m}^{(1)} \sum_{l \neq -n} d_l^{(2)} e^{i(l+n)\kappa_2 z} + d_{-n}^{(2)} \sum_{k \neq -m} d_k^{(1)} e^{i(k+m)\kappa_1 z} + \sum_{k \neq -m} d_k^{(1)} e^{i(k+m)\kappa_1 z} \sum_{l \neq -n} d_l^{(2)} e^{i(l+n)\kappa_2 z} \right),$$

and they are

$$2d_{-n}^{(2)} w_0 \sum d_{[-m-q]}^{(1)} w_q \qquad\qquad , (k+m)\kappa_1 + q\kappa_1 = 0 \qquad\qquad \text{(B.17a)}$$

$$+\ 2d_{-m}^{(1)} w_0 \sum d_{[-n-q]}^{(2)} \omega_q \qquad\qquad , (l+n)\kappa_2 + q\kappa_1 = 0 \qquad\qquad \text{(B.17b)}$$

$$+\ 2d_{-n}^{(2)} w_0 \sum d_{[-m-q\frac{\kappa_2}{\kappa_1}]}^{(1)} \omega_q \qquad\qquad , (k+m)\kappa_1 + q\kappa_2 = 0 \qquad\qquad \text{(B.17c)}$$

$$+\ 2d_{-m}^{(1)} w_0 \sum d_{[-n-q\frac{\kappa_1}{\kappa_2}]}^{(2)} w_q \qquad\qquad , (l+n)\kappa_2 + q\kappa_2 = 0 \qquad\qquad \text{(B.17d)}$$

$$+\ 2w_0 \sum d_l^{(2)} d_{[-(m+q)-(l+n)\frac{\kappa_2}{\kappa_1}]}^{(1)} w_q \quad , (k+m)\kappa_1 + (l+m)\kappa_2 + q\kappa_1 = 0 \quad \text{(B.17e)}$$

$$+\ 2w_0 \sum d_k^{(1)} d_{[-(n+q)-(k+m)\frac{\kappa_1}{\kappa_2}]}^{(2)} \omega_q. \quad , (k+m)\kappa_1 + (l+m)\kappa_2 + q\kappa_2 = 0 \quad \text{(B.17f)}$$

From (B.17) ζ_3 is the deduced,

$$\zeta_3 = \frac{d_n^{(2)}}{\kappa_1} \sum_{l,\, q \neq 0} \frac{d_l^{(2)} d_{[-(m+q)-(l+n)\frac{\kappa_2}{\kappa_1}]}^{(1)} d_{[m+q]}^{(1)}}{q} + \frac{d_m^{(1)}}{\kappa_2} \sum_{k,\, q \neq 0} \frac{d_k^{(1)} d_{[-(n+q)-(k+m)\frac{\kappa_1}{\kappa_2}]}^{(2)} d_{[n+q]}^{(2)}}{q}. \quad \text{(B.18)}$$

In case that the two periods do not share common harmonics only the terms (B.13a-B.13b), (B.15a-B.15b), and (B.17a-B.17b) in the above survive and

$$\zeta_1 = \frac{d_n^{(2)} d_{-n}^{(2)}}{\kappa_1} \sum_{q \neq 0} \frac{d_{[q-m]}^{(1)} d_{[m-q]}^{(1)}}{q} + \frac{d_m^{(1)} d_{-m}^{(1)}}{\kappa_2} \sum_{q \neq 0} \frac{d_{[q-n]}^{(2)} d_{[n-q]}^{(2)}}{q}, \quad \text{(B.19a)}$$

$$\zeta_2 = \frac{d_n^{(2)} d_n^{*(2)}}{\kappa_1} \sum_{q \neq 0} \frac{d_{[m+q]}^{(1)} d_{[m+q]}^{*(1)}}{q} + \frac{d_m^{(1)} d_m^{*(1)}}{\kappa_2} \sum_{q \neq 0} \frac{d_{[n+q]}^{(2)} d_{[n+q]}^{*(2)}}{q}, \quad \text{(B.19b)}$$

$$\zeta_3 = \frac{d_n^{(2)} d_{-n}^{(2)}}{\kappa_1} \sum \frac{d_{[m+q]}^{(1)} d_{[-m-q]}^{(1)}}{q} + \frac{d_m^{(1)} d_{-m}^{(1)}}{\kappa_2} \sum \frac{d_{[n+q]}^{(2)} d_{[-n-q]}^{(2)}}{q}. \quad \text{(B.19c)}$$

B.3   Averaged equations and nonlinearities

When the grating function is real and odd, which is the case for a square grating, the Fourier coefficients of (B.2) obey $d_{-n}^{(j)} = d_n^{*(j)} = -d_n^{(j)}$ and

$$\eta = \eta_1 = \eta_2 = d_m^{(1)} d_n^{(2)} + \sum_{k \neq m} d_k^{(1)} d_{[-(k-m)\kappa_1/\kappa_2 + n]}^{(2)}, \tag{B.20a}$$

$$\gamma = \zeta_1 = -\zeta_2 = -\zeta_3$$
$$= \frac{d_n^{(2)}}{\kappa_1} \sum_{l,\, q \neq 0} \frac{d_l^{(2)} d_{[(m+q)-(l-n)\frac{\kappa_2}{\kappa_1}]}^{(1)} d_{[m+q]}^{(1)}}{q} + \frac{d_m^{(1)}}{\kappa_2} \sum_{k,\, q \neq 0} \frac{d_k^{(1)} d_{[(n+q)-(k-m)\frac{\kappa_1}{\kappa_2}]}^{(2)} d_{[n+q]}^{(2)}}{q}, \tag{B.20b}$$

or in case the QPM frequencies share no common harmonics

$$\eta \quad = \quad \eta_1 = \eta_2 = d_m^{(1)} d_n^{(2)}, \tag{B.21a}$$

$$\gamma \quad = \quad \zeta_1 = -\zeta_2 = -\zeta_3$$
$$= \quad \frac{d_n^{(2)} d_{-n}^{(2)}}{\kappa_1} \sum_{q \neq 0} \frac{d_{[m+q]}^{(1)^2}}{q} + \frac{d_m^{(1)} d_{-m}^{(1)}}{\kappa_2} \sum_{q \neq 0} \frac{d_{[n+q]}^{(2)^2}}{q}. \tag{B.21b}$$

With the averaged nonlinearities given by (B.20) or (B.20) the equations governing the averaged fields (B.8) become

$$i\frac{\partial w_0}{\partial z} + \frac{1}{2}\frac{\partial^2 w_0}{\partial x^2} + \eta w_0^* v_0 + \gamma(|w_0|^2 - |v_0|^2)w_0 = 0, \tag{B.22a}$$

$$i\frac{\partial v_0}{\partial z} + \frac{\alpha}{2}\frac{\partial^2 v_0}{\partial x^2} - \epsilon v_0 + \eta w_0^2 - 2\gamma|w_0|^2 v_0 = 0. \tag{B.22b}$$

Interaction equations for saturable media

The procedure for deriving the soliton interaction equations describing interaction between two localized beams in saturable media is the same as the one followed in appendix A for interaction in combined $\chi^{(2)}$ and $\chi^{(3)}$ media. Therefore comments and details will be more sparse.

The propagation of a beam $\Psi = \Psi(x, y, z)$ in saturable media is described by the Euler-Lagrange equations of the Lagrangian density

$$\mathcal{L} = i\frac{1}{2}\left(\Psi\frac{\partial\Psi^*}{\partial z} - \Psi^*\frac{\partial\Psi}{\partial z}\right) + \nabla_\perp\Psi\cdot\nabla_\perp\Psi^* - |\Psi|^2 + \ln(1 + |\Psi|^2). \quad \text{(C.1)}$$

Substituting the superposition of two overlapping beams, $\Psi = A + B$, into (C.1) yields

$$\begin{aligned}\mathcal{L} = \ &i\frac{1}{2}\left((A + B)\left(\frac{\partial A^*}{\partial z} + \frac{\partial B^*}{\partial z}\right) - (A^* + B^*)\left(\frac{\partial A}{\partial z} + \frac{\partial B}{\partial z}\right)\right)\\ &+ (\nabla_\perp A + \nabla_\perp B)\cdot(\nabla_\perp A^* + \nabla_\perp B^*)\\ &- (A + B)(A^* + B^*) + \ln(1 + (A + B)(A^* + B^*)). \quad \text{(C.2)}\end{aligned}$$

The Euler-Lagrange equation for both A and B is

$$i\left(\frac{\partial A}{\partial z} + \frac{\partial B}{\partial z}\right) + \nabla_\perp^2(A + B) + \frac{(A + B)(A^* + B^*)}{1 + (A + B)(A^* + B^*)}(A + B) = 0. \text{ (C.3)}$$

The nonlinearity is split into three contributions. One contribution involves only A, another only B, and the third contribution, R, involves both A and B.

$$\frac{(A+B)(A^*+B^*)}{1+(A+B)(A^*+B^*)}(A+B) = \frac{|A|^2}{1+|A|^2}A + \frac{|B|^2}{1+|B|^2}B + R, \quad \text{(C.4)}$$

where

$$R = \frac{A(1+|B|^2)(|B|^2+AB^*+A^*B) + B(1+|A|^2)(|A|^2+AB^*+A^*B)}{(1+|A|^2)(1+|B|^2)(1+|A|^2+|B|^2+AB^*+A^*B)}. \quad \text{(C.5)}$$

Rewriting (C.3) yields

$$i\frac{\partial A}{\partial z} + \nabla_\perp^2 A + \frac{|A|^2}{1+|A|^2}A + \left[i\frac{\partial B}{\partial z} + \nabla_\perp^2 B + \frac{|B|^2}{1+|B|^2}B\right] + R = 0. \quad \text{(C.6)}$$

Now the fields A and B are expanded in asymptotic series according to

$$A(x,y,z) = \left[A_0(x-x^{(1)}, y-y^{(1)}) + \sum_{n=1}^\infty \epsilon^n A_n(x,y,z)\right] e^{i\phi^{(1)}}, \quad \text{(C.7a)}$$

$$B(x,y,z) = \left[B_0(x-x^{(2)}, y-y^{(2)}) + \sum_{n=1}^\infty \epsilon^n B_n(x,y,z)\right] e^{i\phi^{(2)}}, \quad \text{(C.7b)}$$

where $\epsilon \ll 1$ is a small parameter and

$$x^j(z) = \int_0^z \nu_x^j(Z')\mathrm{d}Z' + x_0^j \quad \Rightarrow \quad \frac{\partial x^j(z)}{\partial z} = \nu_x^j(Z), \quad \text{(C.8a)}$$

$$y^j(z) = \int_0^z \nu_y^j(Z')\mathrm{d}Z' + y_0^j \quad \Rightarrow \quad \frac{\partial y^j(z)}{\partial z} = \nu_y^j(Z), \quad \text{(C.8b)}$$

$$\phi^j(z) = \int_0^z \lambda^j(Z')\mathrm{d}Z' + \phi_0^j \quad \Rightarrow \quad \frac{\partial \phi^j(z)}{\partial z} = \lambda^j(Z), \quad \text{(C.8c)}$$

where $j = 1, 2$. x^j and y^j express the soliton center position in the transverse plane and ϕ^j is the accumulated phase of soliton j. Subscript 0 denotes initial values. To zeroth order in ϵ A and B are assumed not to interact. Considering A, then collecting terms of the first order in ϵ order yields

$$\nabla_\perp^2 A_1 - i\nu_x^{(1)}\frac{\partial A_1}{\partial x} - i\nu_y^{(1)}\frac{\partial A_1}{\partial y} - \lambda^{(1)} A_1 \qquad \text{(C.9)}$$

$$+(2-3|A_0|^2)|A_0|^2 A_1 + (1-2|A_0|^2)A_0^2 A_1^* = -\tilde{R} + A_0\frac{\partial \phi}{\partial Z} - i\frac{\partial A_0}{\partial Z}.$$

In (C.9) the A-only contribution of the nonlinearity from (C.6) has been expanded in a power series around $A = 0$ and $\tilde{R}$ is

$$\tilde{R} = \frac{A_0(1+|B_0|^2)(|B_0|^2+h) + B_0(1+|A_0|^2)(|A_0|^2+h)e^{i\phi}}{g(1+|A_0|^2)(1+|B_0|^2)}, \quad \text{(C.10)}$$

where $\phi = \phi^{(2)} - \phi^{(1)}$ and

$$h = A_0 B_0^* e^{-i\phi} + A_0^* B_0 e^{i\phi}, \quad \text{and} \quad g = 1 + |A_0|^2 + |B_0|^2 + h. \tag{C.11}$$

Equation (C.9) and its conjugate is put into matrix form

$$\hat{K} \begin{bmatrix} A_1 \\ A_1^* \end{bmatrix} = i\frac{\partial}{\partial Z} \begin{bmatrix} -A_0 \\ A_0^* \end{bmatrix} + \begin{bmatrix} A_0 \\ A_0^* \end{bmatrix} \frac{\partial \phi}{\partial Z} - \begin{bmatrix} \tilde{R} \\ \tilde{R}^* \end{bmatrix}, \tag{C.12}$$

where

$$\hat{K} = \begin{bmatrix} \nabla_\perp^2 - i\nu_x^{(1)}\frac{\partial}{\partial x} - i\nu_y^{(1)}\frac{\partial}{\partial y} - \lambda^{(1)} + 2|A_0|^2 - 3|A_0|^4 & (1 - 2|A_0|^2)A_0^2 \\ \nabla_\perp^2 + i\nu_x^{(1)}\frac{\partial}{\partial x} + i\nu_y^{(1)}\frac{\partial}{\partial y} - \lambda^{(1)} + 2|A_0|^2 - 3|A_0|^4 & (1 - 2|A_0|^2)A_0^{*2} \end{bmatrix}. \tag{C.13}$$

Via Fredholm's alternative three solvability conditions are found, one for each of the known solution vectors

$$\bar{V}_{h1} = i \begin{bmatrix} A_0 \\ -A_0^* \end{bmatrix}, \quad \bar{V}_{h2} = \frac{\partial}{\partial x} \begin{bmatrix} A_0 \\ A_0^* \end{bmatrix}, \quad \text{and} \quad \bar{V}_{h3} = \frac{\partial}{\partial y} \begin{bmatrix} A_0 \\ A_0^* \end{bmatrix}, \tag{C.14}$$

of the homogeneous system corresponding to (C.12).

For the solution vector $\bar{V}_{h1}$ one gets

$$\int \left(-\frac{\partial |A_0|^2}{\partial Z} + i(A_0^* \tilde{R} - A_0 \tilde{R}^*) \right) d\vec{r}_\perp = 0$$

$$\Updownarrow$$

$$\frac{\partial}{\partial Z} \int |A_0|^2 d\vec{r}_\perp - \frac{\partial}{\partial \phi^{(1)}} \int \left(\ln g - \frac{g}{1 + |B_0|^2} \right) d\vec{r}_\perp = 0$$

$$\Updownarrow$$

$$\frac{\partial P^{(1)}}{\partial Z} - \frac{\partial U_1}{\partial \phi^{(1)}} = 0, \tag{C.15}$$

where $P^{(1)}$ is the to the zeroth order conserved power and

$$U_1 = \int \left(\ln g - \frac{g}{1 + |B_0|^2} \right) d\vec{r}_\perp. \tag{C.16}$$

The second solution vector $\bar{V}_{h2}$ yields

$$\int \left(-i\frac{\partial A_0^*}{\partial x}\frac{\partial A_0}{\partial Z} + i\frac{\partial A_0}{\partial x}\frac{\partial A_0^*}{\partial Z} - \frac{\partial A_0^*}{\partial x}\tilde{R} - \frac{\partial A_0}{\partial x}\tilde{R}^* \right) d\vec{r}_\perp = 0$$

$$\Updownarrow$$

$$-\frac{i}{2}\frac{\partial}{\partial Z} \int \left(A_0\frac{\partial A_0^*}{\partial x} - \frac{\partial A_0}{\partial x}A_0^* \right) d\vec{r}_\perp + \int \left(\frac{\partial A_0^*}{\partial x^{(1)}}\tilde{R} + \frac{\partial A_0}{\partial x^{(1)}}\tilde{R}^* \right) d\vec{r}_\perp = 0$$

$$\Updownarrow$$

$$\frac{\partial M_x^{(1)}}{\partial Z} + \frac{\partial U_2}{\partial x^{(1)}} = 0, \tag{C.17}$$

where $M_x^{(1)}$ is the to the zeroth order conserved momentum along the x-axis and

$$U_2 = \int \left(\ln \frac{g}{1 + |A_0|^2} - \frac{h}{1 + |B_0|^2} \right) d\vec{r}_\perp. \tag{C.18}$$

The third solvability condition is trivially found to be

$$\frac{\partial M_y^{(1)}}{\partial Z} + \frac{\partial U_2}{\partial y^{(1)}} = 0, \tag{C.19}$$

where $M_y^{(1)}$ is the to the zeroth order conserved momentum along the y-axis and U_2 is given by (C.18).

By inspection it is obvious that $\frac{\partial U_1}{\partial \phi} = \frac{\partial U_2}{\partial \phi}$ and that

$$U_2 \to \ln(1 + |B_0|^2) \text{ for } x^{(1)} - x^{(2)} \to \infty. \tag{C.20}$$

Hence $\ln(1 + |B_0|^2)$ is subtracted U_2 leading to the final interaction potential $U^{(1)} = U_2 - \ln(1 + |B_0|^2)$. If everywhere in equations (C.15,C.17,C.19) the superscripts are rotated, i.e. $A \leftrightarrow B$, the equivalent equations for the second soliton are found.

To sum up, the full set of interaction equations governing the variation of two generally non-identical interacting solitons in the general nonplanar case is

$$\frac{\partial P^{(1)}}{\partial Z} - \frac{\partial U^{(1)}}{\partial \phi^{(1)}} = 0, \tag{C.21a}$$

$$\frac{\partial P^{(2)}}{\partial Z} - \frac{\partial U^{(2)}}{\partial \phi^{(2)}} = 0, \tag{C.21b}$$

$$\frac{\partial M_x^{(1)}}{\partial Z} + \frac{\partial U^{(1)}}{\partial x^{(1)}} = 0, \tag{C.21c}$$

$$\frac{\partial M_x^{(2)}}{\partial Z} + \frac{\partial U^{(2)}}{\partial x^{(2)}} = 0, \tag{C.21d}$$

$$\frac{\partial M_y^{(1)}}{\partial Z} + \frac{\partial U^{(1)}}{\partial x^{(1)}} = 0, \tag{C.21e}$$

$$\frac{\partial M_y^{(2)}}{\partial Z} + \frac{\partial U^{(2)}}{\partial x^{(2)}} = 0, \tag{C.21f}$$

where

$$U^{(1)} = \int \left(\ln \frac{g}{(1 + |A_0|^2)(1 + |B_0|^2)} - \frac{h}{1 + |B_0|^2} \right) d\vec{r}_\perp, \tag{C.22a}$$

$$U^{(2)} = \int \left(\ln \frac{g}{(1 + |A_0|^2)(1 + |B_0|^2)} - \frac{h}{1 + |A_0|^2} \right) d\vec{r}_\perp, \tag{C.22b}$$

and

$$g = 1 + |A_0|^2 + |B_0|^2 + h, \quad \text{and} \quad h = A_0 B_0^* e^{-i\phi} + A_0^* B_0 e^{i\phi}. \tag{C.23}$$

Papers

Escape angles in bulk $\chi^{(2)}$ soliton interactions

Steffen Kjær Johansen, Ole Bang, and Mads Peter Sørensen,
Physical Review E, Volume 65, 026601 (February 2002).

We develop a theory for non-planar interaction between two identical type I spatial solitons propagating at opposite, but *arbitrary transverse angles* in quadratic non-linear (or so-called $\chi^{(2)}$) bulk media. We predict quantitatively the outwards escape angle, below which the solitons turn around and collide, and above which they continue to move away from each other. For in-plane interaction the theory allows prediction of the *outcome of a collision* through the inwards escape angle, i.e. whether the solitons fuse or cross. We find an analytical expression determining the inwards escape angle using Gaussian approximations for the solitons. The theory is verified numerically.

Stable self-guided laser beams or optical bright spatial solitons are of substantial interest in basic physics[1] and for technical applications, such as inducing fixed[2] and dynamically reconfigurable waveguides[3]. Several types of spatial solitons have been demonstrated experimentally, including 1D Kerr solitons[4] and 1D and 2D (number of transverse dimensions) solitons in saturable[5], photorefractive[6], and $\chi^{(2)}$ media[7]. Even incoherent solitons, excitable by a light bulb, have been demonstrated in photorefractive media[8]. All solitons exist when diffraction is balanced by the nonlinear self-focusing effect. In bulk Kerr media the self-focusing effect dominates and leads to collapse of both coherent and incoherent 2D solitons[9], their existence requiring an effectively saturable nonlinearity.

An intriguing feature of solitons is their particle like behavior during collision. In 1D Kerr media collisions are fully elastic due to integrability of the 1D nonlinear Schrödinger (NLS) equation[10]. In contrast, saturable, photorefractive, and $\chi^{(2)}$ media are described by non-integrable equations and soliton collisions are therefore inelastic, displaying both fusion (Fig. 1:A), crossing (Fig. 1:B), repulsion, and annihilation, additional solitons can be generated in a fission-type process [11], and solitons can even spiral around each other [12]. All processes depend strongly on the relative phase and have been demonstrated experimentally (see [1] and references therein).

Complex waveguide structures can be generated by soliton interaction, such as directional couplers[13], but their efficient implementation requires a detailed understanding of the nature of soliton collisions. Snyder and Sheppard predicted the outcome of collisions of 1D solitons in saturable media by comparing the collision angle with the critical angle for total internal reflection in an equivalent waveguide[14]. Except for this work most theories are based on the variational approach, which require the solitons to be far apart and breaks down at collision.

Here we focus on $\chi^{(2)}$ materials [15], which are more general than the simpler cubic Kerr and saturable media in the sense that dependent on the phase-mismatch between the fundamental and second-harmonic (SH) waves the nonlinearity can be both purely quadratic (close to phase-matching) and effectively cubic (for a large phase-mismatch). Spatial solitons in $\chi^{(2)}$ materials do not modify the refractive index, and consist of one (type I) or two (type II) fundamental fields resonantly coupled to a SH. The $\chi^{(2)}$ materials are of significant interest to photonics due to the strong and fast nonlinearities they can provide through cascading[16]. Furthermore, soliton induced waveguides in photorefractives can have a strong $\chi^{(2)}$ nonlinearity, which can be used for second-harmonic generation (SHG)[17].

Fusion and crossing (Fig. 1:A,B) of spatial $\chi^{(2)}$ solitons has been demonstrated numerically[18] and experimentally [19], and fission of 1D type I solitons was demonstrated analytically and numerically in the large phase-mismatch limit approximately described by the NLS equation[20]. However, the $\chi^{(2)}$ system is more general and
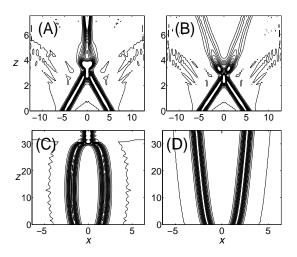
Figure 1: A,B: Planar collision between two Gaussians, $P = 48.3$ and $\beta = 0$. C,D: Outwards launched exact solitons, $P = 122.4$ and $\beta = 5$. The launch angles are $\alpha_x = 58°$ (A), $\alpha_x = 62°$ (B), $\alpha_x = 5.4°$ (C), and $\alpha_x = 5.7°$ (D).

complex than the saturable NLS equation and so far variational theories were only able to predict critical launch angles and relative phases separating regimes of collision and no collision [21]. Elegant non-planar effective particle theories predicted the absence of spiraling type I solitons, but still required weakly overlapping solitons [22]. In this letter we extend the effective particle approach to *arbitrary launch angles* and present the first theory able to correctly predict the *outcome of collisions* between 2D type I solitons in $\chi^{(2)}$ media.

We consider beam propagation under type-I SHG conditions in lossless bulk $\chi^{(2)}$ materials. Neglecting walk-off the system of normalized dynamical equations for the slowly varying envelope of the fundamental wave, $E_1 = E_1(\vec{r})$, and its SH, $E_2 = E_2(\vec{r})$, are [23]

$$i\partial_z E_1 + \tfrac{1}{2}\nabla_\perp^2 E_1 + E_1^* E_2 = 0, \tag{1a}$$

$$i\partial_z E_2 + \tfrac{1}{4}\nabla_\perp^2 E_2 - \beta E_2 + E_1^2 = 0. \tag{1b}$$

Here $\vec{r} = (x, y, z)$, z is the propagation variable, and $\nabla_\perp^2 = \partial_x^2 + \partial_y^2$ accounts for diffraction in the transverse $\vec{r}_\perp = (x, y)$-plane. The normalized phase mismatch is $\beta = l_d(2k_1 - k_2)$, where l_d is the diffraction length of the fundamental and k_1 and k_2 are the wave numbers of the fundamental and SH, respectively. The system (1) can be derived from the Lagrangian density

$$\begin{aligned}
\mathcal{L} &= 2\text{Im}\left(E_1 \partial_z E_1^*\right) + \text{Im}\left(E_2 \partial_z E_2^*\right) + \beta|E_2|^2 \\
&\quad + |\nabla_\perp E_1|^2 + \tfrac{1}{4}|\nabla_\perp E_2|^2 - \text{Re}\left(E_2^* E_1^2\right),
\end{aligned} \tag{2}$$

and conserves the power $P = \int (|E_1|^2 + |E_2|^2) d\vec{r}_\perp$ and momentum $\vec{M} = \int \text{Im}\{E_1^* \nabla_\perp E_1 + \frac{1}{2} E_2^* \nabla_\perp E_2\} d\vec{r}_\perp$, where we have defined $\int d\vec{r}_\perp \equiv \int \int_{-\infty}^{\infty} dx dy$.

The system (1) is known [24, 25] to have a *one-parameter family* of radially symmetric bright 2D solitons of the form $E_1(\vec{r}) = V(r; \lambda) \exp(i\lambda z)$ and $E_2(\vec{r}) = W(r; \lambda) \exp(i2\lambda z)$ where $\lambda > \max(0; -\beta/2)$ is the internal soliton parameter and $r = \sqrt{x^2 + y^2}$. We have found this family numerically, using a standard relaxation method, and approximately, using the variational approach [25] with Gaussians profiles $(V, W) = (V_g, W_g)$,

$$V_g = a_1 \exp(-r^2/b), \ W_g = a_2 \exp(-r^2/b). \tag{3}$$

Here $a_1 = a_2[2(\lambda b - 1)]^{-\frac{1}{2}}$, $a_2 = \frac{3}{2}(\lambda + b^{-1})$, and $b = [1 + (12\lambda^2 + 8\lambda\beta + \beta^2)^{\frac{1}{2}}/(2\lambda + \beta)]/2\lambda$. Because the system is Galilean invariant we can apply a gauge transformation to find moving solitons. Thus the *general three parameter soliton family* $(\tilde{V}, \tilde{W})$ is given by

$$\tilde{V}(x - \nu_x z, y - \nu_y z; \lambda, \nu_x, \nu_y) =$$
$$V(r; \lambda - \tfrac{1}{2}\nu_x^2 - \tfrac{1}{2}\nu_y^2) \exp[-i(\nu_x x + \nu_y y)], \tag{4a}$$
$$\tilde{W}(x - \nu_x z, y - \nu_y z; \lambda, \nu_x, \nu_y) =$$
$$W(r; \lambda - \tfrac{1}{2}\nu_x^2 - \tfrac{1}{2}\nu_y^2) \exp[-2i(\nu_x x + \nu_y y)], \tag{4b}$$

where (V, W) are either the exact soliton profiles (V_s, W_s) found numerically or (V_g, W_g) given by (3). $\nu_{x,y} = \tan(\alpha_{x,y})$ are the initial transverse velocities corresponding to the launch angles $\alpha_{x,y}$ with respect to the z-axis.

We substitute a field composed of two weakly overlapping solitons $(\tilde{V}^{(i)}, \tilde{W}^{(i)})$ into the Lagrangian density (2). We then follow the procedure outlined in [22] and allow the solitons to vary adiabatically through a slow variation of the soliton parameters with $Z = \epsilon z$ being the slow propagation variable. To first order in $\epsilon \ll 1$ the result is a set of dynamical equations governing the collective coordinates $x^{(i)}$, $y^{(i)}$, and $\phi^{(i)}$, being the center positions along the x and y-axis and accumulated phase of soliton $i=1,2$, respectively. We can express the new coordinates as $x^{(i)}(z) = \int_0^z \nu_x^{(i)}(Z')dZ' + x_0^{(i)}$, $y^{(i)}(z) = \int_0^z \nu_y^{(i)}(Z')dZ' + y_0^{(i)}$, and $\phi^{(i)}(z) = \int_0^z \lambda^{(i)}(Z')dZ' + \phi_0^{(i)}$, where subscript 0 denotes initial values.

At this point one traditionally simplifies the system by assuming the velocities to be small ($\partial_z x^{(i)} \sim \epsilon$, $\partial_z y^{(i)} \sim \epsilon$), i.e. the solitons propagate almost in parallel. However, we are interested in velocities that can be considerable, so instead we assume symmetric interaction between in-phase solitons with initially identical profiles, $\lambda = \lambda^{(i)}$ and $P = P^{(i)}$, and equal but opposite velocities, $\nu_{x,y} = \nu_{x,y}^{(1)} = -\nu_{x,y}^{(2)}$. Without loss of generality we set $x_0 = x_0^{(1)} = -x_0^{(2)} \geq 0$ and $y_0 = y_0^{(1)} = -y_0^{(2)} \geq 0$. Symmetry is conserved and the two sets of collective coordinates degenerate to one, $X = x^{(1)} = -x^{(2)}, Y = y^{(1)} = -y^{(2)}$. In cylindrical coordinates with $R = \sqrt{X^2 + Y^2}$

we can then reduce the dynamical equations to the Euler-Lagrange equation of the effective Lagrangian

$$L(R, \dot{R}) = \frac{1}{2} P \dot{R}^2 - U_{\text{eff}}(R, \dot{R}), \tag{5}$$

for the single coordinate R. The effective potential

$$U_{\text{eff}}(R, \dot{R}) = \frac{C_0}{2R^2} P + \frac{1}{2} U(R, \dot{R}) \tag{6}$$

is composed of the classical centrifugal barrier, where $C_0 = (X\dot{Y} - Y\dot{X})^2 = (x_0 \nu_y + y_0 \nu_x)^2$ is constant because of conservation of angular momentum, and of the interaction integral

$$U = - \int V^{(1)} \left[V^{(1)} W^{(2)} \cos(2\phi) + 2W^{(1)} V^{(2)} \cos(\phi) \right] d\vec{r}_\perp \tag{7}$$

where $\phi = 2\nu_x x + 2\nu_y y$. We note that, strictly speaking, U is only a quasi-classical potential since it depends on the velocities (in contrast to the potential used in [22]).

We have now established a picture of an effective particle moving in a potential, U_{eff}, with the kinetic energy $E_{\text{kin}} = \frac{1}{2} P \dot{R}^2 \geq 0$. For small velocities the potential (7) has the shape of a well and hence represents an attractive force. In the general case of non-planar interaction, $C_0 \neq 0$, the centrifugal barrier is always repulsive and goes to infinity at $R = 0$. This does not necessarily rule out fusion since also the velocities go to infinity because of conservation of C_0. The centrifugal barrier also creates a local minimum in the effective potential (still assuming small velocities) which suggests that spiraling configurations may exist. In general, however, we cannot expect our model to yield correct physical results in the vicinity of $R = 0$ since it violates the assumption of weakly overlapping solitons. In fact fusion has been observed numerically, but stable spiraling configurations have not been found[22].

Here we shall not discuss the qualitatively different regimes. Rather we are interested in *quantitative* predictions of escape velocities. For solitons launched with outwards velocities we will all ways be able to theoretically predict the escape velocity. On the other hand, a consistent theory for the determination of the inwards escape velocity only exists for in-plane interaction, when the classical centrifugal barrier vanishes, i.e. $C_0 = 0$.

We first determine the outwards escape angle. For simplicity we focus on in-plane interaction with $y_0 = \nu_y = C_0 = 0$ wherefore $R = |X|$ and $\dot{R} = \nu_x$. In this case the effective particle either escapes the potential, $E_{\text{tot}} = E_{\text{kin}} + E_{\text{pot}} > 0$, or is trapped by it, $E_{\text{tot}} < 0$, and the escape velocity, ν_c, is given by the relation
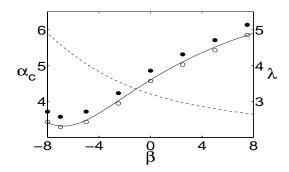
$$\nu_c^2 P = U(x_0, \nu_c). \tag{8}$$

Figure 2: Outwards escape angle in degrees (solid curve) for $FWHM\!=\!1$ and $x_0\!=\!1.5$. Numerical experiments where exact solitons fused ($\bullet$) and where they escaped ($\circ$). The dashed line shows the initial soliton power, P.

Unfortunately we are not able to express the interaction integral $U(x_0, \nu_x)$ in terms of analytical functions and we cannot use Gaussians, since the Gaussian tale asymptotic is different from that of the exact soliton. It is however trivial to solve (8) numerically and in Fig. 2 we have plotted the outwards escape angle, given by $\alpha_c = \mathrm{Arctan}(\nu_c)$, versus the phase mismatch. The initial beam width and separation are kept constant to ensure a weak overlap of the soliton tails at all phase mismatches. The simulations were performed with numerically found exact solitons as initial conditions. They confirm the accuracy of the escape angle predicted by Eq. (8). We found the minimum of about $3°$ around $\beta = -7$ to be global. Note that the angles are expected to be small, since the initial overlap and hence the attractive force between the solitons is weak. As an example of the dynamics we show in Fig. 1:C,D the outcome of the experiments with $\beta\!=\!5$ from Fig. 2. Only the fundamental waves are shown, the evolution of the SH waves being qualitatively the same.

Now considering solitons launched towards each other we first elaborate on the effective particle picture. If we assume the solitons to be initially far apart this corresponds to the effective particle experiencing essentially no potential. Even a small launch angle should then result in a positive total energy and enable the effective particle to cross the bottom of the potential and escape towards infinity, corresponding to soliton crossing. This is off course not the correct physical picture, since our system is not integrable and thus in reality the collision is not elastic. There is transfer of energy into internal soliton modes and shedding of energy as radiation.

In a different picture we assume that the soliton profiles do not change before the point of collision. This seems reasonable when comparing the characteristic length of slow adiabatic change with the relatively short interaction distance occurring for considerable velocities. In this case we can treat the interaction as if the solitons were launched on top of each other ($x_0\!=\!0$) corresponding to the effective particle

being launched in the bottom of the potential, where it experiences the maximum barrier. Then the relation determining the escape velocity becomes $\nu_c^2 P = 2U(0, \nu_c)$ rather than (8). The interaction integral no longer depends on the asymptotic tales but on the entire profiles and hence we can apply the Gaussian approximation (3). The general transcendental equation for the inwards escape angle is then given by

$$\nu_c^2 = \frac{2}{b} \frac{\lambda b + 1}{2\lambda b - 1} \left[e^{-\frac{4}{3} b \nu_c^2} + 2 e^{-\frac{1}{3} b \nu_c^2} \right], \tag{9}$$

which for $\beta{=}0$ simplifies to

$$\beta = 0 : \quad \nu_c = 0.23 \times \sqrt{P}, \tag{10}$$

in terms of the power. In the large phase-mismatch cascading limit, $(\beta \gg \lambda)$ where the nonlinearity is effectively cubic, Eq. (9) simplifies to

$$\beta \gg \lambda : \quad \nu_c = \sqrt{\frac{3}{4} \left(\frac{P}{2\pi} - \beta \right)}. \tag{11}$$

We remark that this approach is equivalent to finding the critical angle of total internal reflection for a waveguide [14]. However, since beam propagation in quadratic media does not induce changes in the refractive index the method used in [14] is not applicable to this case.

In Fig. 3 we have summarized the results for exact phase matching, $\beta{=}0$, and plotted the predicted inwards escape angle, $\alpha_c = \text{Arctan}(\nu_c)$, versus soliton power, both for ν_c given by (10) and for ν_c found with exact solitons. The curves are close and the simple square root dependency on the power excellently predict the escape angle. In the experiments we used Gaussians as initial conditions. These were launched with a distance of $2x_0{=}10$ between them, ensuring practically zero initial overlap. In Fig. 1:A,B we show examples of experiments with $\beta = 0$ and a power of $P = 48.3$. We note that for the exact soliton initial conditions we observed even better agreement than with Gaussians. Close to the escape angle all the power is shed as radiation and thus (10) serves as an *accurate prediction of soliton annihilation* (Fig. 4:B). We also investigated the cases of non-zero mismatches, focusing on $\beta = \pm 3$. In these regimes there is a power threshold for soliton excitation and the collisions are of a much more complex nature than for perfect phase matching, where solitons exist at all powers. For relatively low powers not far above the threshold the collisions mostly resulted in destruction of the solitons (Fig. 4:A). The explanation of this phenomenon is that too much power is shed as radiation in the collision and hence the resulting beams diffract because they do not carry sufficient power to form solitons. For higher powers the predicted escape angles were reasonably close to the observations.

In conclusion we have developed a theoretical description that should hold for systems with all types of local nonlinearities. In particular we have studied bulk $\chi^{(2)}$ media
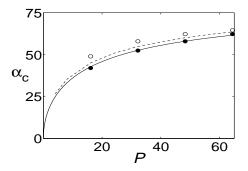
Figure 3: Inwards escape angle in degrees versus soliton power calculated analytically with Gaussians (solid) and with exact solitons (dashed) for $\beta=0$ and $x_0=5$. Numerical experiments where Gaussians crossed ($\circ$) and fused ($\bullet$).
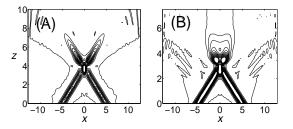

Figure 4: A: Crossing followed by diffraction ($\beta = -3$ and $P = 45.3$). B: Annihilation ($\beta = 0$ and $P = 48.3$).

and determined analytical expressions for the escape angles when the centrifugal barrier vanishes. This happens in the two in-plane cases of outwards and inwards launched solitons. The simple expression for the inwards escape angle represents the first *analytical* prediction of the *outcome* of a soliton collision. We have verified the analytical expressions numerically using Gaussian approximations and observed excellent agreement.

References

[1] For a review see: M. Segev and G. Stegeman, Phys. Today **51** (8), 42 (1998)

[2] M. Klotz *et al.*, Opt. Lett. **24**, 77 (1999).

[3] R. De La Fuente, A. Barthelemy, and C. Froehly, Opt. Lett. **16**, 793 (1991). M. Shih *et al.*, J. Opt. Soc. Am. B **14**, 3091 (1997). Ph. Dittrich *et al.*, Opt. Lett. **24**, 1508 (1999).

[4] J.S. Aitchinson *et al.*, Opt. Lett. **15**, 471 (1990).

[5] V. Tikhonenko, J. Christou, and B. Luther-Davies, J. Opt. Soc. Am. B **12**, 2046 (1995).

[6] G. Duree *et al.*, Phys. Rev. Lett. **71**, 533 (1993).

[7] R. Schiek, Y. Baek, and G.I. Stegeman, Phys. Rev. E **53**, 1138 (1996). W.E. Torruellas *et al.*, Phys. Rev. Lett. **74**, 5036 (1995).

[8] M. Mitchell *et al.*, Phys. Rev. Lett. **77**, 490 (1996). M. Mitchell and M. Segev, Nature **387**, 880 (1997).

[9] P.L. Kelley, Phys. Rev. Lett. **15**, 1005 (1965). O. Bang, D. Edmundson, and W. Królikowski, Phys. Rev. Lett. **83**, 5479 (1999).

[10] R.Y. Chiao, E. Garmire, and C.H. Townes, Phys. Rev. Lett. **13**, 479 (1964). V.E. Zakharov and A.B. Shabat, Sov. Phys. JETP **34**, 62 (1972).

[11] W. Królikowski and S.A. Holstrom, Opt. Lett. **22**, 369 (1997).

[12] M. Shih, M. Segev, and G. Salamo, Phys. Rev. Lett. **78**, 2551 (1997).

[13] S. Lan *et al.*, Opt. Lett. **24**, 475 (1999).

[14] A.W. Snyder and A.P. Sheppard, Opt. Lett. **18**, 482 (1991).

[15] For a review see L. Torner, in *Beam Shaping and Control with Nonlinear Optics*, eds. F. Kajzar and R. Reinisch (Plenum, New Yourk, 1998).

[16] For a review see G.I. Stegeman, D.J. Hagan, and L. Torner, J. Opt. Quantum Electron. **28**, 1691 (1996).

[17] S. Lan *et al.*, Opt. Lett. **24**, 1145 (1999).

[18] Type I: M.J. Werner and P.D. Drummond, J. Opt. Soc. Am. B **10**, 2390 (1993). Type II: G. Leo, G. Assanto, and W.E. Torruellas, Opt. Lett. **22**, 7 (1997).

[19] Type I: Y. Baek *et al.*, Opt. Lett. **22**, 1550 (1997). Type II: B. Costantini *et al.*, Opt. Lett. **23**, 424 (1998).

[20] L. Torner, J.P. Torres, and C.R. Menyuk, Opt. Lett. **21**, 462 (1996).

[21] Type I: C.B. Clausen, P.L. Christiansen, and L. Torner, Opt. Commun. **136**, 185 (97). Type II: B. Costantini *et al.*, Opt. Lett. **22**, 1376 (1997).

[22] V.V. Steblina, Y.S. Kivshar, and A.V. Buryak, Opt. Lett. **23**, 156 (1998). A.V. Buryak and V.V. Steblina, J. Opt. Soc. Am. B **16**, 245 (1999).

[23] C. R. Menyuk, R. Schiek, and L. Torner, J. Opt. Soc. Am. B **11**, 2434 (1994). O. Bang, *ibid.* **14**, 51 (1997).

[24] A.V. Buryak, Y.S. Kivshar, and V.V. Steblina, Phys. Rev. A **52**, 1670 (1995).

[25] V.V. steblina *et al.*, Opt. Commun. **118**, 345 (1995).

Engineering of spatial solitons in two-period QPM structures

Steffen Kjær Johansen, Silvia Carrasco, Lluís Torner, and Ole Bang,
Optics Communications, Volume 203, Issue 3-6, pp. 393-402 (March 2002).

We report on a scheme which might make it *practically* possible to engineer the effective competing nonlinearities that on average govern the light propagation in quasi-phase-matching (QPM) gratings. Modulation of the QPM period with a second longer period, introduces an extra degree of freedom, which can be used to engineer the effective quadratic and induced cubic nonlinearity. However, in contrast to former work here we use a *simple phase-reversal grating* for the modulation, which is practically realizable and has already been fabricated. Furthermore, we develop the theory for *arbitrary relative lengths of the two periods* and we consider the effect on solitons and the bandwidth for their generation. We derive an expression for the bandwidth of multicolor soliton generation in two-period QPM samples and we predict and confirm numerically that the bandwidth is broader in the two-period QPM sample than in homogeneous structures.

Quasi-phase-matching (QPM) is a major alternative over conventional phase match-
ing in many laser applications based on frequency-conversion processes in quadratic
nonlinear media (for reviews, see [1, 2]). Besides other practical advantages, QPM
allows tailoring the nonlinearity of the material to form complex structures. This
opens a range of new possibilities, which have become experimentally feasible with
the recent progress in poling techniques. For example, engineerable pulse compression
in frequency-doubling schemes in synthetic QPM gratings has been demonstrated in
aperiodically poled lithium niobate and potassium niobate [3, 4, 5, 6], and transverse
QPM gratings have been made both for shaping second-harmonic beams and to ex-
tend the spectral coverage of optical parametric oscillators[7, 8]. Bandwidth enhanced
parametric interactions can be obtained in modulated-period structures [9], multi-
ple nonlinear interactions can be achieved in quasi-periodic schemes [10, 11, 12, 13],
and simultaneous generation of multiple color laser light has been demonstrated in
QPM crystals doped with active lasing ions [14]. QPM engineering also finds novel
important applications beyond pure frequency-conversion devices, e.g., to generate
enhanced cascading phase-shifts [15], all-optical diode operation [16], and multicolor
soliton formation [17, 18, 19, 20, 21, 22].

Here we show that two-period QPM structures offer new opportunities for soliton
control.

Multicolor solitons mediated by second-harmonic generation (SHG) form by mutual
trapping of the beams at the fundamental frequency (FF) and at the second harmonic
frequency (SH). Here we focus on bright solitons whose basic properties are well
known. Whole dynamically stable families exist above a certain power threshold for
all phase mismatches. At lowest order the effect of QPM grating is to average the
quadratic nonlinearity [2]. However, taking higher order perturbations into account
reveals that the corresponding averaged field equations include effective cubic, Kerr-
like terms[19, 23, 24]. Such terms modify the average properties of CW waves [25, 26]
and the soliton families of the averaged equations [19, 24, 27], which can be analyzed
as sustained by competing quadratic and effective cubic nonlinearities [28, 29, 30, 31,
32].

Nevertheless, in standard QPM the strength of the induced averaged cubic nonline-
arity is proportional to the ratio between the QPM grating period and the soliton
characteristic length (i.e., the diffraction length in the case of spatial solitons). At
optical wave lengths, the former is typically of the order of ten μm, whereas the latter
is a few mm. Therefore, the strength of the induced cubic nonlinearities is extremely
small. The question thus naturally arises whether and how QPM engineering can be
employed to bring the effective cubic nonlinearities to compete with the quadratic
in the average fields. One solution is to add a strong dc-part to the nonlinear QPM
grating, i.e. as done in [33, 34]. This adds a term to the induced Kerr terms, which
is proportional to the QPM grating period and the dc-value squared, and thus can
be large[24]. Another potentially more versatile technique is to modulate the QPM

period with a second longer period, as it was shown theoretically in [23]. This introduces an extra degree of freedom, which can be used to engineer the effective quadratic and induced averaged cubic nonlinearity.

Here we consider the latter technique. However, in contrast to the rather complicated long-period modulation used in [23] we use here a *simple phase-reversal grating* for the modulation, similar to the two-period QPM sample recently employed by Chou and co-workers [12] for multiple-channel wavelength conversion in the third telecommunication window. Furthermore, we develop the theory for *arbitrary relative lengths of the two periods* and we consider the effect of the modulation on multicolor solitons. We expect soliton formation to be possible for a variety of phase-reversal periods, in view of the fact that multicolor solitons have been shown to be robust against strong perturbations, including quasi-periodic QPM gratings[21] and even periodic gain and loss[35]. Using the induced averaged cubic nonlinearities we derive an expression for the bandwidth of multicolor soliton generation in two-period QPM samples and we show that the bandwidth is broader in the two-period QPM sample than in homogeneous quadratic nonlinear materials. Importantly, all our results are confirmed numerically.

We consider beam propagation under type-I SHG conditions in a lossless QPM $\chi^{(2)}$ slab waveguide. The slowly varying envelope of the fundamental wave, $E_1 = E_1(x, z)$, and its SH, $E_2 = E_2(x, z)$, are[36]

$$i\frac{\partial E_1}{\partial z} + \frac{1}{2}\frac{\partial^2 E_1}{\partial x^2} + d(z)E_1^* E_2 e^{-i\beta z} = 0, \tag{1}$$

$$i\frac{\partial E_2}{\partial z} + \frac{\alpha}{2}\frac{\partial^2 E_2}{\partial x^2} + d(z)E_1^2 e^{i\beta z} = 0, \tag{2}$$

where in all cases of practical interest $\alpha \simeq 0.5$. The normalized wave-vector mismatch is introduced via the real parameter $\beta = k_1 \omega_0^2 \Delta k$, where $\Delta k = 2k_1 - k_2$, and ω_0 is the beam width, and $k_{1,2}$ are the linear wave numbers of the fundamental and SH, respectively. The scaled transverse coordinate, x, is measured in units of ω_0 and the propagation coordinate, z, is measured in units of $2l_d$ where $l_d = k_1 \omega_0^2/2$ is the diffraction length of the fundamental wave. The spatial periodic modulation of the nonlinearity is described by the grating function $d(z)$ whose amplitude is normalized to 1, and whose domain length we define as $\Lambda = \pi/\kappa$, where κ is the spatial grating frequency or the QPM frequency, which we assume real and positive. In the case of second-harmonic generation in lithium niobate pumped at $\lambda_\omega \sim 1.5$ μm with a beam width of $\omega_0 \sim 20$ μm, the intrinsic material wave vector mismatch is of the order $|\beta| \sim 10^3$. Thus the QPM frequency must also be of this order which corresponds to a domain length of ~ 10 μm. For such values, a scaled grating frequency of the order $\kappa \sim 10$ correspond to a domain length of about 1 mm.

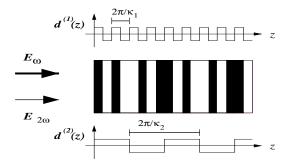The two-period grating function, $d(z)$, consists of a primary grating, $d^{(1)}(z)$, and a

Figure 1: Two-period QPM grating.

superimposed secondary grating, $d^{(2)}(z)$. We expand $d(z)$ in a Fourier series

$$d(z) = \sum_k d_k^{(1)} \exp(ik\kappa_1 z) \times \sum_l d_l^{(2)} \exp(il\kappa_2 z) \qquad (3)$$

where the summations are over all (k, l) from $-\infty$ to ∞. If we assume the grating functions to be square, only the odd harmonics enters into the expansion, $d_{2l+1} = 2/i\pi(2l+1)$ and $d_{2l} = 0$. In the case of low-depletion SHG, the effect of the super-imposed period is to split each peak of the original one-period QPM grating into an infinite family of peaks[12]. More formally, one has peaks at all spatial QPM frequencies $m\kappa_1 + n\kappa_2$ where m and n are the QPM orders related to the primary and secondary grating, respectively. These peaks are not delta-like, though for simplicity they are depicted as such in Fig. 2, but rather sinc-like functions around the relevant QPM frequency. The SHG-efficiency is higher the lower the order. Hence, in one-period QPM one would choose to match to the first peak ($m = \pm1$). In two-period QPM there is an equivalent rule, i.e. the low-depletion SHG-efficiency is highest for $m = n = \pm1$. To be able to treat the problem mathematically we have to neglect all overlap between peaks in order to avoid resonances. Thus we must assume $\kappa >> 1$ in the one-period case. In the general two-period case the spectrum becomes dense, as in the case of a Fibonacci grating[21]. In order to be able to neglect any overlap between the peak we are looking at, and the rest of the dense spectrum, we have to assume, not only high spatial QPM frequencies, but also that the two frequencies are of different order. We remark that soliton excitation is expected to be possible no matter what the spectrum looks like, as long as the power is high enough[21]. Our numerical simulations presented here agree with this expectation. It is the lack of analytical tools which necessitates the assumption of well separated peaks.

By applying the asymptotic expansion[37] technique we have established a perturbation theory describing the propagation of the averaged fields in this two-period QPM system. We make the transformation $E_1(x, z) = w(x, z)$ and $E_2(x, z) = v(x, z) \exp(i\epsilon z)$, where $\epsilon = \beta - m\kappa_1 - n\kappa_2$, is the residual phase mismatch, which is assumed to be
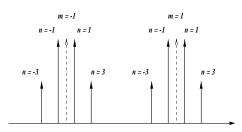
Figure 2: Peak splitting in the two-period QPM grating. Dashed peaks indicate the location of the 1'st order peaks in the one-period case.

small. The functions $w(x, z)$ and $v(x, z)$ are assumed to vary slowly on the scale given by the QPM periods and can be expanded in the Fourier series

$$w(x, z) = w_0(x, z) + \sum_{k \neq 0} w_k(x, z)e^{ik\kappa_1 z} + \sum_{l \neq 0} \omega_l(x, z)e^{il\kappa_2 z}, \tag{4}$$

$$v(x, z) = v_0(x, z) + \sum_{k \neq 0} v_k(x, z)e^{ik\kappa_1 z} + \sum_{l \neq 0} \nu_l(x, z)e^{il\kappa_2 z}. \tag{5}$$

We remark that this assumption is valid also when the QPM frequencies share common harmonics. In this case the SHG spectrum discussed above becomes discrete as in the one-period case. However, to avoid overlap between peaks the QPM frequencies must still be assumed of different order. Furthermore we formally assume that $\beta \gg 1$, $\kappa_1 \gg 1$, and $\kappa_2 \gg 1$. Substituting (4-5) into (1-2) and matching leading order terms yields the relations for the harmonic coefficients[19]. One gets

$$w_q = \frac{1}{q\kappa_1} d_n^{(2)} d_{(q+m)}^{(1)} w_0^* v_0, \quad v_n = \frac{1}{q\kappa_1} d_{-n}^{(2)} d_{(q-m)}^{(1)} w_0^2, \tag{6}$$

$$\omega_q = \frac{1}{q\kappa_2} d_m^{(1)} d_{(q+n)}^{(2)} w_0^* v_0, \quad \nu_n = \frac{1}{q\kappa_2} d_{-m}^{(1)} d_{(q-n)}^{(2)} w_0^2, \tag{7}$$

and the equations governing the averaged fields are of the form

$$i\frac{\partial w_0}{\partial z} + \frac{1}{2}\frac{\partial^2 w_0}{\partial x^2} + \eta w_0^* v_0 + \gamma(|w_0|^2 - |v_0|^2)w_0 = 0, \tag{8}$$

$$i\frac{\partial v_0}{\partial z} + \frac{1}{4}\frac{\partial^2 v_0}{\partial x^2} - \epsilon v_0 + \eta w_0^2 - 2\gamma|w_0|^2 v_0 = 0. \tag{9}$$

System (8-9) conserves the same power as system (1-2), $P = \int(|w_0|^2 + |v_0|^2)dx =$

$\int (|E_1|^2 + |E_2|^2)dx$. The strengths of the averaged nonlinearities are given by

$$\eta = d_m^{(1)} d_n^{(2)} - \sum_k d_k^{(1)} d_{[(k-m)\frac{\kappa_1}{\kappa_2}+n]}^{(2)}, \tag{10}$$

$$\gamma = \frac{d_{-n}^{(2)}}{\kappa_1} \sum_{q,l} \frac{d_l^{(2)} d_{[(m+q)-(l-n)\frac{\kappa_2}{\kappa_1}]}^{(1)} d_{[m+q]}^{(1)}}{q} + \frac{d_{-m}^{(1)}}{\kappa_2} \sum_{q,k} \frac{d_k^{(1)} d_{[(n+q)-(k-m)\frac{\kappa_1}{\kappa_2}]}^{(2)} d_{[n+q]}^{(2)}}{q}. \tag{11}$$

In these expressions, q, l, and k are integers, and the summations are everywhere over all integers from $-\infty$ to ∞ except zero. We emphasize that the averaged model (8-9) is valid for arbitrary values of κ_1 and κ_2 as long as the assumptions $\kappa_1 >> 1$, and $\kappa_2 >> 1$ are not violated. However care must be taken when calculating the sums in (10) and (11). When necessary, k and l, themselves integers, must always be chosen such that the $(k-m)\kappa_1/\kappa_2$ and $(l-n)\kappa_2/\kappa_1$ are integers. This ensures that the Fourier coefficients $d_k^{(1)}$ and $d_l^{(1)}$ exist. We remark that if one of the QPM frequencies is an irrational number expressions (10) and (11) are greatly simplified

$$\eta = d_m^{(1)} d_n^{(2)}, \tag{12}$$

$$\gamma = \frac{d_n^{(2)} d_{-n}^{(2)}}{\kappa_1} \sum_q \frac{d_{[m+q]}^{(1)2}}{q} + \frac{d_m^{(1)} d_{-m}^{(1)}}{\kappa_2} \sum_q \frac{d_{[n+q]}^{(2)2}}{q}. \tag{13}$$

To make the cubic self- and cross-phase modulation symmetric in (8-9) we have had to assume that $d_n^{*(i)} = d_{-n}^{(i)} = -d_n^{(i)}$, which is the case for square grating functions. Otherwise expressions (10-13) hold for any grating function of the form (3). Rewriting (10) and (11) for square grating functions we get

$$\eta = -\frac{4}{\pi^2} \left(\frac{1}{mn} - \sum_s \frac{1}{(2s+m)\left(2s\frac{\kappa_1}{\kappa_2}+n\right)} \right), \tag{14}$$

$$\gamma = -\frac{16}{\pi^4} \left(\frac{1}{n\kappa_1} \sum_{q,r} \frac{1}{2q(2r+n)\left(2q-2r\frac{\kappa_2}{\kappa_1}+m\right)(m+2q)} \right.$$

$$\left. + \frac{1}{m\kappa_2} \sum_{q,s} \frac{1}{2q(2s+m)\left(2q-2s\frac{\kappa_1}{\kappa_2}+n\right)(n+2q)} \right), \tag{15}$$

where the summations now are over all integers q, r, and s from $-\infty$ to ∞ except zero. Notice the different sign of the lowest-order contribution to (14) at the $(m = 1, n = 1)$-peak, and the $(m = 1, n = -1)$-peak. Such change of sign has implications to the soliton features, as shall be discussed below. Equations (8-9) were first derived in [19]. They have the same form regardless of the specific type of grating, the parameters still merely being given as sums over the Fourier coefficients of the grating. Thus they were derived in [24] for QPM with both a linear and a nonlinear grating with

or without a dc-value of the nonlinear grating. They were also derived in [23] for a more exotic two-period grating.

By letting $w_0(x,z) = \bar{w}(x,z)/\eta$ and $v_0(x,z) = \bar{v}(x,z)/\eta$ we can reduce system (8-9) to

$$i\frac{\partial \bar{w}}{\partial z} + \frac{1}{2}\frac{\partial^2 \bar{w}}{\partial x^2} + \bar{w}^*\bar{v} + \tilde{\gamma}(|\bar{w}|^2 - |\bar{v}|^2)\bar{w} = 0, \tag{16}$$

$$i\frac{\partial \bar{v}}{\partial z} + \frac{1}{4}\frac{\partial^2 \bar{v}}{\partial x^2} - \epsilon\bar{v} + \bar{w}^2 - 2\tilde{\gamma}|\bar{w}|^2\bar{v} = 0. \tag{17}$$

The stationary bright solitary families of system (16-17) are of the form $\bar{w}(x,z) = u_1(x)\exp(i\lambda z)$, $\bar{v}(x,z) = u_2(x)\exp(i2\lambda z)$. They are parametrized by the soliton parameter $\lambda > \max\{0, -\epsilon/2\}$. The stationary solutions of (8-9) are parametrized by exactly the same parameter but since this system is characterized by three (ϵ, η, and γ) rather than the two parameters of (16-17) (ϵ and $\tilde{\gamma} = \gamma/\eta^2$) each solution of (16-17) corresponds to an infinite family of solutions of (8-9), i.e. an infinite number of QPM frequency combinations and thus physical setups. System (16-17) conserves the renormalized power $\bar{P} = \int(|\bar{w}|^2 + |\bar{v}|^2)dx = \eta^2 P$. We note that also the assumed slow variation of the functions $w(x,z)$ and $v(x,z)$ imposes constraints on the choice of the soliton parameter λ. The characteristic soliton scale length, $2\pi/\lambda$, must be much larger than the QPM period $\Lambda = \pi/\kappa$, where κ in the two-period case is the smallest QPM frequency.

Merely looking at expressions (14-15) suggests that in principle there is ample room for engineering of the averaged nonlinearities. The main parameters are the QPM frequencies κ_1 and κ_2. In general we can state that the higher the QPM frequencies are, the lower the induced averaged cubic terms become. Thus $\gamma \to 0$ for $\kappa_1, \kappa_2 \to \infty$. One also notices that the ratio between κ_1 and κ_2 and vice versa plays an important role in the sums in expressions (14) and (15). We observe that the smaller the ratio the more significant the corresponding sums. From (14) it is obvious that the induced part of the averaged quadratic nonlinearity depends *only* on the ratio κ_2/κ_1. Thus we can realize the same averaged quadratic nonlinearity at large QPM frequencies (no induced averaged cubic terms) and at low QPM frequencies (significant induced averaged cubic terms). We note that if we let the second grating function $d^{(2)}(z) = 1$, the only Fourier coefficient left in the expansion of $d^{(2)}(z)$ is $d_0^{(2)} = d_n^{(2)} = d_{-n}^{(2)} = 1$ and hence $\eta = d_m^{(1)}$ and $\gamma = \frac{1}{\kappa_1}\sum d_{[m+q]}^{(1)^2}/q$. The whole system thus degenerates into the one-period case and the results of [19] are reproduced.

Depending on our objectives we can make the individual terms of the averaged nonlinearities more or less significant. Thus we can essentially make the two-period QPM system behave like the one-period system with induced averaged cubic nonlinearities by choosing $\kappa_1 >> \kappa_2$ while still assuming $\kappa_2 >> 1$. In this way one can use κ_1 to reduce a large intrinsic phase mismatch, β, to a small effective mismatch which can
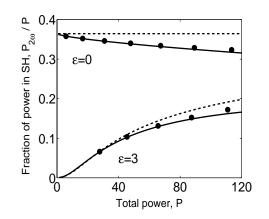
Figure 3: Fraction of power in the SH for the two-period QPM system with $(\kappa_1, \kappa_2) = (997, 13)$ as a function of total power. Solid line and •: Theoretical and numerically measured values, respectively. Dashed curves: Zero-order approximation, $\gamma = 0$. The value of ϵ is indicated at each pair of curves.

then be manipulated further with κ_2. Thus, if we let $\kappa_1 \to \infty$ the averaged nonlinearities of for the system with square grating functions (14-15) with $m = n = 1$ reduces to

$$\eta = -\frac{4}{\pi^2}, \qquad \gamma = \frac{4}{\kappa_2 \pi^2} \left(1 - \frac{8}{\pi^2} \right). \tag{18}$$

To verify the model in this $\kappa_1 \to \infty$ limit we have made a series of simulations launching soliton initial conditions, found from (16-17), in a real two-period structure described by (1-2) with κ_1 chosen to be a high prime and κ_2 a small prime. Choosing primes effectively eliminates contributions from the remaining sums in (14-15) because r and s must be chosen such that $r\kappa_2/\kappa_1$ and $s\kappa_1/\kappa_2$ are positive integers. We measure the fraction of power in the SH after any initial transient has died out and compare this to the theoretically predicted value. In Fig. 3 we have summarized the results of this investigation for different powers and different effective phase mismatches.

If both QPM frequencies are of the same order, the full non-simplified expressions (14-15) must be used to calculate the averaged nonlinearities. Because of the way the ratio κ_1/κ_2 enters in (14-15), one has *discrete resonances* between the QPM frequencies. At these discrete resonances the induced averaged nonlinearities become stronger. The strength depends on the order of the resonance, the lower the order the higher the strength. To show how the strength of the averaged nonlinearities are calculated we concentrate on the summations involving $s\kappa_1/\kappa_2$. The contribution of the terms involving $r\kappa_2/\kappa_1$ is handled in an analogous way. First-order resonances arise when κ_1/κ_2 is a positive integer; then s is summed over all integers except zero

from $-\infty$ to ∞. Second-order resonances arise when $\kappa_1 = (2p-1)\kappa_2/2$ where p is a positive integer. In this case s only spans the even integers. Third-order resonances occur when $\kappa_1 = p * \kappa_2/3$ where $p = 1, 2, 4, 5, 7, 8, \cdots$; then s must be summed over the integers $\pm 3, \pm 6, \pm 9, \cdots$. And so on and so forth for higher-order resonances.

We emphasize that resonances in principle must be taken into account whenever the gratings periods are rational values. In actual practice, the values of the grating periods are not integers but may be approximated by rational numbers. For example, let $(\kappa_1, \kappa_2) = (194.7, 13.3)$. In this particular case, we can write $\kappa_1 = p\kappa_2/133$, where p is any integer which has no common divisor with 133 except 1, showing that we are thus dealing with a 133'rd order resonance. In this particular case, $p = 1947$, and s must be summed over $\pm 133, \pm 266, \pm 399, \cdots$.

In Fig. 4 we show the induced averaged cubic nonlinearity of the reduced system, $\tilde{\gamma} = \gamma/\eta^2$, as a function of the QPM frequency κ_1 (κ_2 is fixed). We have plotted the values for the lowest order resonances together with the no-resonance curve, i.e. the limiting curve where the average nonlinearities are given by (12-13) which in the case of square grating functions reduces to

$$\eta = -\frac{4}{\pi^2}, \tag{19}$$

$$\gamma = \frac{4}{\pi^2}\left(1 - \frac{8}{\pi^2}\right)\left(\frac{1}{\kappa_1} + \frac{1}{\kappa_2}\right). \tag{20}$$

It is evident from Fig. 4 that the higher order resonances quickly converge towards the no-resonance curve with κ_1 and that only the first order resonances yield induced averaged cubic nonlinearity significantly higher than the no-resonance case. We note that the resonance peaks shown are truly discrete. Furthermore, when the grating periods are non-integer numbers, only very high-order resonances occur. The point labelled $\circ$ in Fig. 4 illustrates the idea. It corresponds to $(\kappa_1, \kappa_2) = (8.66, 13)$. While the very similar structure corresponding to $(\kappa_1, \kappa_2) = (26/3, 13)$ yields a third-order resonance contribution, $(\kappa_1, \kappa_2) = (8.66, 13)$ yields a 650th order resonance. Hence, the negligible deviation relative to the no-resonance curve. The conclusion is thus that only the no-resonance curve is of practical experimental interest.

However, to verify that the model is correct we still need to analyze the full resonant structure of the averaged nonlinearities. Thus in Fig. 5 we focus on the first order resonances and show how the effective averaged quadratic nonlinearity changes with the ratio κ_1/κ_2. In the same figure we have also plotted $\tilde{\gamma}$ to emphasize the interplay between $\tilde{\gamma}$ and η. Recall that the graphs are not continuous but discrete functions of κ_1/κ_2, i.e. the plot only holds for values of κ_1 which are integers of κ_2 ($\kappa_2 = 13$ in this case). In Fig. 6 we have made a series of numerical experiments to confirm that the averaged model derived in this paper does predict correct behavior also at the QPM frequency resonances. Again we launch soliton found from (16-17) in the real
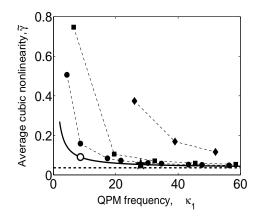
Figure 4: Averaged cubic nonlinearity at the $(m = n = 1)$-peak in the reduced system as a function of the QPM frequency κ_1 ($\kappa_2 = 13$). Full curve: No-resonance limit. $\blacklozenge$: 1'st order resonances. $\blacksquare$: 2'nd order resonances. $\bullet$: 3'rd order resonances. The lines between $\bullet$, $\blacklozenge$ and $\blacksquare$'s are only to help the eye. Dashed line: $\kappa_2 \to \infty$ approximation. $\circ$: Indicates a point, $(\kappa_1, \tilde{\gamma}) = (8.66, 0.090)$ very close to the $p = 2$ 3'rd order resonance point $(\kappa_1, \tilde{\gamma}) = (26/3, 0.157)$. $\bigstar$: Indicates the point where $\tilde{\gamma} \approx 0.050$ (see text).

Figure 5: Averaged nonlinearities at the first order resonances from Fig. 4. $\kappa_2 = 13$ and $\kappa_1 = p * 13$ (p is an integer). $\blacksquare$: The effective cubic nonlinearity, $\tilde{\gamma}$, of the averaged system. $\bullet$: Amplitude of the averaged quadratic nonlinearity, η. The curves are discrete and the lines in between the $\bullet$'s and $\blacksquare$'s are just to help the eye. The dashed and dotted lines indicate the asymptotic values of $\tilde{\gamma}$ ($\kappa_1 \to \infty$) and $|\eta|$, respectively. $\bigstar$ indicates the point where $\tilde{\gamma} \approx 0.050$ (see text).
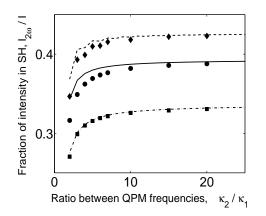
Figure 6: Fraction of peak-intensity in SH at the first order resonances from Fig. 5. $\kappa_2 = 13$ and $\kappa_1 = p * 13$ (p is an integer). The input power is kept constant at $P = 15$ and $\epsilon = 0$. The lines represent theoretically predicted values whereas $\blacklozenge$, $\bullet$ and $\blacksquare$ are numerically measured values. Dashed line and $\blacklozenge$: Maximum value. Solid line and $\bullet$: Average value. Dashed dotted line and $\blacksquare$: Minimum value. Notice that the lines actually represent the discrete integer values. They are drawn as lines just to help the eye.

system described by (1-2), but now we keep the input power fixed, while we change κ_1 in integer steps of κ_2. Simulations where carried out in the actual two-period QPM structure. As before we let the evolution continue until any initial transient has died out. Then we sample the minimum, maximum, and averaged peak intensities and compare those with the theoretically predicted values.

It is worth recalling that for every soliton solution of the reduced system (16-17) we have a whole family of solutions of the form (4-5). In Fig. 7 we have shown how one specific solution for $\tilde{\gamma} \approx 0.050$ leads to different initial conditions for two different physical setups. The two setups here chosen corresponds to the point $\bigstar$ indicated on both Fig. 4 and Fig. 5. We also show the evolution of these initial conditions in Fig. 7, i.e. the evolution of the peak intensities.

For the induced averaged nonlinearities addressed in this paper to be of potential practical importance, they have to impact the observable soliton properties, including their excitation conditions. To show that this seems to be the case, in Fig. 8 we show the behavior found for the soliton content[38], SC, as a function of the residual phase mismatch in a two-period structure with QPM frequencies $(\kappa_1, \kappa_2) = (195, 13)$. We also include the outcome of the numerical experiments performed for a structure with the non-integer values $(\kappa_1, \kappa_2) = (194.7, 13.3)$, to show that the effect predicted is not restricted to a particularly suitable choice of these parameters. We launch a FF signal,
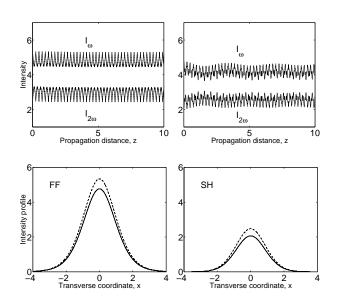
Figure 7: Evolution of solitons in the real two-period system (1-2). Top figures show peak intensities. Bottom figures compare intensity profiles for the FF's (left) and SH's (right). Top left figure and dashed curves in bottom figures are for $(\kappa_1, \kappa_2) = (195, 13)$. Top right figure and solid curves in bottom figures are for $(\kappa_1, \kappa_2) = (32.9, 13)$. The two initial conditions stem from the same soliton of system (16-17) with $\tilde{\gamma} \approx 0.050$, $\epsilon = 0$, and $\lambda = 0.4$.
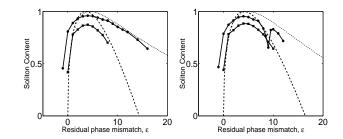
Figure 8: Soliton content for sech input FF as a function of the residual phase mismatch $\epsilon = \beta - \kappa_1 - \kappa_2$ ($m = n = 1$). Input power is $P_{in} = 50$. Left plot is for $(\kappa_1, \kappa_2) = (195, 13)$ ($\eta \simeq -0.38, \tilde{\gamma} \simeq 0.050$) and right plot for $(\kappa_1, \kappa_2) = (194.7, 13.3)$ ($\eta \simeq -4/\pi^2, \tilde{\gamma} \simeq 0.038$). •': SC for two-period QPM. '■': SC for purely quadratic model. The discrete points are the outcome of numerical experiments; the full lines in between are only to help the eye. The dashed and dotted lines are estimates from the limiting NLSE for a pure quadratic model and for a model with cubic terms, respectively.

with a sech-shape, and no SH seeding and calculate how much of the initial power, P_{in}, is bound in the soliton which eventually forms. We propagate until a steady state has emerged and then we collect the energy flow in a window wide enough to enclose substantially all the soliton. Typical values are propagation until $z = 10^3$ and collection of energy flow in a window of $x = \pm 10$, but these values were adapted whenever needed in order to capture always all the soliton energy. Simulations where carried out in the actual two-period QPM structure. The bandwidth of the SC for sech inputs can be estimated by using the Zakharov-Shabat scattering equations associated with the (1+1)-dimensional nonlinear Schrödinger equation, NLSE. With cubic terms, i.e. for system (8-9), one gets the estimate

$$\text{SC} \simeq \frac{2\sqrt{\frac{\eta^2 \epsilon}{\eta^2 + \gamma\epsilon}}}{\eta^2 P_{in}} \left(\sqrt{2\eta^2 P_{in}} - \sqrt{\frac{\eta^2 \epsilon}{\eta^2 + \gamma\epsilon}} \right). \tag{21}$$

In the plot we also include the actual value of SC that is numerically found in the corresponding homogeneous pure quadratic case. Compared to the pure quadratic model, the bandwidth for the two-period structure is found to get wider. This effect can be understood by comparing the approximate theoretical expressions for the two cases given by (21). There is also an expected significant increase in the efficiency owing to the fact that in systems with induced cubic terms the exited solitons are closer to the initial sech-shape than in purely quadratic systems. To explain the "dip" in the SC in the case of $(\kappa_1, \kappa_2) = (194.7, 13.3)$ again one must turn to the SHG spectrum. We find that the ($m = -1, n = 31$)-peak is located exactly at $\epsilon = 9.6$, which is where the bottom of the "dip" seems to be. Thus we conclude that the efficiency of soliton excitation is diminished because of resonances between the ($m = n = 1$)- and the ($m = -1, n = 31$)-peak.
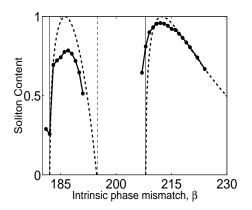
Figure 9: Soliton content for sech input FF as a function of intrinsic phase mismatch β with $(\kappa_1, \kappa_2) = (195, 13)$. Input power is $P_{in} = 50$. The discrete points are the outcome of numerical experiments; the full lines in between are only to help the eye. The dashed curves are estimates from the limiting NLSE. The vertical lines located at $\beta = 182$ and $\beta = 208$ indicate the $m = 1, n = -1$ and $m = n = 1$ peaks, respectively. The dashed vertical line at $\beta = 195$ indicates the location of the peak in the absence of a second period (see Fig. 2).

In Fig. 9 we plot the soliton content for the $(\kappa_1, \kappa_2) = (195, 13)$ case, but now we scan mismatches not only around the $(m = n = 1)$-peak but also around the $(m = 1, n = -1)$-peak. In the absence of resonances and average cubic nonlinearities, i.e. $\eta = \pm 4/\pi^2$, no differences are found in the behavior of soliton excitation at each peak. However, such is not the case when the soliton generation efficiencies can interfere with each other, as shown in Fig. 9. For example, in the particular case shown, one observes that soliton generation around the $(m = 1, n = -1)$-peak takes place within a narrower band of mismatches and is less efficient than around the $(m = 1, n = 1)$-peak. This is because the average nonlinearities (14-15) are nonlinear functions of m and n and hence they change their relative strengths at the two peaks. A different behavior than that displayed in Fig. 9 might be obtained with different values of the two-grating periods and input light conditions, as shown in Fig. 10. When resonances are involved we note that at the $(m = 1, n = -1)$-peak the induced part of the average second order nonlinearity is stronger than the no-resonance value $4/\pi^2$ whereas it is weaker at the $(m = 1, n = 1)$-peak. Notice also that the soliton content vanishes in the intermediate region between the $(m = 1, n = \pm 1)$-peaks. This is because in the intermediate region between both peaks, e.g., at the mismatch that would be exactly compensated with a single-period QPM structure, the interference between the two peaks acts as a periodic amplitude modulation of the effective nonlinear coefficient, with a period comparable with the characteristic soliton length. Such modulation constitutes a very strong perturbation that prevents soliton formation.
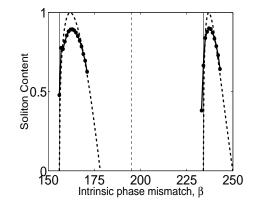
Figure 10: Same as in Fig. 9, but here $(\kappa_1, \kappa_2) = (195, 39)$

.

We remark that one finds soliton generation around other peaks than the ($m = 1, n = \pm 1$)-peak. For example, in the $(\kappa_1, \kappa_2) = (195, 13)$ case we observe a band (not shown in the plot) around $\epsilon = 39$ corresponding to the ($m = 1, n = 3$)-peak. However, soliton formation in this band is much less efficient than in the ($m = 1, n = \pm 1$)-band and therefore we did not include it the plot. Similarly, other bands with higher QPM order also exist but one has to launch correspondingly high powers to excite solitons.

In conclusion, we derived an averaged model for the soliton propagation in two-period QPM systems of the form (8-9), and we showed that the model gives an accurate description of stationary soliton propagation under a variety of input light and material conditions. We have shown that one can use one grating period of the QPM structure to reduce the intrinsic phase mismatch and the other grating period to induce averaged cubic nonlinearities. We found the induced averaged cubic nonlinearities to be strongest when one QPM frequency is a multiple of the other, but we showed that those are strictly discrete resonances that cannot occur when experimentally feasible grating periods are taking into account. However, our investigations predict that also the no-resonance averaged contributions can be important. In particular, we found that the QPM engineered averaged cubic nonlinearities, induced in feasible two-period samples, enhances the peak-efficiency and residual mismatch-bandwidth of the soliton excitation process with non-soliton single frequency pump light.

References

[1] R. L. Byer, Quasi-phasematched nonlinear interactions and devices, J. Nonlinear Opt. Phys. 6 (4) (1997) 549–592.

[2] M. M. Fejer, in *Beam shaping and control with nonlinear optics*, F. Kajzar and R. Reinisch, eds. (Plenum Press, New York, 1998), pp. 375-406.

[3] M. A. Arbore, M. M. Fejer, M. E. Fermann, A. Hariharan, A. Galvanauskas, D. Harter, Frequency doubling of femtosecond erbium-fiber soliton lasers in periodically poled lithium niobate, Opt. Lett. 22 (1) (1997) 13–15.

[4] M. A. Arbore, A. Galvanauskas, D. Harter, M. H. Chou, M. M. Fejer, Engineerable compression of ultrashort pulses by use of second-harmonic generation in chirped-period-poled lithium niobate, Opt. Lett. 22 (17) (1997) 1341–1343.

[5] P. Loza-Alvarez, D. T. Reid, P. Faller, M. Ebrahimzadeh, W. Sibbett, H. Karlsson, F. Laurell, Simultaneous femtosecond-pulse compression and second-harmonic generation in aperiodically poled $KTiOPO_4$, Opt. Lett. 24 (15) (1999) 1071–1073.

[6] G. Imeshev, M. A. Arbore, M. M. Fejer, Galvanauskas, M. Fermann, D. Harter, Ultrashort-pulse second-harmonic generation with longitudinally nonuniform quasi-phase-matching gratings: pulse compression and shaping, J. Opt. Soc. Am. B 17 (2) (2000) 304–318.

[7] G. Imeshev, M. Proctor, M. M. Fejer, Lateral patterning of nonlinear frequency conversion with transversely varying quasi-phase-matching gratings, Opt. Lett. 23 (9) (1998) 673–675.

[8] P. E. Powers, T. J. Kulp, S. E. Bisson, Continuous tuning of a continuous-wave periodically poled lithium niobate optical parametric oscillator by use of a fan-out grating design, Opt. Lett. 23 (3) (1998) 159–162.

[9] K. Mizuuchi, K. Yamamoto, M. Kato, H. Sato, Broadening of the phase-matching bandwidth in quasi-phase-matched second harmonic generation, IEEE J. Quantum Electron. 30 (7) (1994) 1596–1604.

[10] S.-N. Zhu, Y.-Y. Zhu, N.-B. Ming, Quasi-phase-matched third-harmonic generation in a quasi-periodic optical superlattice, Science 278 (1997) 843–846.

[11] K. Fradkin-Kashi, A. Arie, Multiple-wavelength quasi-phase-matched nonlinear interactions, IEEE J. Quantum Electron. 35 (11) (1999) 1649–1656.

[12] M. H. Chou, K. R. Parameswaran, M. M. Fejer, I. Brener, Multiple-channel wavelength conversion by use of engineered quasi-phase-matching structures in $LiNbO_3$ waveguides, Opt. Lett. 24 (16) (1999) 1157–1159.

[13] H. Liu, Y. Y. Zhu, S. N. Zhu, C. Zhang, N. B. Ming, Aperiodic optical superlattices engineered for optical frequency conversion, Appl. Phys. Lett. 79 (6) (2001) 728–730.

[14] J. Capmany, Simultaneous generation of red, green, and blue continuous-wave laser radiation in Nd^{3+}-doped aperiodically poled lithium niobate, Appl. Phys. Lett. 78 (2) (2001) 144–146.

[15] M. Cha, Cascaded phase shift and intensity modulation in aperiodic quasi-phase-matched gratings, Opt. Lett. 23 (4) (1998) 250–252.

[16] K. Gallo, G. Assanto, K. R. Parameswaran, M. M. Fejer, All-optical diode in a periodically poled lithium niobate waveguide, Appl. Phys. Lett. 79 (3) (2001) 314–316.

[17] L. Torner, C. B. Clausen, O. Bang, P. L. Christiansen, Y. S. Kivshar, M. M. Fejer, Soliton control by QPM engineering, Optics & Photonics News 10 (12) (1999) 44.

[18] L. Torner, C. B. Clausen, M. M. Fejer, Adiabatic shaping of quadratic solitons, Opt. Lett. 23 (12) (1998) 903–905.

[19] C. B. Clausen, O. Bang, Y. S. Kivshar, Spatial solitons and induced Kerr effects in QPM media, Phys. Rev. Lett. 78 (1997) 4749–4752.

[20] C. B. Clausen, L. Torner, Spatial switching of quadratic solitons in engineered quasi-phase-matched structures, Opt. Lett. 24 (1) (1999) 7–9.

[21] C. B. Clausen, O. Bang, Y. S. Kivshar, P. L. Christiansen, Quasi-periodic envelope solitons, Phys. Rev. Lett. 83 (23) (1999) 4740–4743.

[22] S. Carrasco, J. P. Torres, L. Torner, R. Schiek, Engineerable generation of quadratic solitons in synthetic phase matching, Opt. Lett. 25 (17) (2000) 1273–1275.

[23] O. Bang, C. B. Clausen, P. L. Christiansen, L. Torner, Engineering competing nonlinearities, Opt. Lett. 24 (1999) 1413–1415.

[24] J. F. Corney, O. Bang, Solitons in quadratic nonlinear photonic crystals, Phys. Rev. E 64 (4) (2001) 047601.

[25] A. Kobyakov, F. Lederer, O. Bang, Y. S. Kivshar, Nonlinear phase shift and all-optical switching in quasi-phase-matched quadratic media, Opt. Lett. 23 (7) (1998) 506–508.

[26] O. Bang, T. W. Graversen, J. F. Corney, Accurate switching intensities and length scales in quasi-phase-matched materials, Opt. Lett. 26 (13) (2001) 1007–1009.

[27] J. F. Corney, O. Bang, Modulational instability in periodic quadratic nonlinear materials, Phys. Rev. Lett. 87 (13) (2001) 133901.

[28] A. V. Buryak, Y. S. Kivshar, S. Trillo, Optical soliton supported by competing nonlinearities, Opt. Lett. 20 (19) (1995) 1961–1963.

[29] O. Bang, Dynamical equations for wave packets in materials with both quadratic and cubic responses, J. Opt. Soc. Am. B 14 (1997) 51–61.

[30] L. Bergé, O. Bang, J. J. Rasmussen, V. K. Mezentsev, Self-focusing and soliton-like structures in materials with competing quadratic and cubic nonlinearities, Phys. Rev. E 55 (3) (1997) 3555–3570.

[31] O. Bang, L. Bergé, J. J. Rasmussen, Wave collapse in bulk media with quadratic and cubic responses, Opt. Commun. 146 (1998) 231–235.

[32] O. Bang, Y. S. Kivshar, A. V. Buryak, A. D. Rossi, S. Trillo, Two-dimensional solitary waves in media with quadratic and cubic nonlinearity, Phys. Rev. E 58 (4) (1998) 5057–5069.

[33] A. S. Helmy, D. C. Hutchings, T. C. Kleckner, J. H. Marsh, A. C. Bryce, J. M. Arnold, C. R. Stanley, J. S. Aitchison, C. T. A. Brown, K. Moutzouris, M. Ebrahimzadeh, Quasi phase matching in GaAs-AlAs superlattice waveguides through bandgap tuning by use of quantum-well intermixing, Opt. Lett. 25 (18) (2000) 1370–1372.

[34] Y. Shuto, T. Watanabe, S. Tomaru, I. Yokohama, M. Hikita, M. Amano, Quasi-phase-matched second-harmonic generation in diazo-dye-substituted polymer waveguides, IEEE J. Quantum Electron. 33 (3) (1997) 349–357.

[35] L. Torner, J. P. Torres, O. Bang, Robustness of quadratic solitons with periodic gain, Opt. Commun. 185 (2000) 479–485.

[36] C. R. Menyuk, R. Schiek, L. Torner, Solitary waves due to $\chi^{(2)} : \chi^{(2)}$ cascading, J. Opt. Soc. Am. B 11 (12) (1994) 2434–2443.

[37] Y. S. Kivshar, N. Grønbech-Jensen, R. D. Parmentier, Kinks in the presence of rapidly varying perturbations, Phys. Rev. E 49 (5) (1994) 4542–4551.

[38] L. Torner, J. P. Torres, D. Artigas, D. Mihalache, D. Mazilu, Soliton content with quadratic nonlinearities, Opt. Commun. 164 (1999) 153–159.